1-1-2005

Mechanical behavior, modeling, and color change of electrospun fiber mats.

Angelo Pedicini
University of Massachusetts Amherst

MECHANICAL BEHAVIOR, MODELING, AND COLOR CHANGE OF ELECTROSPUN FIBER MATS

A Dissertation Presented

by

ANGELO PEDICINI

Submitted to the Graduate School of the
University of Massachusetts Amherst in partial fulfillment
of the requirements for the degree of

DOCTOR OF PHILOSOPHY

February 2005

Polymer Science & Engineering

MECHANICAL BEHAVIOR, MODELING AND COLOR CHANGE OF ELECTROSPUN FIBER MATS

A Dissertation Presented

by

ANGELO PEDICINI

Approved as to style and content by:

Richard J. Farris, Chair

William J. MacKnight, Member

Thomas J. Lardner, Member

Heidi Schreuder-Gibson, Consulting Member

Shaw Ling Hsu, Department Head
Polymer Science & Engineering

DEDICATION

To my sisters for believing in me

To my parents for teaching us the value of education

ACKNOWLEDGMENTS

There are many people to thank who played a part in helping me get to this point. The goals we achieve are milestones in life's journey; the people and places along the way make the journey itself more important than the final destination.

To begin, I'd like to thank Dr. Lynn Penn for letting me experience laboratory research as an undergraduate student, and for suggesting UMASS, Amherst, as a potential graduate school choice. Toward the completion of this work and dissertation, I owe great thanks to my advisor, Professor Richard Farris. Professor Farris teaches all his students how to be good scientists, as well as how to be good people, through example. I feel truly privileged to have had Professor Farris as a mentor, teacher, and role model. In addition, I'd like to thank my committee members—Professor William MacKnight, Professor Thomas Lardner, and Dr. Heidi Schreuder-Gibson—for their time, effort, and contributions to the quality of this dissertation. Special thanks to Dr. Schreuder-Gibson for her especially close involvement with the work. Our many discussions and her insightful suggestions were a great help to my research.

I wish to thank the members of the Farris research group whom I had the pleasure of working with daily. In addition, many students and members of the Polymer Science and Engineering Department have made my time here not only educational, but truly fruitful and pleasurable.

A few special thanks go to my classmates, especially Firat, Manuel, and Margarita. Firat was my first lab partner and friend in Amherst. Manuel and Margarita over the past few years have become very dear friends and I consider them two of the

truly good people in the world. I'd also like to thank Kishore for being the most selfless friend a person could ever hope to have. Through his actions, Kishore reminded me every day that it's more rewarding to give than to receive.

I want to thank the town of Amherst for being a wonderful place to live, learn, and just be. Everyone should be so lucky to live in a town like Amherst, Massachusetts, at least once.

Finally, I want to thank Bhavini and my family. Bhavini left familiar surroundings in Kentucky to come to UMASS so we could spend four years of experiences together. She taught me that even graduate students can enjoy themselves outside of school and I've cherished our time in Amherst together. Thanks also to Bhavini's family, whom I now consider part of my own, for their encouragement.

To my parents I want to thank for their constant support and love. Thank you for always making sure I finished my homework, from my first day of school to now. And thanks to my sisters for reminding me that even with a Ph.D., I'm still just their little brother. Thanks to my brothers-in-law, Jerry and David, for their support and encouragement.

Finally, the smallest people on my list of thanks, but whom occupy the most volume in my heart, my nephews Samuel and Nicholas. Their existence brings me greater joy and happiness than any academic or professional achievement ever could.

ABSTRACT

MECHANICAL BEHAVIOR, MODELING, AND COLOR CHANGE IN ELECTROSPUN FIBER MATS

FEBRUARY 2005

ANGELO PEDICINI, B.A., UNIVERSITY OF KENTUCKY

M.A., UNIVERSITY OF MASSACHUSETTS AMHERST

Ph.D., UNIVERSITY OF MASSACHUSETTS AMHERST

Directed by: Professor Richard J. Farris

The process of electrospinning and the physical properties of electrospun fibers are presented in this thesis. In electrospinning, polymeric fibers having diameters ranging from 50 nanometers to 1 micrometer are prepared by applying high static charge to a polymer solution. The mechanical properties and molecular morphology of some electrospun polymers are shown to be fundamentally different compared to their bulk analogs. Experimental results indicate that the mechanical behavior of electrospun polyurethane fiber mats is influenced by fiber mat morphology, molecular orientation, and surface flaws on electrospun fibers.

This research characterizes the mechanical behavior of randomly oriented electrospun polyurethane mats and sheds light on general differences in behavior between electrospun and bulk materials. Further, the mechanical response of random fiber mats is modeled based on the mechanical characterization of aligned electrospun fibers. Also, empirical models are employed to relate the tensile properties of electrospun materials to their bulk analogs.

The crystallinity and melting behavior of a family of electrospun polyesters is studied and provides insight to the rapid cooling and effects on solidification and crystallization of electrospun polymeric fibers. The results indicate a commonly accepted idea in electrospinning, that electrospun fibers result from rapid solvent evaporation and experience quench-like solidification from a jet of polymer solution.

A qualititative study illustrates a color change phenomenon in a series of electrospun polymer/solvent systems. Color change is produced by electrospinning, and subsequent heating, and occurs at characteristic temperatures dependent on the polymer system used. These color change systems are also demonstrated as candidates for imageable media.

TABLE OF CONTENTS

LIST OF TABLES

Table

Page

LIST OF FIGURES

Figure

Page

CHAPTER 1

ELECTROSPINNING: HISTORY, BASIC PRINCIPLES AND APPLICATIONS

1.1 Electrospinning History

Over 400 years ago, Sir William Gilbert discovered that static charge had the ability to physically deform a drop of fluid. Those observations are described in his treatise *On the Loadstone and Magnetic Bodies and on the Great Magnet the Earth*: "a rubbed piece of amber held at suitable distance pulls toward itself the nearest particles of a spherical drop of water standing into a cone." [1]

In the early 20th century, the physical phenomenon described by Gilbert was applied to two-component solutions and patented separately by two individuals in the early 20th century. Cooley in 1902 described "a method of electrically dispersing fluids by subjecting them to the disruptive and dispersive action . . . of electricity at high tension." [2] Also in 1902, Morton[3] patented ". . . the electrical method of dispersing fluids, whereby volatile fluids are separated from their combination or association with relatively non-volatile or fixed substances in composite fluids composed thereof, resulting also in the evaporation of the volatile fluids and a state of condensation or solidification of the relatively non-volatile or fixed substances, whereby fiber may be artificially produced." These basic principles continue to form the basis of electrospinning research today. In 1934, Formhals[4-5] employed a more applied approach to electrospinning by collecting fibers onto a reel, spool, or drum made of conducting material so fibers could " . . . pile up in parallelism on the thread receiving device in such a way that they can be unwound continuously in solid form in

skeins or ropes . . ." Shortly after, a similar patent in 1936[6] included molten materials such as gums, pitches, synthetic rosins, and glass that could be spun into fine filaments by the process. In addition, external assists were applied to the process such as air directed through a nozzle to facilitate dispersion and travel across the potential gap. Electrospinning solutions were also subjected to air blasts transverse to their trajectory and electrodes positioned at opposite sides of the path of travel of the fibers upon which alternating charge delivered sidewise impulses. As fibers proceed toward the target, their trajectory becomes more crooked and irregular to make them suitable for their intended use at the time, packing and insulation.

The early patents discussed above outline the most basic elements of the electrospinning process: a polymer solution or melt, a high voltage source with an electrode to deliver charge to the fluid, and a counter-electrode acting as a target. These elements are presented schematically in Figure 1. The more recent research interest in the electrospinning field and electrospun fibers as potentially useful materials stems from the relative ease of the process and most notably the size of fibers produced—typically in the range of 50 to 500 nanometers in diameter. Fibers in this size range are attractive materials for many applications: fiber-reinforced composites, filtration applications due to the fine pore size of electrospun fibers mats, and biological scaffolds owing to their porosity and large surface area.

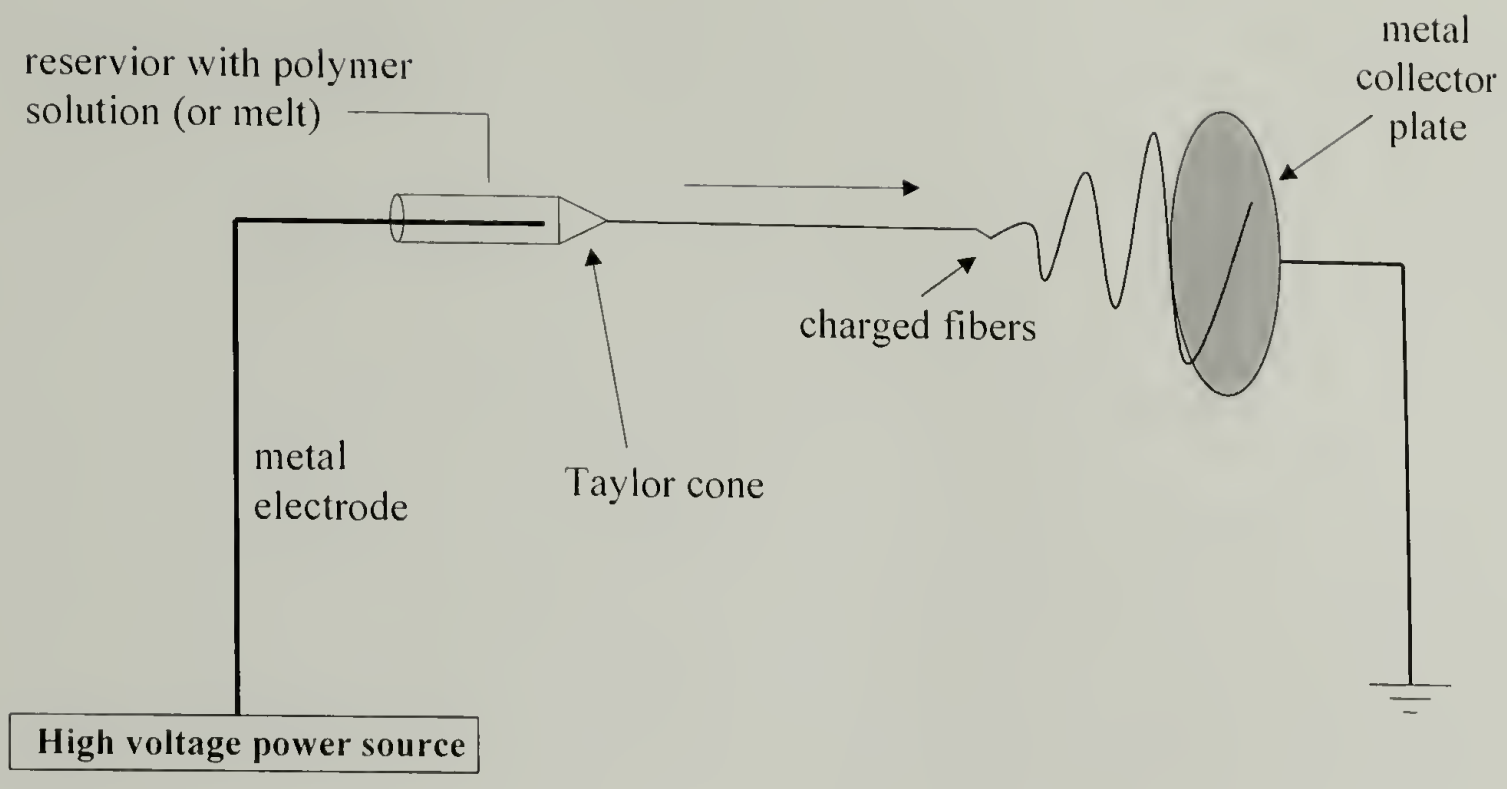

Figure 1.1 - Schematic diagram of the electrospinning process

1.2 Modeling the Electrospinning Process

An analytical approach to the relationship between static electricity and the movement of fluids is taken in several studies.[7-11] The formation of a cone described by Gilbert has been treated theoretically and experimentally, and the physical parameters governing the jet dimensions and shape of the cone have been studied.[12] In the current literature, the deformed conical shape experienced by a pendant drop of fluid when static charge is applied bears the name of the pioneering researcher: Taylor cone.

The principles that govern electrified fluids are also applicable and can be extended to describe the behavior of polymer solutions and melts in electrospinning. Some important differences between electrospraying and electrospinning have been

studied and modeled.[13-14] In the earlier view of electrospinning, applying a static charge to a solution in a nozzle results in the formation of the Taylor cone, from which a single jet is ejected. As the jet travels the gap between nozzle and target, charge repulsion causes the jet to split, or "splay," into multiple filaments. Hence, a micron size jet produces nanoscale fibers by splitting multiple times. At high electric fields in which the jet becomes unstable after traveling a short distance, the "splaying" description of events appears to be correct when the unstable region is imaged at an exposure time of 1 microsecond or greater. While isolated incidents of jet splay have been observed in electrospun systems, high-speed photography confirms that the cone-shaped instability envelope is actually created by a single unstable jet.[15-16] The instability results in the spinning jet following a bending and spiraling path in three dimensions. The jet grows longer and thinner as the loop diameter increases. Theoretical calculations suggest that the longitudinal strain rate in the loops is of the order of $10^5 s^{-1}$.[17] Theory also suggests that the transformation from a random coil to a stretched macromolecule occurs when the strain rate multiplied by the conformational relaxation time of the molecule is greater than 0.5.[18-19] Even polymers with relatively short relaxation times, when multiplied by strain rates of $\approx 10^5 s^{-1}$, are likely to become stretched in the direction of the electrospinning jet axis. Evidence of molecular orientation—through optical birefringence and infrared (IR) dichroism—induced by electrospinning will be presented in this work.

The effect of longitudinal strain in the electrospinning jet and the consequences on polymer chain conformation and orientation has been illustrated for electrospun nylon. Raman spectroscopy has shown that electrospun nylon 6 adopts

an altered crystalline conformation, the γ-form, relative to bulk nylon 6, which has the α-form.[20] The γ-form is also obtained when nylon 6 is melt-spun and collected at high take-up speeds that result in high stress on the fibers. High stresses may also be experienced by polymer chains during electrospinning and the rapid solidification of the nanofibers kinetically locks in the γ-form. Other studies of electrospun nylon 6 also indicate molecular orientation, determined by x-ray diffraction.[21]

1.3 Electrospun Polymer Systems

Electrospinning is a robust process and more than 40 different polymers have been electrospun and reported in the literature. Among these include glassy polymers—polystyrene, poly(methyl methacrylate), and polycarbonate[22]; semicrystalline polymers—poly(vinyl alcohol),[23] poly(acrylonitrile),[24] poly(vinyl chloride),[25] and nylon 4,6[26]; biopolymers—DNA,[27] silk,[28] and collagen[29]; high-performance polymers such as poly (*p*-phenylene terephthalamide)[30]; and polyolefins from the melt.[31-32] In addition to the many homopolymers, various blends[33] and copolymers[34-35] have been electrospun into nanofibers. In addition to two-component polymer/polymer systems, polymer solutions with carbon nanotubes and silicate clays have been electrospun to create so called 'nanocomposite' fibers. Bergshoef and coworkers prepared optically transparent composite fibers of nylon 4,6 filled with montmorillonite clay[26] and the orientation of carbon nanotubes in electrospun fibers was studied by Dror and coworkers.[36] The reinforcing effect of single-walled carbon nanotubes (SWNT) in electrospun fiber mats is reviewed later.

1.4 Fundamental Studies

Fundamental studies have elucidated some of the more salient variables influencing the electrospinning process that affect the size, morphology, and intrinsic properties of electrospun fibers. Specifically, polymer solution rheology and surface tension play critical roles in fiber size and morphology and have been studied quantitatively by several groups.[37-39] The essential conclusions to be drawn from the literature and from our own investigations are that for a particular polymer/solvent system, solutions of relatively high concentration and viscosity and lower surface tension produce relatively large, defect-free fibers. Solutions of relatively low concentration and viscosity and higher surface tension result in fibers of smaller diameter and a higher probability of defects such as beads. A fiber electrospun from solution is like a liquid cylinder supported along its axis. It is not stable and liquid will flow spontaneously into evenly spaced droplets strung along the core fiber.[40] This beading effect is obviously promoted by higher surface tension and lower volatility solvents which remain as part of the spinning jet for a longer period of time. An illustration of the qualitative relationship between electrospinning solution and choice of solvent and the resultant fiber morphology is demonstrable in a variety of electrospun polymer/solvent systems. Examples are shown below.

The effect of solution concentration and choice of solvent on electrospun fiber morphology is shown for poly(ethylene oxide) in Figure 1.2. An electrospinning solution of 2% wt. PEO in water produces fibers with a bead-on-string morphology, as shown in Figure 1.2a. By increasing the concentration of PEO in water to 5% by weight, beads are eliminated and fibers of cylindrical geometry are produced. PEO

fibers electrospun from 5% wt. solution in water are shown in Figure 1.2b. Similar morphological changes result when the polymer concentration is held at 2% wt. and a highly volatile solvent, chloroform, is substituted for water. Cylindrical fibers, free of beads, result when PEO is electrospun from 2% wt. solution in chloroform, illustrated in Figure 1.2c. The chloroform in the 2% wt. PEO solution evaporates more rapidly than the water in the 2% wt. aqueous solution and the spinning jet quickly solidifies to maintain a cylindrical fiber geometry free of bead-on-string defects.

Another observable effect of changing solvent and/or solution concentration is fiber diameter. The micrographs in Figure 1.2, taken at the same magnification, qualitatively illustrate the difference in average fiber diameter among the three electrospun solutions. Comparison of the 5% aqueous solution and 2% chloroform solution shows that fibers electrospun from solution in chloroform have a larger diameter than fibers spun from aqueous solution.

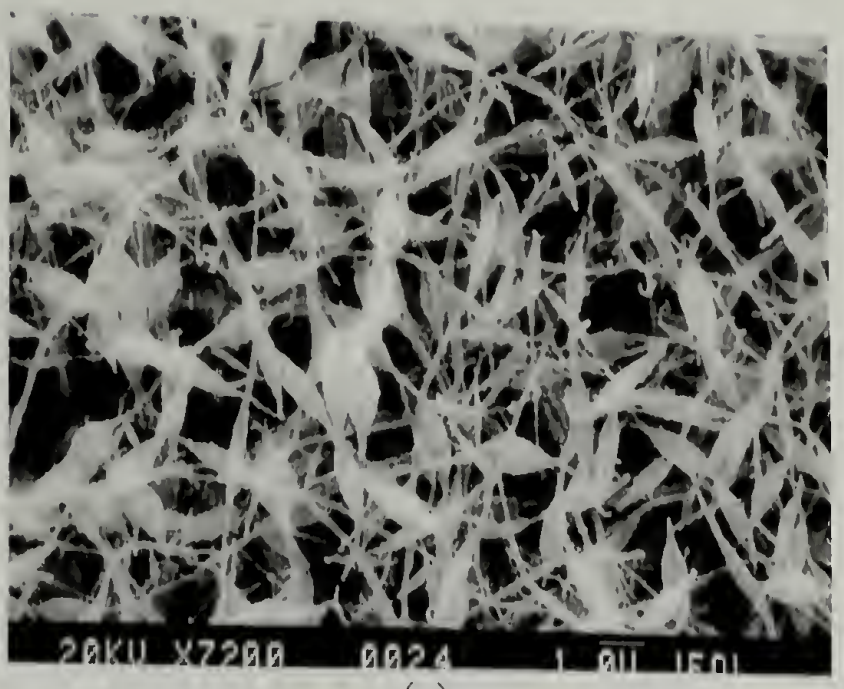

(a)

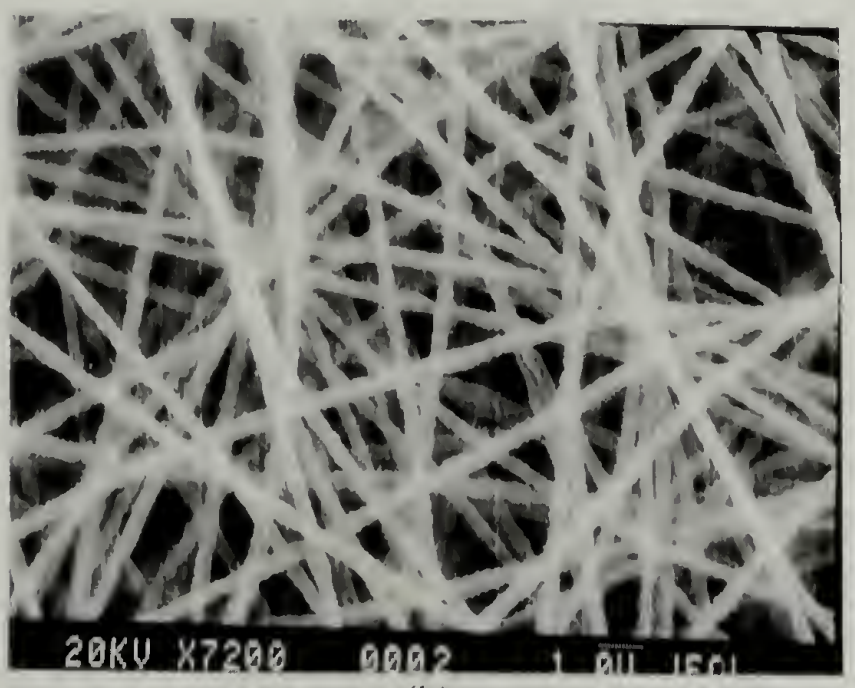

(b)

(c)

Figure 1.2 – Electrospun poly(ethylene oxide): (a) 2% wt. in water, (b) 5% wt. in water, (c) 2% wt. in chloroform.

Similar results are seen with electrospun polystyrene. A variety of morphologies are obtainable by electrospinning polystyrene from different solvents and at different concentrations. Even the beads can vary in their morphology, depending on the solvent used in the electrospinning solution. The morphologies for a variety of electrospun polystyrene/solvent systems are shown in Figure 1.3.

(a)

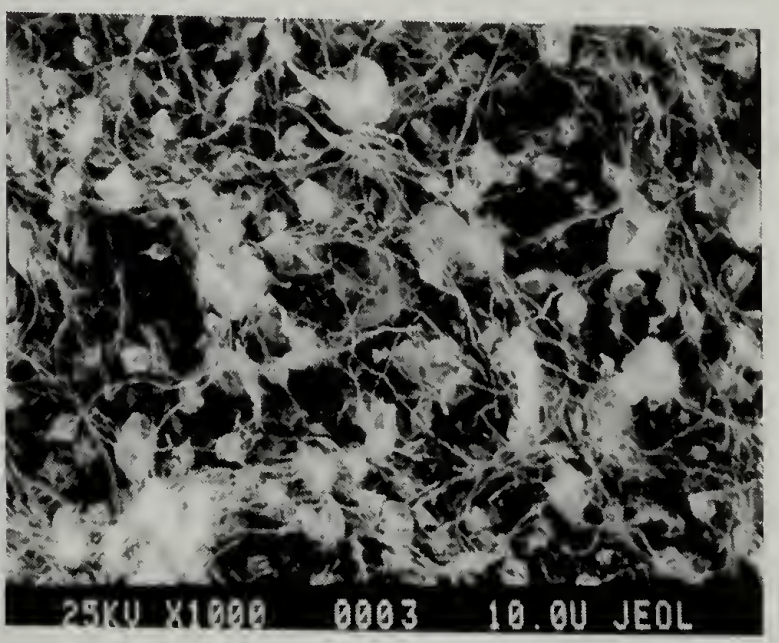

(b)

(b)

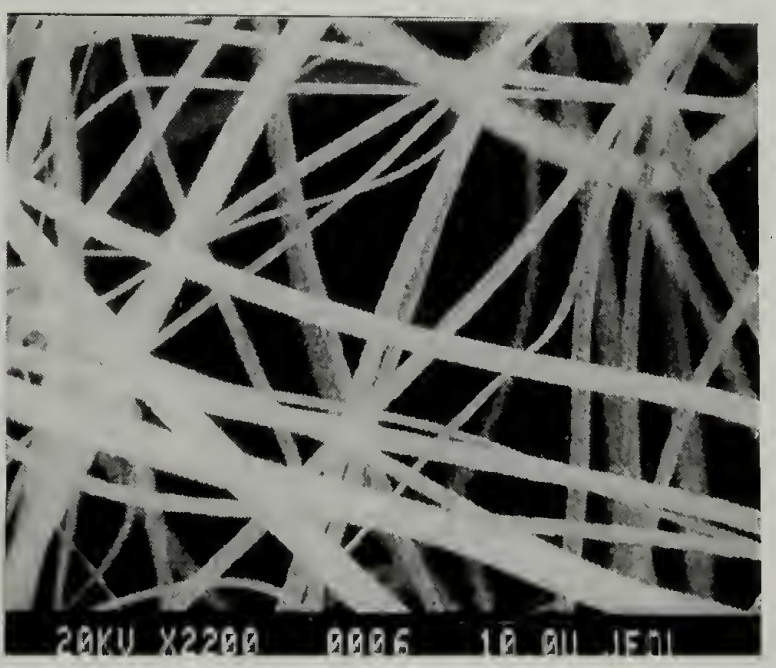

(d)

Figure 1.3 – Electrospun polystyrene: (a) 15% wt. in cyclohexanone; (b) 15% wt. in methyl ethyl ketone; (c) 15% wt. in THF/DMF (8:2); (d) 30% wt. in THF

The bead-on-string morphology has also been reported in the literature.[41-42] Examples from reference 41 are shown in Figure 1.4.

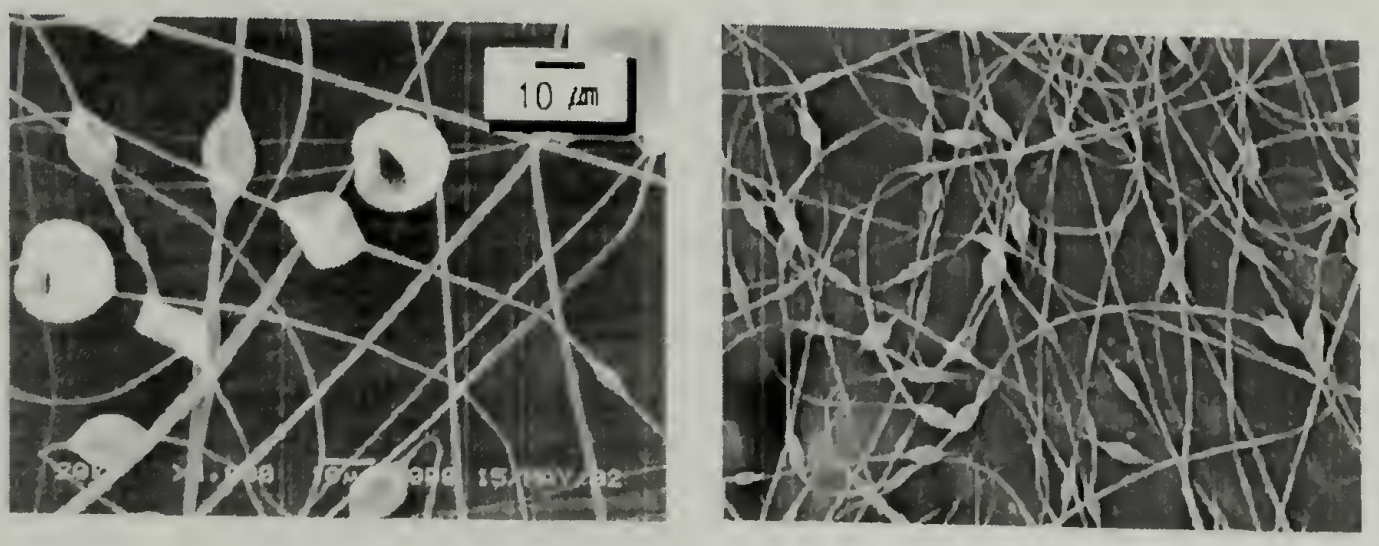

Figure 1.4 – Electrospun polystyrene (left) and poly(ethylene oxide) (right). (reproduced from reference 41)

A major limitation of the electrospinning process is low output. Typically, several hours are required to spin enough material to form a fibrous mat large and thick enough to obtain 5-10 standard size tensile test specimens. However, electrospun fiber mats of particular biocompatible polymers have been identified and studied for use in smaller scale applications as scaffolds for cell growth and tissue engineering. [43] Additionally, several patents have been issued for use of electrospun materials in biomedical applications such as fibrillar lining for prosthetic device such as an artificial internal organ,[44] synthetic blood vessel prostheses, [45] and synthetic vascular grafts.[46]

1.5 Applications

Potential applications for electrospun nonwoven mats include filtration media[47] and semi-permeable membranes. The transport properties of some electrospun polymers have been characterized with regard to breathability and air flow resistance and compared to commercial PTFE membrane laminates—Gore-Tex®—and other commercial membranes, films, and fabrics used in fabric laminate systems for military and sport clothing.[48] The transport properties of electrospun polyurethanes are shown to be comparable to commercial membranes, and have the advantage of being produced by the relatively simple electrospinning process. Transport properties of electrospun nylon fiber mats have also been reported.[49]

As filtration media, ceramic nanofiber mats are promising. To this end, organic/inorganic composite fibers are electrospun as precursors, and subsequently calcined, to form purely ceramic fiber mats of titania,[50] alumina-borate oxide,[51] vanadium pentoxide, zinc oxide,[52-53] lead zirconate titanate,[54] nickel ferrite,[55] Co_3O_4,[56] magnesium titanate[57] and copper oxide.[58] Typically, a soluble metal oxide precursor is dissolved in a common solvent with a high molecular weight poly (vinyl pyrollidone) and electrospun to form a mat of composite nanofibers. Subsequent calcination of the composite fibers results in degradation of the polymer, leaving pure crystalline metal oxide nanofibers. Morphology of the precursor fibers, resultant ceramic fibers, and effect of calcination time and temperature on final morphology has been studied and reported. Other potential applications of ceramic nanofiber mats are for high-

temperature insulation, catalyst support in high-temperature reactions, sensors, membrane-based separation or purification, and mechanical reinforcement.

The use of electrospun materials in practical applications including reinforcement, biomedical, and membrane applications requires some measure of control over the process in terms of fiber diameter, average pore size of electrospun mats, and fiber alignment. A model has been developed to address control of fiber diameter.[59] More numerous studies have focused on the alignment and controlled deposition of electrospun fibers. Collection of aligned fibers onto the edge of a rotating disk[60-61] and more conventionally onto a rotating drum[62-64] has been demonstrated. Analogous to the 1936 patent[6] which describes using external charged sources to increase the instability of the electrospinning jet, Deitzel and coworkers utilized an external charge to control the spinning jet by increasing the length of the stable spinning region and more precisely directing the deposition of fibers.[65] Patterned electrospun fiber mats have been prepared by varying the conductivity of the target substrate.[66-67] The controlled alignment of electrospun fibers is particularly important pertaining to their use in fiber-reinforced composites. For a unidirectional fiber-reinforced composite, the longitudinal modulus is directly proportional to the fiber aspect ratio, according to the Halpin-Tsai equations.[68] Aspect ratios for continuous nanofibers are orders of magnitude larger than for conventional fibers. Further, the longitudinal modulus, E_{11}, for a discontinuous unidirectional composite is always less that that for a continuous unidirectional composite. Based on a simple shear lag analysis, producing long continuous fibers is more desirable than relatively short fibers for maximizing composite tensile strength as well. The longer the

reinforcing fiber, the more stress is transferred to and carried by the fibers. This effect is further enhanced by the fact that the surface area to volume ratio for typical electrospun nanofibers is very large compared to conventional fibers, promoting more efficient load transfer from the matrix to the reinforcing fibers.

1.6 Motivation

The motivation for this research comes from the need to gain a fundamental understanding of the physical characteristics and mechanical behavior of electrospun materials. Further, modeling the mechanical behavior and properties will be useful as a predictive tool and necessary for the practical use of electrospun fibers and fiber mats. The relationship between bulk and electrospun material behavior will be influenced by changes in physical characteristics such as crystallinity and molecular orientation, as well as more subtle changes on the molecular and nanometer length scales.

1.7 Dissertation Overview

Chapter 2 presents and discusses the mechanical behavior of electrospun polyurethanes. The mechanical behavior of electrospun thermoplastic polyurethane elastomers is presented in the form of stress-strain data, and comparison of behavior between the bulk material and isotropic and aligned electrospun polyurethane fiber mats. The observed differences in mechanical response among the three morphologies are discussed.

Chapter 3 addresses a variety of models proposed to describe the mechanical behavior of electrospun fiber mats. The stress-strain behavior of an isotropic electrospun mat is modeled based on the stress-strain behavior for an aligned mat of the same electrospun material. Experimental evidence indicates that when strain is applied to an isotropic electrospun mat, fibers oriented at angles relative to the direction of applied strain rotate and subsequently bear load in the material as they are uniaxially deformed, while a certain population of fibers are oriented at angles such that they buckle as a result of the Poisson effect and contribute essentially nothing to the measured force in the material. The tensile strength of isotropic electrospun mats is related to the strength of the bulk material based on a simple density relationship. The tensile strength of the electrospun materials is modeled with the assumption that the void volume of the electrospun mat has an elastic modulus of zero and therefore carries no load in the material. Electrospun mats from two polyurethane systems, at several mat densities are tested and compared to the model. Finally, the elastic modulus of isotropic electrospun polyurethane fiber mats is compared to that of their aligned electrospun fiber analogs.

Chapter 4 presents a color change phenomenon for electrospun systems containing fillers of color. A color change from solution to electrospun fiber mat is observed for several polymer/solvent systems. Subsequently, heating the electrospun mats reverts the materials back to their original solution color. This is observed for both glassy and semicrystalline polymers, and the thermal color change occurs with the glass transition themperature (T_g) or crystalline melting temperature (T_m), respectively.

The phenomenon is shown to make material that can be used as a medium for creating images with local heating.

Chapter 5 presents observed melting behavior for the electrospun fibers of a family of linear aromatic polyesters—poly(ethylene terephthalate) (PET), poly(trimethylene terephthalate) (PTT) and poly(butylene terephthalate) (PBT). Melting behavior is studied by differential scanning calorimetry (DSC) and the electrospun materials are compared to the bulk starting materials (in pellet form) as well as cast samples from the same solutions from which fibers are electrospun. The melting behavior of the electrospun polymer analogs are explained based on studies in the literature that show similar melting behavior for those polymers crystallized from the melt at intermediate cooling rates.

Chapter 6 summerizes the thesis and presents ideas for future research in the field of electrospinning.

CHAPTER 2

MECHANICAL BEHAVIOR OF ELECTROSPUN POLYURETHANE

2.1 Introduction

Few studies in the literature address the mechanical properties of electrospun polymers. Typically, mechanical data is included as a minor part of a larger analysis and characterization of electrospun fiber morphology, size, etc. In two reported cases, electrospun homopolymers are characterized by conventional tensile tests and tensile properties such as elastic modulus, tensile strength, and elongation at break are reported.

Poly(glycolic acid), a biocompatible polymer of interest in the field of tissue engineering, was electrospun to form aligned, as well as randomly oriented, nonwoven fiber mats.[42] Aligned mats were tested in longitudinal and transverse directions, and elastic modulus and peak strains were reported for mats electrospun from a series of solutions differing in polymer concentration. Aligned mats consistently show higher modulus and lower peak strain values than both orthogonal tests and random mats across the solution concentration profile. The random mats and aligned mats tested transverse to the fiber direction have statistically similar values of strain at break.

The second case in which a homopolymer is electrospun and mechanical properties reported is for poly(trimethylene terephthalate) (PTT).[69] Stress-strain curves are presented for electrospun PTT fiber mats tested in the machine direction and transverse to the machine direction, although electron micrographs show little or no difference in the two directions in terms of a preferred fiber orientation. Moreover, the stress-strain curves are counter-intuitive, as the tensile properties observed for the

transverse direction are superior to tensile properties in the machine direction. Also lacking in the experimental description is the rotational velocity of the collecting drum.

Two-component polymer blends have also been electrospun from solution, and mechanical properties reported as a function of varying concentration of respective components.[70] An inherently stiff material, poly(vinyl chloride) (PVC) and an elastomeric material, polyurethane (PU), were electrospun as homopolymers and blends and tested as a function of varying PVC/PU concentrations. Expected results are presented in the form of stress-strain curves and tensile properties. Electrospun PVC has a lower tensile strength and strain to failure than electrospun PU. Electrospun PVC becomes stronger and breaks at higher strain with the addition of 25% and 50% PU to the electrospinning solution, respectively. At a weight ratio of 75/25 (PU/PVC) the tensile behavior and properties of the electrospun mat more closely resemble pure electrospun PU. The 50/50 (PU/PVC) electrospun mat has strength and failure strain intermediate to the pure electrospun PVC and PU, respectively. The observed tensile behavior is attributed in part to the number of junction points in the electrospun mats. The pure PVC contains relatively few junction points, and therefore fibers slip past one another with minimal friction, resulting in the mat having poor tensile properties. As the PU concentration is increased, the 25/75 (PU/PVC) and 50/50 blend have elastic regions followed by plastic deformation, attributed to the material being held together by elastic PU junction points, followed by breakage of junction points and subsequent plastic deformation of the PVC fibers. The elastic modulus of the blends increases to a peak at 50/50 weight fraction. At 75/25 (PU/PVC), behavior is elastic, dominated by the electrospun PU behavior. The existence and quality of fiber junction points is a

relavent issue that will be discussed further in the analysis of electrospun polyurethanes presented in this chapter. Lacking, in the study of Lee and coworkers however, is a discussion of how these electrospun blends behave relative to conventional solution cast or melt-processed blends.

So-called nanocomposite electrospun fibers have also been prepared and studied by adding single-walled carbon nanotubes (SWNT) to electrospinning solutions of polystyrene and polyurethane.[71] Mechanical properties were reported for electrospun polyurethanes with as-prepared and ester-functionalized SWNTs. For both varieties of SWNT, improvements were observed in tensile strength and tensile modulus for the nanotube-filled electrospun fiber mats. The greatest improvements of strength and modulus were seen with the ester-functionalized SWNTs, while elongation at break remained essentially unchanged for both filled systems compared to the unfilled electrospun polyurethane.

Mechanical properties have also been determined for biocompatible and biodegradable polymers. Tensile strength and behavior of electrospun tissue engineering scaffold material, poly (glycolide-co-lactide), was determined as a function of in vitro degradation time[72] and compared to the tensile properties of cartilage and skin.[73]

In a single report, electrospun fibers were incorporated into epoxy and rubbery matrices, respectively.[74] Poly(benzimidazole) (PBI) nanofibers were incorporated into two different matrix materials and tensile and fracture properties for the composites were determined. In one composite, PBI nanofibers were electrospun onto a rotating target to prepare aligned fiber mats, which were subsequently layed up unidirectionally

into 8 to 32 ply laminate specimens impregnated with a thermoset epoxy resin and cured. The composite was tested in three-point bend tests to determine the elastic modulus, E, and in a double torsion test to determine fracture toughness (k_c) and fracture energy (G_c). Both fracture properties were found to increase with increasing fiber content. Electrospun PBI filled composites were approximately equal in fracture toughness and fracture energy to composites prepared with conventional PBI fibers. Another set of tests were performed on SBR rubber filled with chopped electrospun PBI nanofibers. Rubber composites were characterized by tensile and tear tests, and compared to rubber specimens filled with carbon black. Nanofiber filled rubber specimens were found to have higher elastic modulus by approximately one order of magnitude over the carbon black filled and unfilled systems, approximately equal tensile strength to carbon black filled and unfilled, and approximately equal tear strength to the carbon black filled system. Both nanofiber and carbon black filled composites had twice the tear strength of the unfilled rubber.

In the reported studies that deal with mechanical characterization of electrospun polymers, blends, and composites, very little discussion is included that addresses the mechanical response of the electrospun material relative to the mechanical response of the bulk material from which the spinning solutions and fiber mats are prepared. In fact, no point of reference is given in references 64 or 65 as to the mechanical properties of commercially produced fibers of PTT or PGA used for tissue scaffolds, respectively. In no study is molecular orientation, crystallization, or the effect of fiber morphology and size directly related to, or characterized in terms of influencing ultimate properties of the electrospun materials.

Molecular orientation in individual fibers will have an effect on the properties of electrospun fiber mats, even if the mats are collected in the form of isotropic nonwoven mats. In addition to molecular orientation as an element to producing strong fibers, the extremely fine diameter fibers produced by electrospinning are one of the key elements of why the process is of such interest to researchers and why the materials produced by electrospinning have such intriguing applications potential.

The relatively few reported data on the mechanical properties of electrospun fiber mats and composites incorporating electrospun nanofibers leaves much to be explored and learned from the behavior of electrospun materials. The many potential applications reviewed above require a thorough understanding of the fundamental mechanical properties and behavior of electrospun materials, as well as predictive and modeling tools to provide knowledge about materials for applications based on the behavior of the starting materials. A basic qualitative understanding of the critical parameters of electrospinning and how they influence fiber structure and morphology—both on the molecular and macroscopic level—are necessary to relate the observed properties of the electrospun fiber mats. The novelty of the electrospinning process also allows us to study how the extreme size scale—tens to hundreds of nanometers—and rapidity of fiber formation associated with the process affect characteristic morphological attributes such as crystallinity and molecular orientation, and how these changes affect subsequent processability of particular electrospun polymer fibers.

2.2 Mechanical Characterization

Based on theoretical calculations pertaining to the elongation of the electrospinning jet and the trajectory of the jet as it travels from the tip of a nozzle to a target, and from limited data in the literature, the possibility exists for the production of polymer nanofibers with molecular orientation by electrospinning. The mechanical properties of electrospun nanofibers will be determined. There are obvious practical issues in attempting to characterize nanoscale fibers by conventional methods. Alternatively, a polymer/solvent system will be identified that can be electrospun to make nonwoven fiber mats which can be tested by standard methods. Single-fiber properties may be estimated from these measurements.

If molecular orientation is induced by electrospinning, the response of an aligned fiber mat is expected to be correspondingly higher in tensile modulus and strength than the bulk material. Even for a randomly oriented nonwoven fiber mat, which is globally isotropic, the stress-strain response will reflect the molecular orientation within individual fibers. For applications such as filtration and separation membranes, the properties of the nonwoven fiber mat are critical. It is expected that the nature of the junction points among fibers in the mat will also have a distinct influence on the mechanical behavior of the electrospun fiber mat. Good adhesion among electrospun fibers in a mat should result in a material with structural integrity, while a mat with little or no adhesion among fibers will be relatively weak. However, electrospun polymers that exhibit inherently weak fiber-fiber adhesion, may be post-treated to enhance fiber junction points and increase material strength. As illustrated in the work of Fennessey and Farris [62], electrospun fiber yarns of substantial tensile strength and modulus are

produced by inducing a twist in electrospun fiber mats to increases the friction among electrospun fibers. Alternatively, heat and pressure can be used to effectively "sinter" electrospun fibers, as shown later in this chapter.

In this chapter, mechanical behavior of electrospun polyurethane fiber mats is presented. The mechanical stress-strain response of bulk and electrospun forms of commercial thermoplastic polyurethanes (TPU) are compared. One system, Pellethane® 2103-80AE is studied in depth, while another, Pellethane® 2363-55DE, is included to illustrate different mechanical behavior. Differences in their response to applied strain are observed and described through morphological and spectroscopic analysis.

2.3 Experimental

2.3.1 Materials

N,N-dimethyl formamide (DMF) and tetrahydrofuran (THF) were purchased from the Aldrich Chemical Company, and used as received to prepare electrospinning solutions. Pellethane® 2103-80AE, Pellethane® 2363-55DE, and Pellethane® 2103-70A are polyether-based thermoplastic polyurethanes, received in pellet form from Dow Chemical Company. A description of the chemistry of the polyurethanes is included in Appendix A. Electrospinning solutions were prepared by dissolving the polymer in solvent at room temperature and stirring vigorously for at least 24 hours prior to electrospinning. Solution cast films were prepared by casting polymer solution in a petri dish and allowed to dry at room temperature and atmospheric pressure for at least

one week prior to mechanical testing. Other bulk films were prepared by thermally processing plaques from polymer pellets.

List of electrospun and bulk samples:

1. Electrospun Pellethane® 2103-80AE: 7% wt. solution of polymer in DMF/THF (3:1) (for electrospinning isotropic mats); 12% wt. polymer in DMF (for eleetrospinning aligned fiber mats)
2. Electrospun Pellethane® 2363-55DE: 7% wt. solution of polymer in DMF/THF
3. Solution cast films: 6% wt. polymer in THF; cast in glass pctri dish and dried in a fume hood at room temperature and atmospheric pressure for at least one week
4. Melt pressed film: eompression molded at 240° C, with applied pressure of approximately 900 psi for 10 minutes; followed by eooling with eireulating cold water in press while maintaining pressure until platens cooled to 35° C.

2.3.2 Electrospinning process

Isotropie fiber mats for tensile tests and infrared spectroscopy experiments were prepared by electrospinning polyurethane solutions from a 1 mL glass Pastuer pipette with a capillary tip of approximately 1 millimeter inner diameter. A stainless steel electrode is submerged in the polymer solution and the solution is spun onto a grounded aluminum foil target. Oriented elcetrospun samples were prepared by spinning the PU solution from a 10 ml syringe with metal capillary tip of 1mm inner diameter and a backpressure applied with a syringe pump set at a volume flow rate of 0.040 ml/minute. An alligator style clip eharges the syringe tip, and solution is electrospun onto a rotating

stainless steel drum. The electric field for electrospinning is supplied by a high voltage power supply (Gamma High Voltage Research) capable of generating voltages up to 20 kilovolts. A schematic diagram of the electrospinning process is shown in Chapter 1 (Figure 1.1); a schematic diagram of the modified electrospinning process for collecting aligned fiber mats is shown in Figure 2.1.

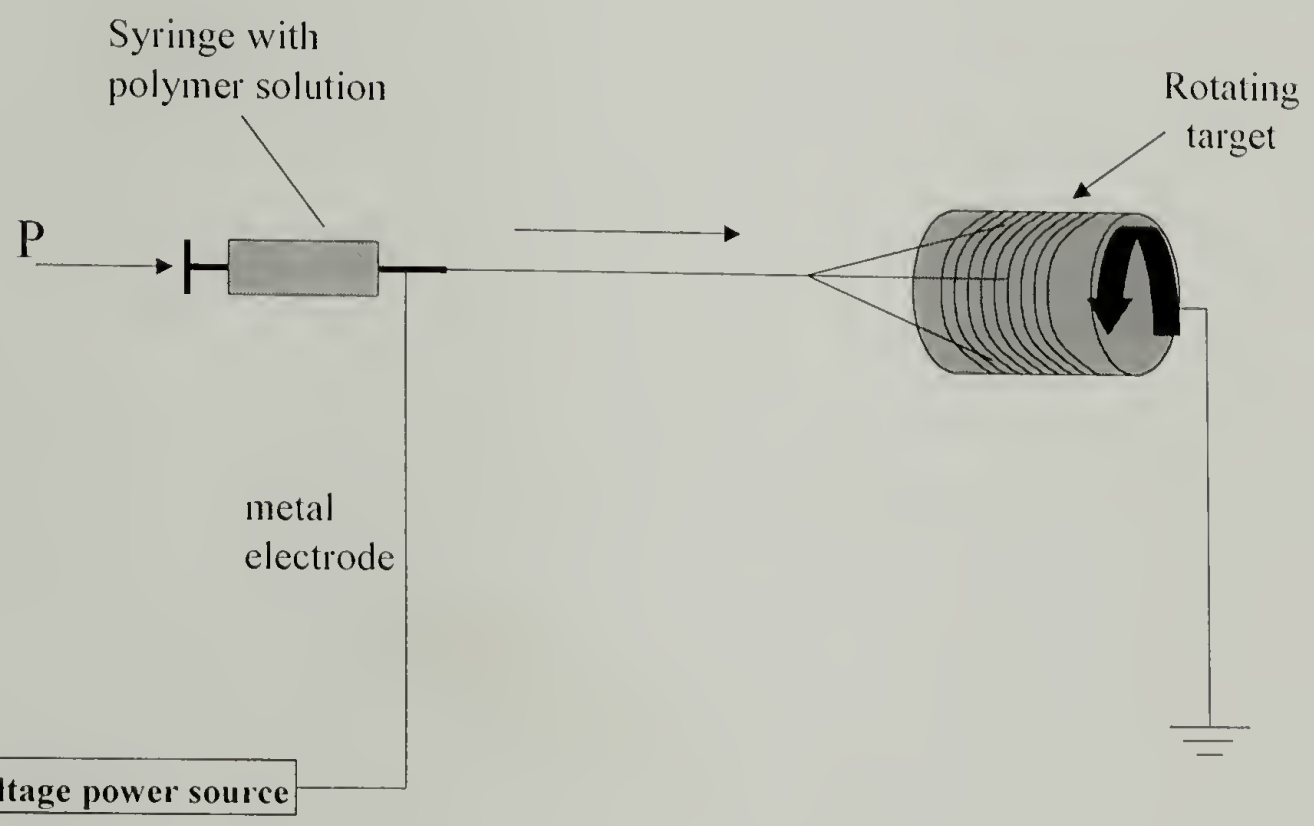

Figure 2.1 – Schematic diagram of modified electrospinning for collection of aligned fiber mat.

2.3.3 Mechanical behavior

The tensile behavior of the electrospun and bulk PU was tested on an Instron 5500R with a crosshead speed of 10 mm/minute ($\approx 0.5\ min^{-1}$ strain rate) at room temperature. ASTM 1708D dumbbell-shaped tensile specimens were prepared by die-

cutting samples from isotropic electrospun polyurethane mats, as well as from compression molded and solution cast films.

2.3.4 Morphology

The morphology of the electrospun fiber mats was studied by high resolution scanning electron microscopy (FE-SEM, JEOL 6320 Field Emission Scanning Electron Microscope) operating at an accelerating voltage of 5 kV. All specimens were sputter-coated with gold prior to SEM.

2.3.5 Infrared dichroism

Infrared spectroscopy dichroism studies were carried out using a BIO-RAD FT-IR spectrometer at a rate of 300 scans per specimen. Dichroic ratios were computed using peak values obtained from IR spectra of aligned electrospun samples with linearly polarized light parallel and perpendicular to the principle direction of fiber alignment.

2.4 Results and Discussion

2.4.1 Processing bulk film samples

The electrospun materials studied in this chapter are spun from solution. Commercially, these thermoplastic polyurethanes are typically melt-processed to make products. It should be noted that the mechanical response of melt-processed samples differs from samples cast from solution. Figure 2.2 shows the stress-strain curves for melt and solution cast bulk film samples. From this point forward, all comparisons of

mechanical behavior and properties are between the respective electrospun materials and their solution cast bulk analogs.

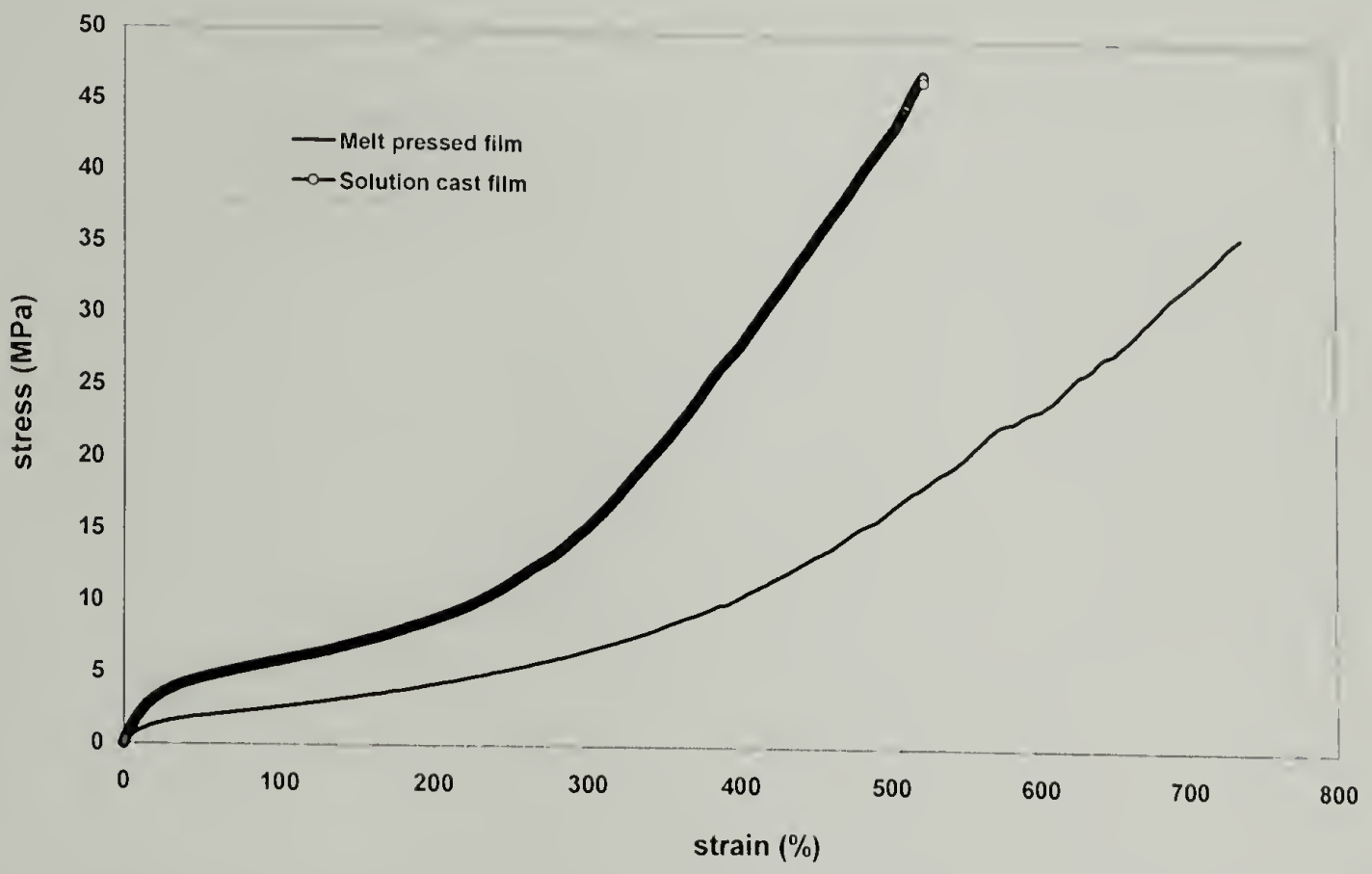

Figure 2.2 – Stress-strain curves for melt and solution processed Pellethane® 2103-80AE films.

2.4.2 Morphology of electrospun Pellethane® 2103-80AE

Images of electrospun Pellethane® 2103-80AE from field emission scanning electron microscopy (SEM) are shown in Figure 2.3. The morphology of the fibers is cylindrical and they have average diameters of approximately 500 nanometers. The electrospun mats are fibrous and highly porous yet have structural integrity and macroscopically appear as films. The fibers are held together by the adhesion to one another at multiple bonding sights throughout the mats. Figure 2.4 illustrates the inter-

fiber adhesion that leads to the film-like character and structural integrity of the electrospun fiber mats.

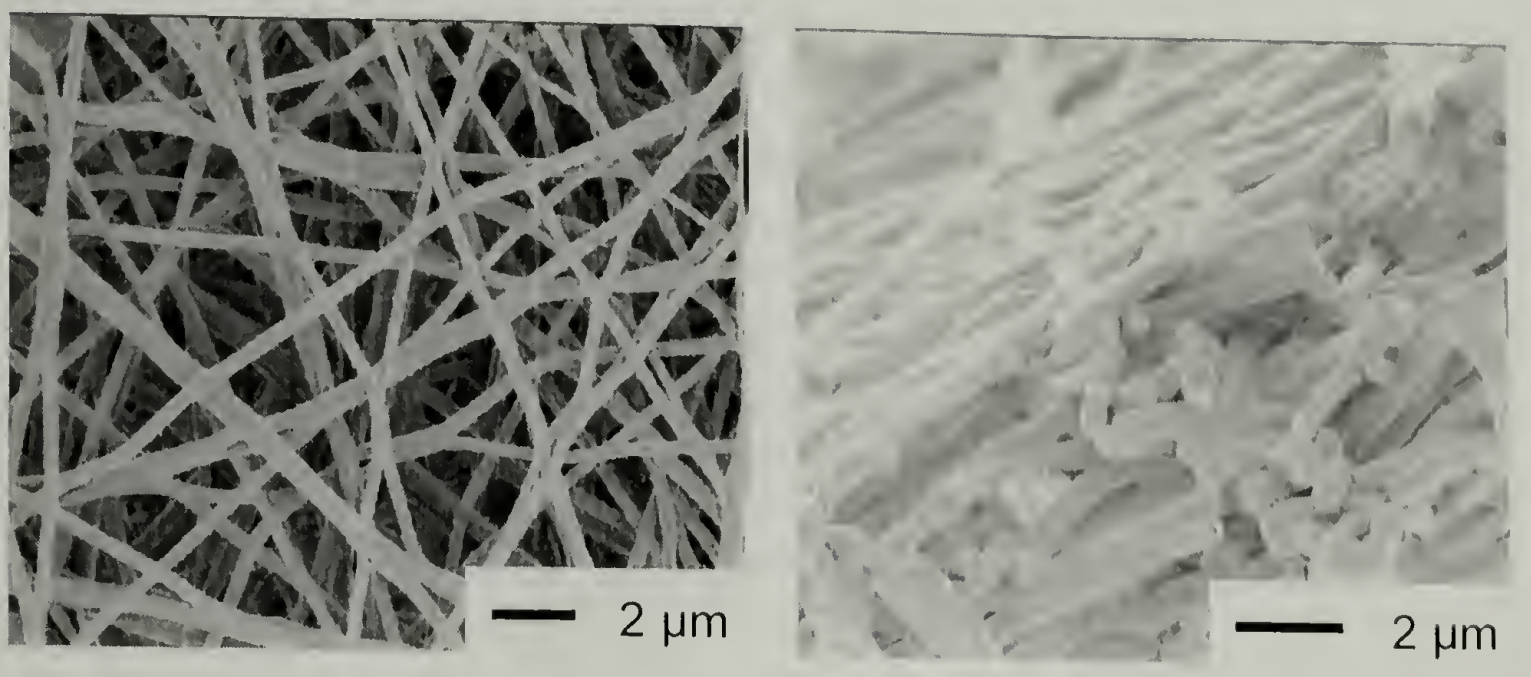

Figure 2.3 – Electrospun Pellethane® 2103-80AE: (a) top view of fiber mat; (b) cross-section of cryo-fractured fiber mat.

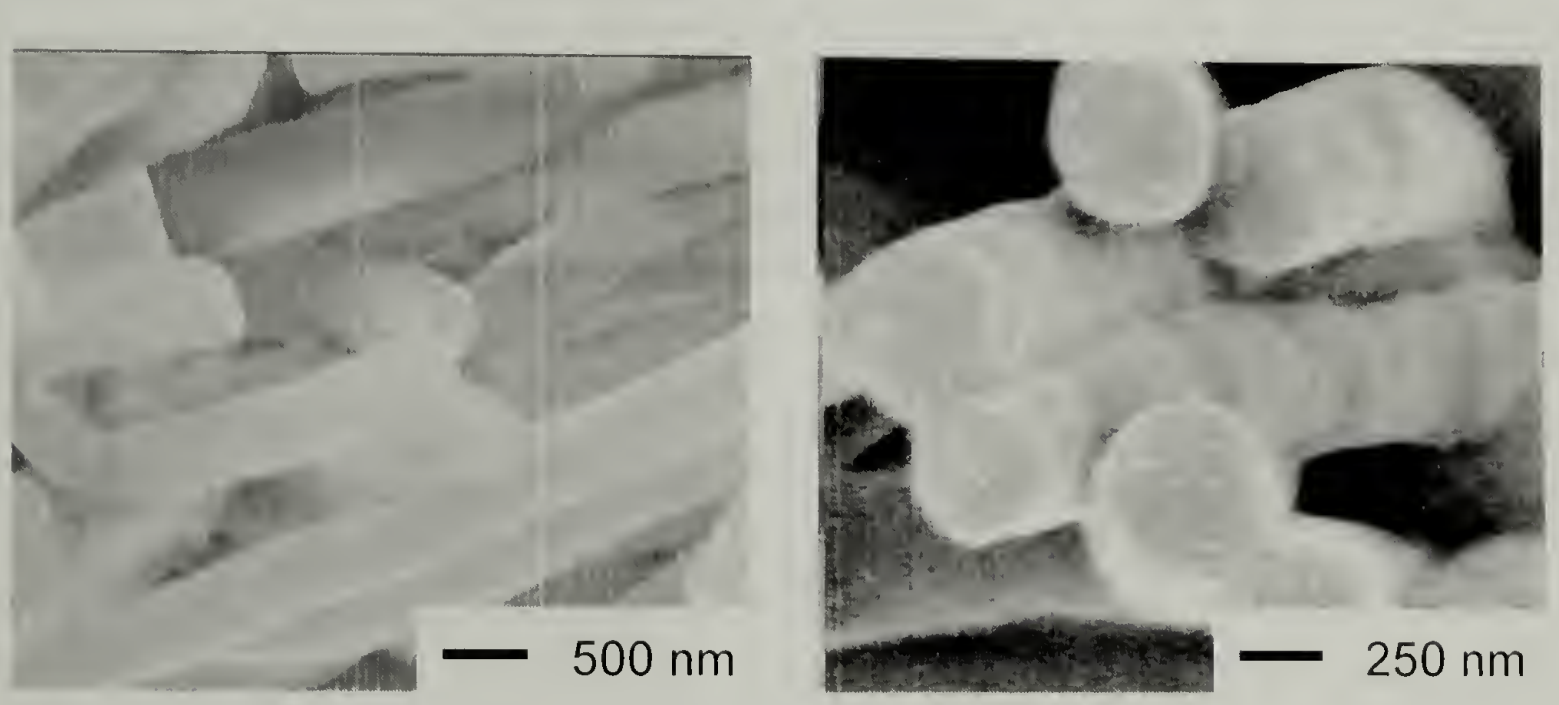

Figure 2.4 – Electrospun Pellethane® 2103-80AE: cross-section of cryo-fractured fibers.

2.4.3 Stress-strain behavior of electrospun Pellethane® 2103-80AE

Uniaxial tensile tests show the stress-strain behavior of electrospun Pellethane® 2103-80AE to be distinctly different from the bulk. Figure 2.5 is a plot comparing the engineering stress-strain curves from electrospun and bulk Pellethane® 2103-80AE. It should be noted that the stress-strain curves presented in this chapter for all electrospun materials have been adjusted to account for the difference in density between the electrospun and bulk analogs of each material, respectively. In the case of Pellethane® 2103-80AE electrospun from 7% wt. solution in DMF/THF (3:1), the density of the electrospun mat is approximately 0.30 g/cm^3. The density of the bulk material is 1.13 g/cm^3. The experimental stress strain curve of the electrospun material is adjusted by a density correction factor of 0.30 divided by 1.13, equal to 0.256. The bulk material response is typical of elastomeric materials—sigmoidal in shape, with strain hardening of the material resulting from molecular orientation at high degrees of strain. Qualitatively, the electrospun mat is also elastomeric in nature, but the shape of the stress-strain curve of the electrospun material is characteristically different. The stress-strain curve for the electrospun material has an initially low slope, with an inflection point at approximately 30-40% strain.

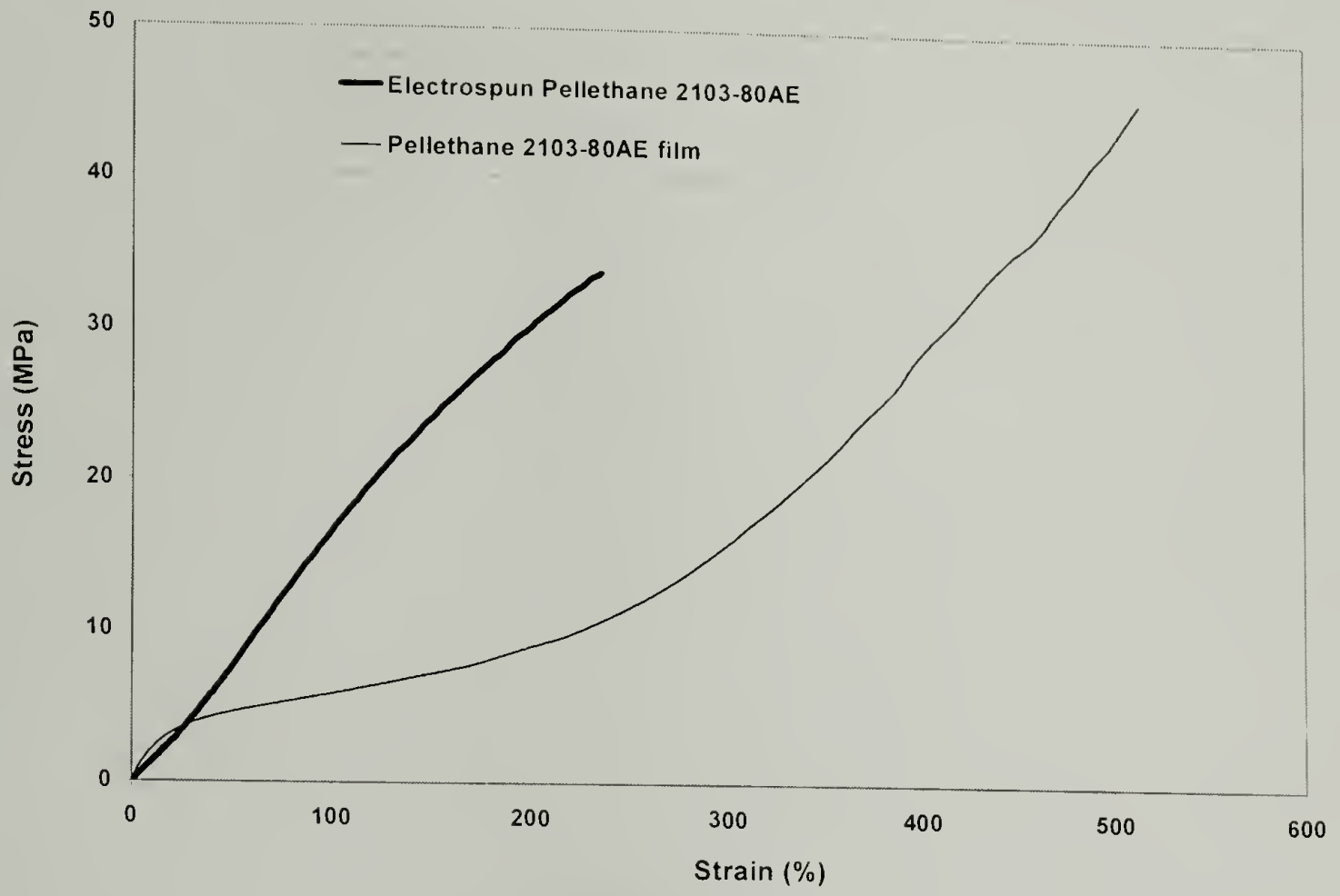

Figure 2.5 – Stress-strain curves for electrospun and bulk Pellethane® 2103-80AE.

From 30-40% strain until the break strain, the electrospun material has significantly higher stress than the bulk. However, the ultimate tensile strength of the electrospun material is less than the bulk, and the elongation at break is significantly lower than for the bulk material. Most importantly, the shape of the stress-strain curve of the electrospun material is fundamentally different than the response of the bulk.

2.4.4 Tensile Strength

Tensile strength is a flaw-limited material measure. Although the stress in the electrospun material is higher than in the bulk at equivalent strain until break of the electrospun material, the ultimate tensile strength of the bulk is higher than the electrospun mat. This is potentially due to flaws in the electrospun material that apparently result from the electrospinning process. Figure 2.6 shows several images of electrospun Pellethane® 2103-80AE prior to mechanical testing, illustrating the existence of cracks in the electrospun fibers. These images are representative of the material as a whole, indicating that the cracks are widespread and act as points of stress concentration throughout the material.

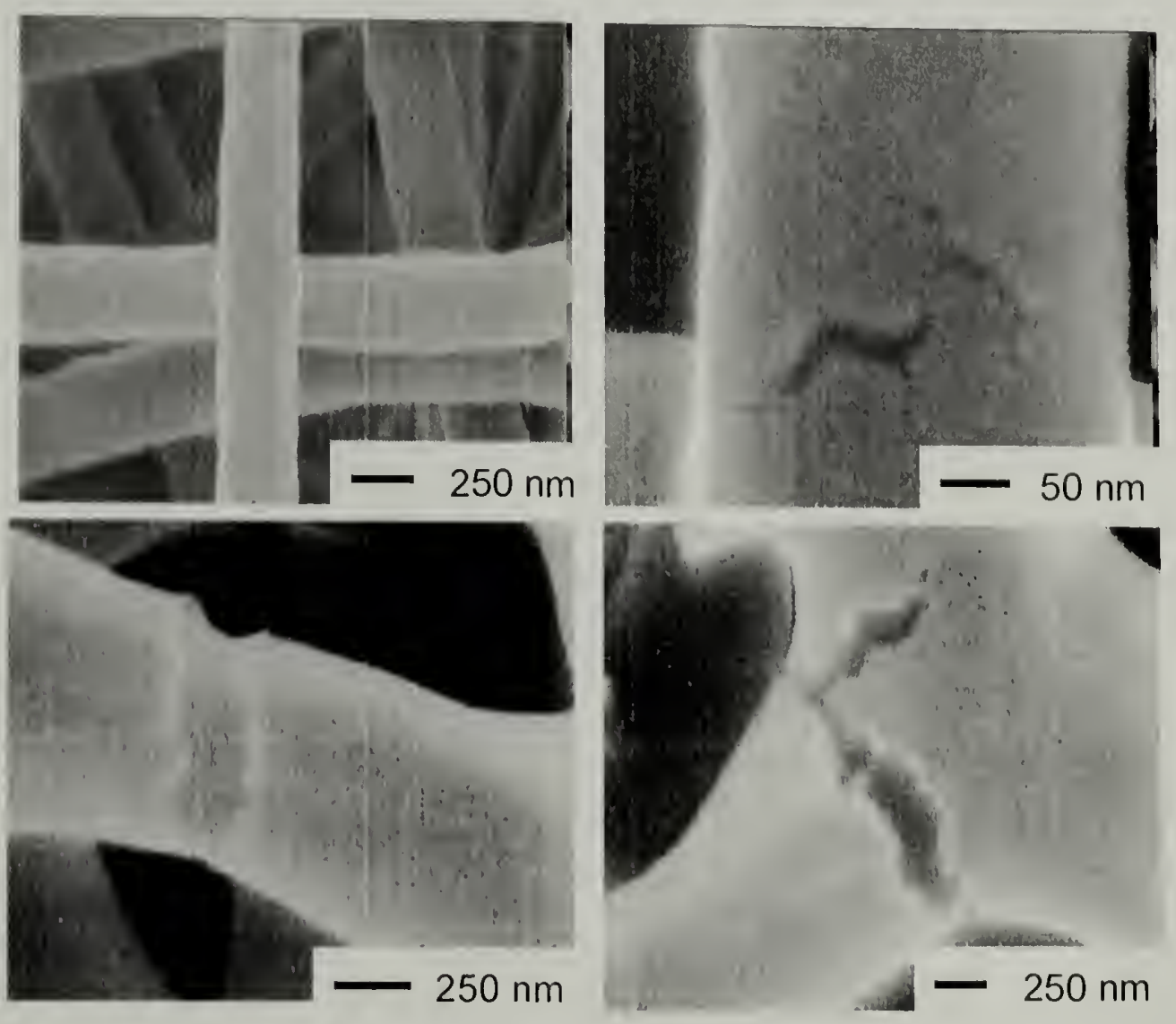

Figure 2.6 – Cracks in electrospun Pellethane® 2103-80AE fibers.

The existence of these cracks in the electrospun fibers also, in part, accounts for the significantly reduced strain at break for the electrospun material, relative to the bulk. Another example of the influence of pre-existing cracks in electrospun fiber mats is illustrated in another thermoplastic polyurethane system, Pellethane® 2363-55DE. Figure 2.7 illustrates the prolific existence of surface cracks in electrospun Pellethane® 2363-55DE fibers.

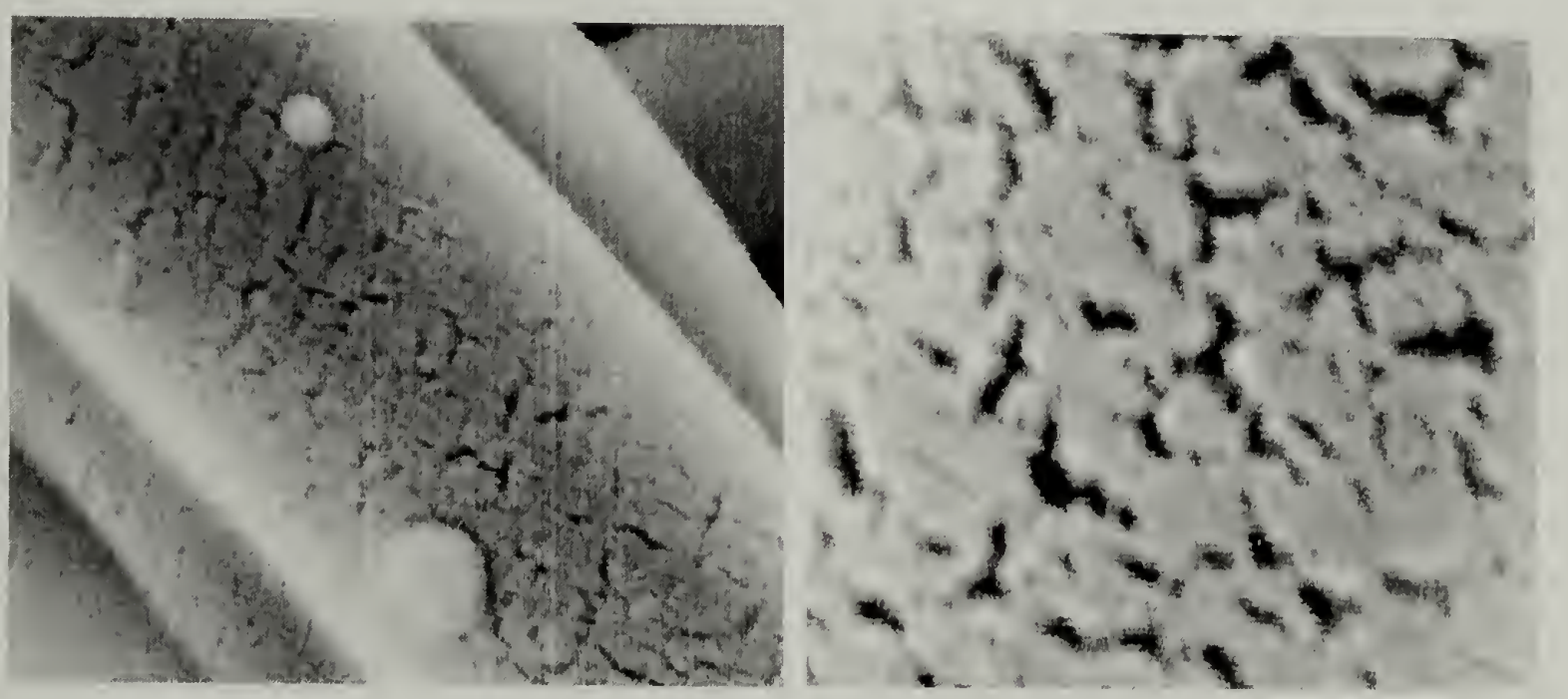

Figure 2.7 – Cracks in electrospun Pellethane® 2363-55DE.

The surface cracks in this system appear to be more widespread that those seen in the Pellethane® 2103-80AE electrospun system, and the effect on tensile behavior is reflected in the stress-strain curve of electrospun Pellethane® 2363-55DE, shown in Figure 2.8. The rise in stress of the electrospun material is not as significantly higher

relative to the bulk analog, as in the previous system, and the ultimate tensile strength of the electrospun Pellethane® 2363-55DE is approximately 60% of the tensile strength of the bulk. The tensile strength of electrospun Pellethane® 2103-80AE is approximately 75% of the bulk. The decreased tensile properties of the electrospun Pellethane® 2363-55DE relative to the bulk material can be attributed to the higher degree of cracking experienced by the electrospun fibers, and not to decreased inter-fiber adhesion. As illustrated in Figure 2.9, the inter-fiber adhesion among electrospun fibers of Pellethane® 2363-55DE appear to be at least as good, if not better, than the electrospun Pellethane® 2103-80AE fibers.

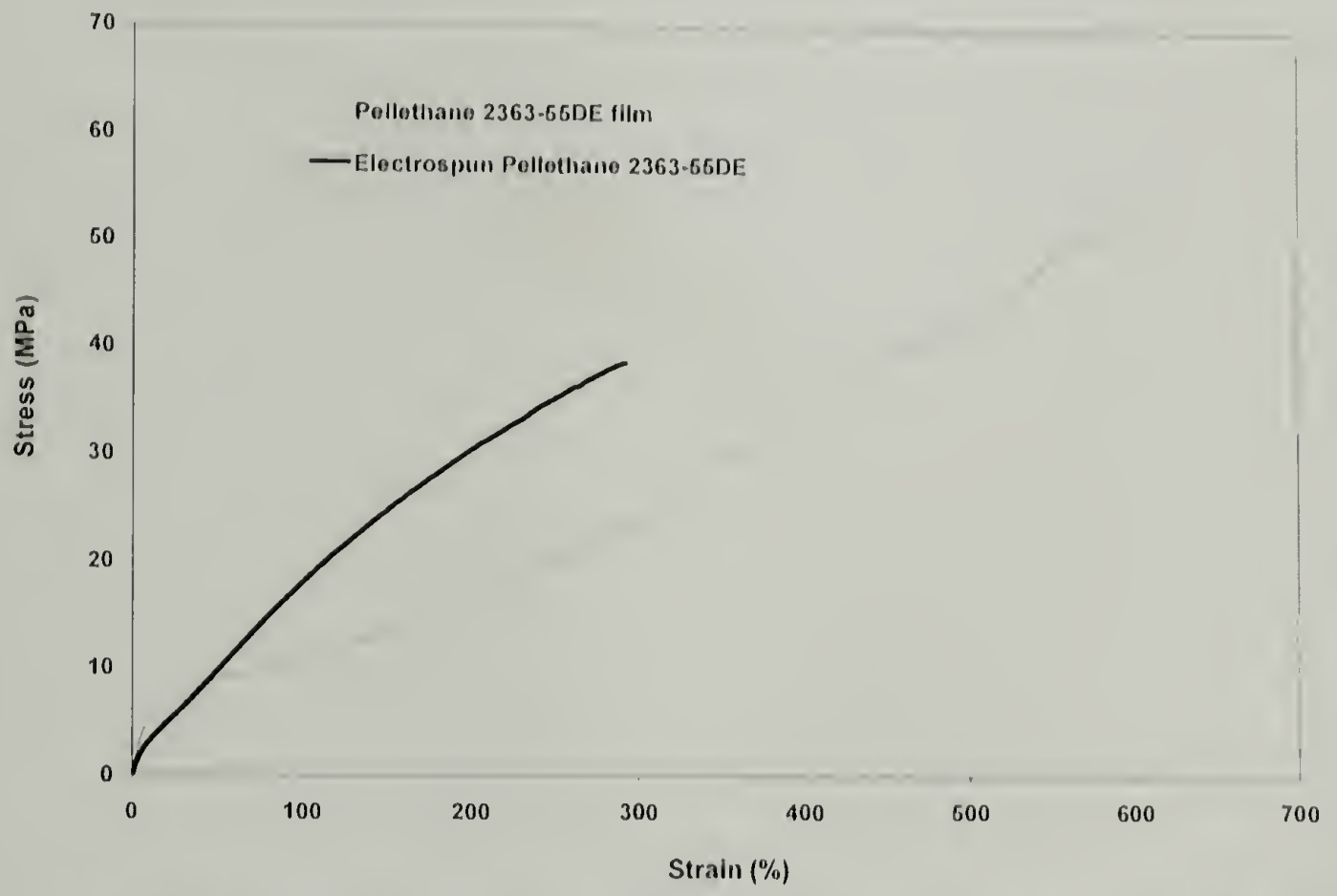

Figure 2.8 – Stress-strain curves for bulk and electrospun Pellethane® 2363-55DE.

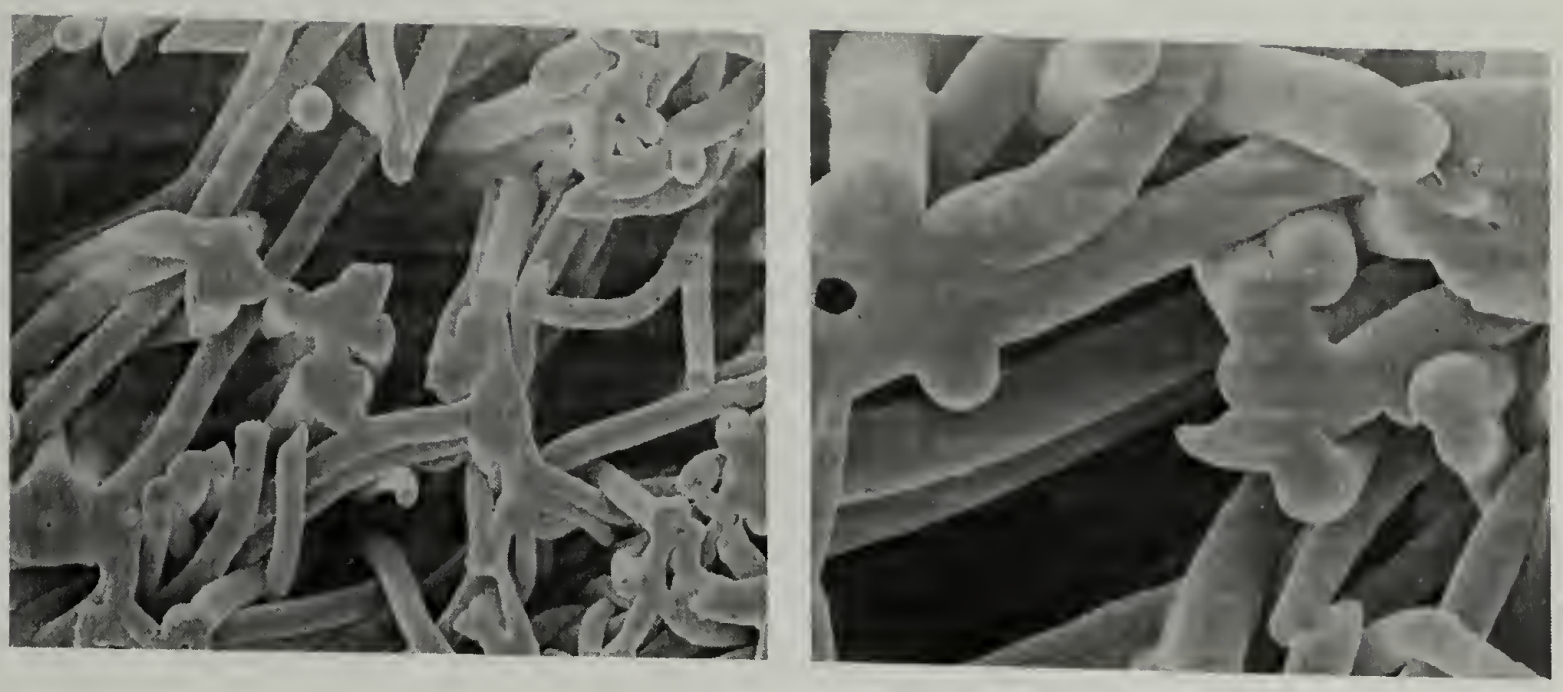

Figure 2.9 – Cross-section view of fractured electrospun Pellethane® 2363-55DE.

2.4.5 Stress-strain response

When strain is applied to the electrospun mat, fibers oriented in the direction of the applied strain are considered to be stretched uniaxially, while fibers oriented at some angle relative the principal strain direction experience first rotation, followed by uniaxial strain. As mentioned previously, Pellethane® 2103-80AE electrospun from 7% solution in DMF/THF (3:1) has a density of approximately one-third that of the bulk. Low density and random fiber orientation are factors that explain the relatively low stress in the electrospun material from 0-50% strain. As the strain in the electrospun mat increases and fibers are oriented into the direction of applied strain, the ratio of fibers stretched to fibers rotated increases, and the stress in the electrospun mat increases. In fact, from approximately 60% strain until break, the stress in the electrospun material increases more rapidly and is higher than the stress in the bulk. Strain-induced alignment of the electrospun mat is illustrated in Figure 2.10 and 2.11.

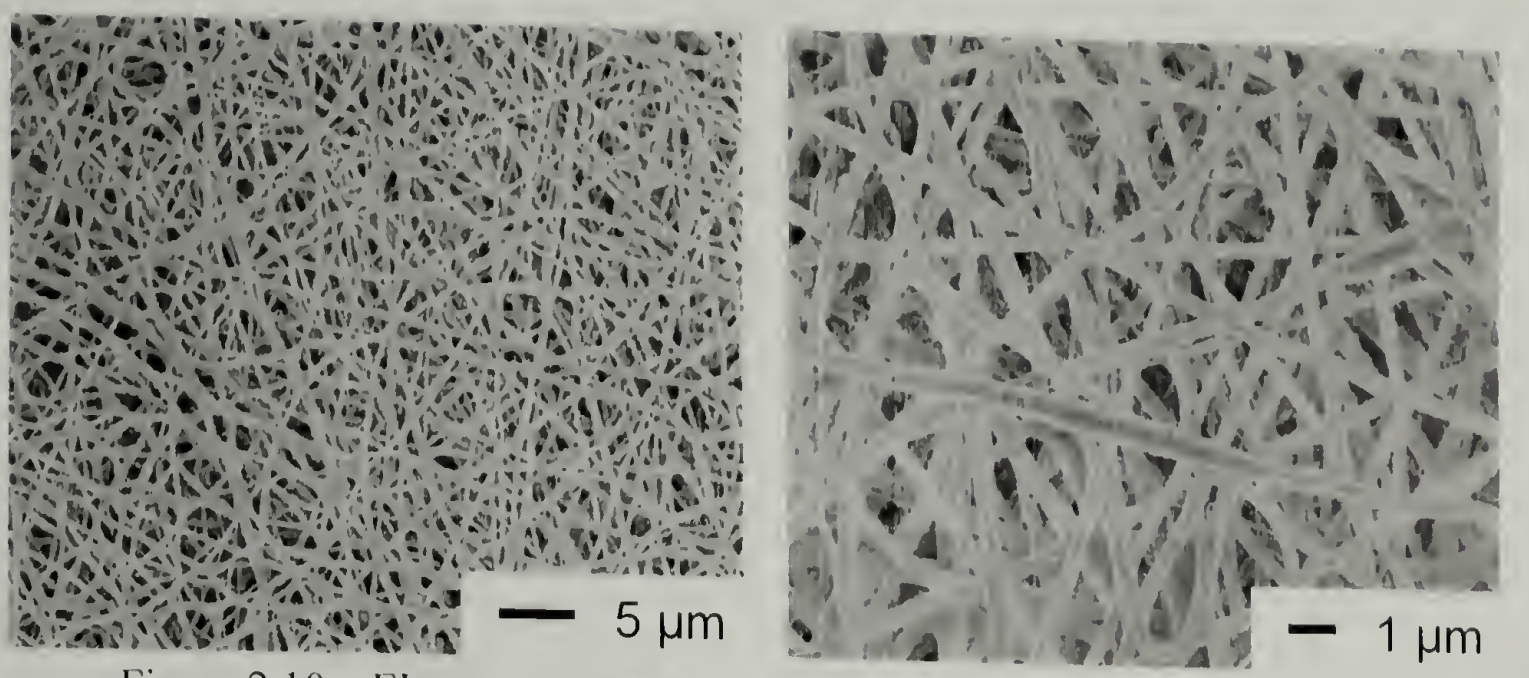

Figure 2.10 – Electrospun Pellethane® 2103-80Ae at 0% strain.

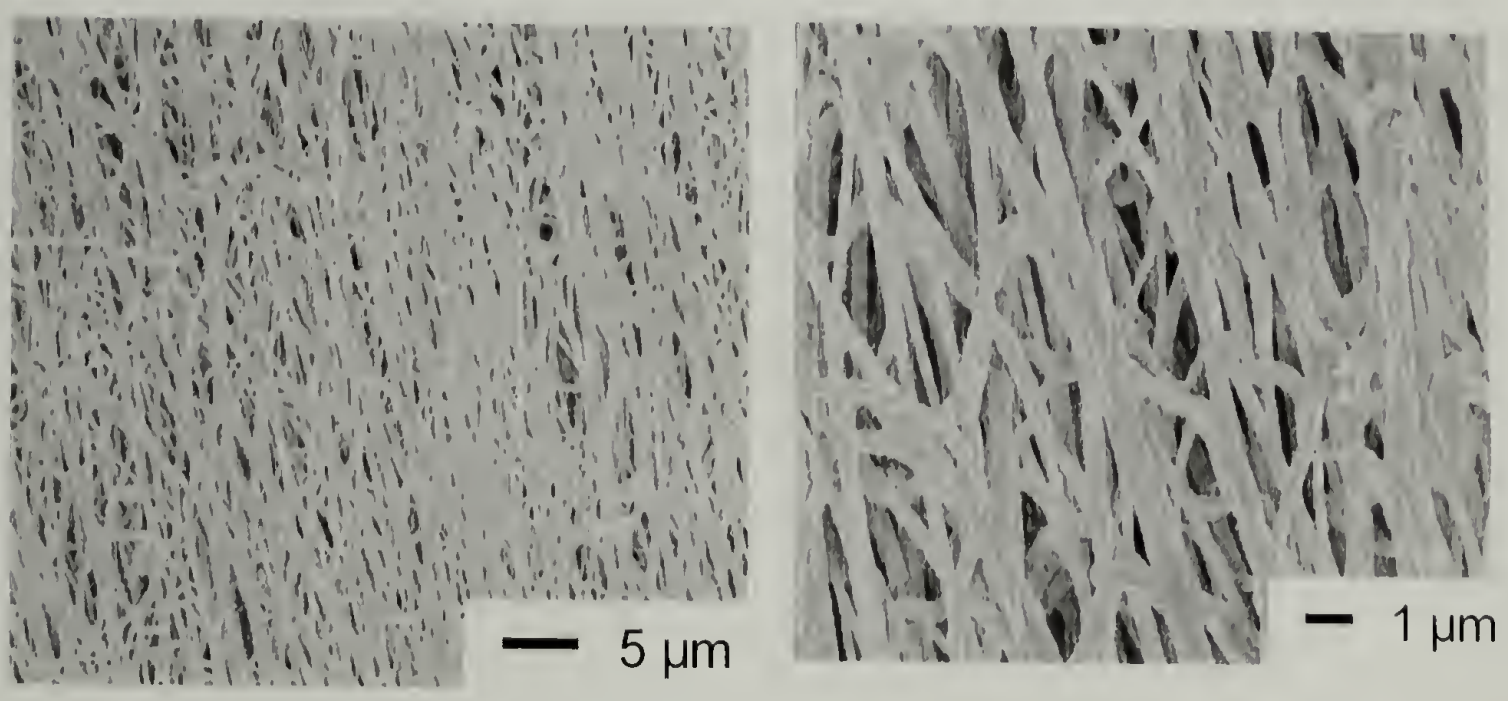

Figure 2.11 – Electrospun Pellethane® 2103-80AE at 75% strain.

At equal amounts of strain, the electrospun material maintains a higher stress until failure at approximately 300% strain. This seemingly premature failure is another difference between the two stress-strain curves, as the bulk PU has an ultimate strain to

failure of over 700% strain. Reasons for low failure strain were discussed previously. The fundamental differences observed in the stress-strain behavior of the two forms of the PU may be explained by comparing morphology and molecular orientation in each.

2.5 Morphological characterization

To determine if molecular scale morphology changes result from electrospinning, and if they have an effect on the mechanical response of the electrospun polyurethane, crystallinity was determined by wide angle x-ray diffraction (WAXD) and differential scanning calorimetry (DSC). Molecular orientation in electrospun fibers was determined qualitatively by polarized optical microscopy, and quantitatively by infrared (IR) dichroism.

DSC thermograms of both bulk and electrospun Pellethane® 2103-80AE are shown in Figure 2.12. No melting endotherms or other thermal transitions are present in the heating scans of either material that would indicate crystalline morphology.

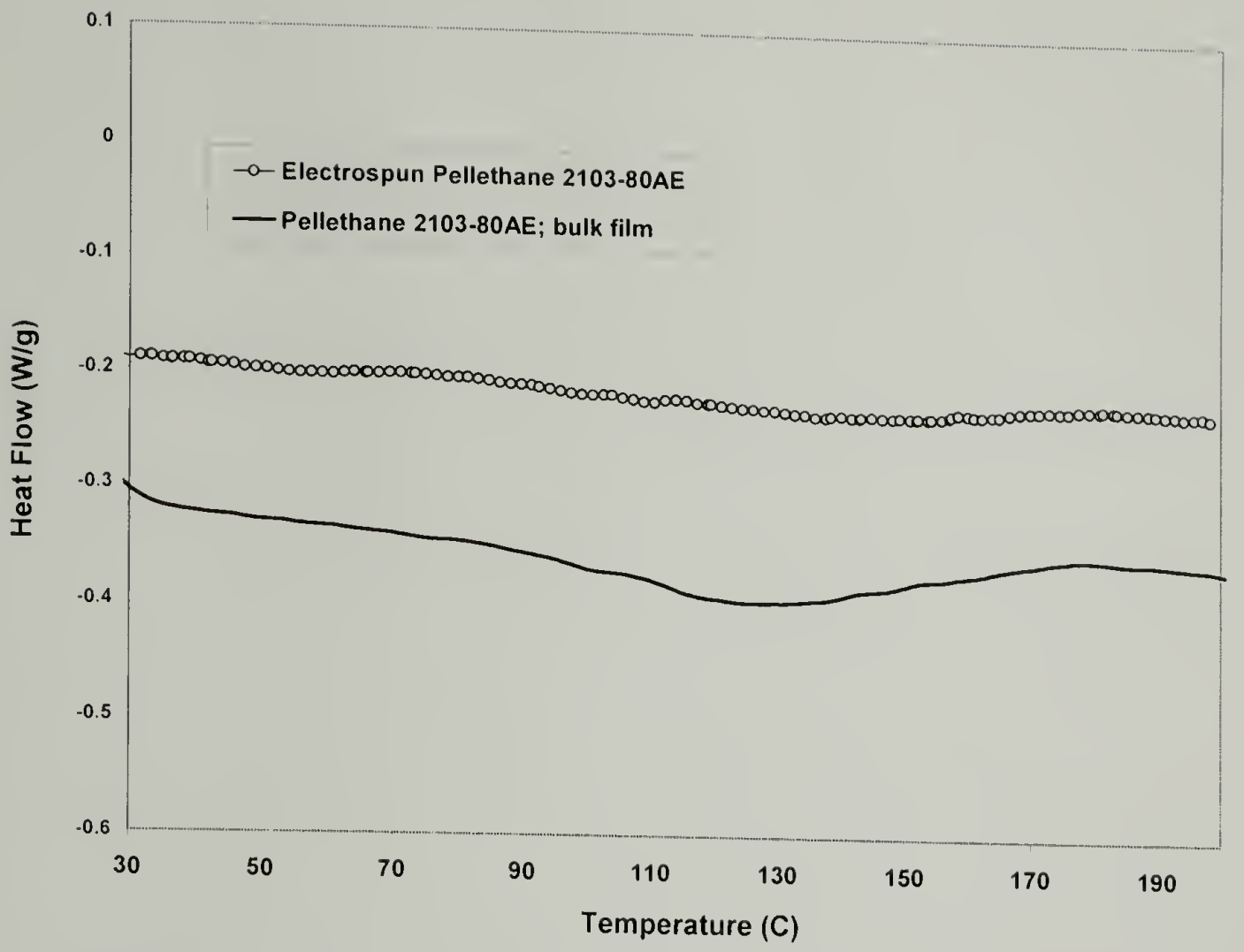

Figure 2.12 – DSC heating scans for bulk and electrospun Pellethane® 2103-80AE.

Wide angle x-ray diffractograms for both materials are shown in Figure 2.13, and corroborate the DSC data indicating no crystallinity in either material. The single broad peak for bulk and electrospun forms are indicative of amorphous materials.

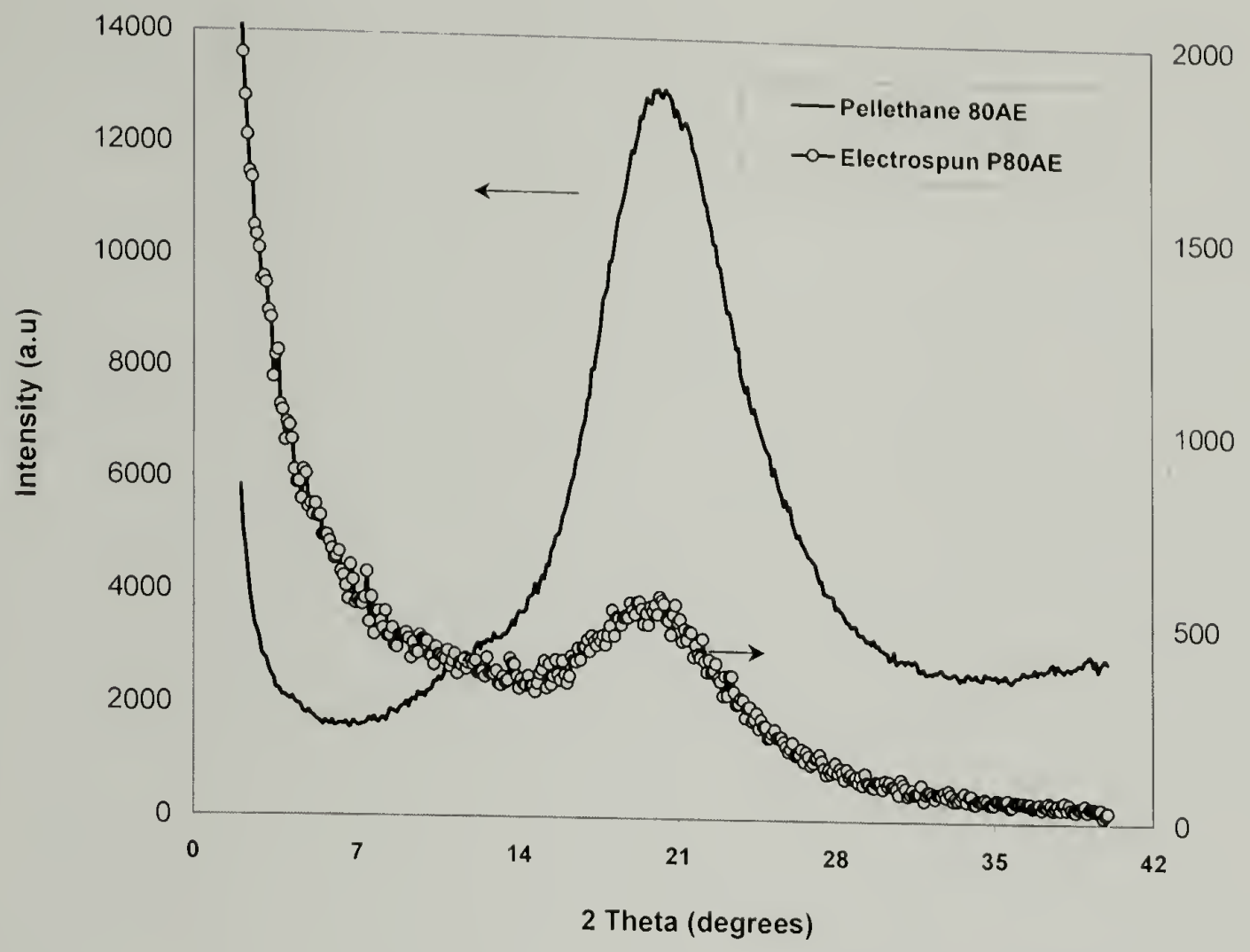

Figure 2.13 – WAXD of bulk and electrospun Pellethane® 2103-80AE.

The absence of crystallinity in this particular thermoplastic polyurethane is to be expected based on the chemistry of the material. The hard segment content for Pellethane® 2103-80AE, as determined by NMR, is approximately 9% by weight. Similar polyether-based segmented polyurethane systems with slightly higher hard segment content—approximately 15% by weight—were studied by Bonart and coworkers[75] who reported that in WAXD, no hard segment interferences of any kind were observed, and the diisocyanate blocks are dispersed in a matrix of soft segments.

2.6 Infrared dichroism

The strain applied to the electrospun mat serves to orient both the fibers and the molecules within the fibers. Molecular orientation also occurs in the bulk material when a strain is applied. Strain-induced molecular orientation is illustrated in the stress-strain curve of the bulk material at high degrees of strain. While the electrospun mat is globally isotropic, the individual fibers comprising the mat have a slight degree of molecular orientation prior to stretching. Qualitatively, molecular orientation in the electrospun fibers is evidenced by polarized light microscopy. Images of individual electrospun Pellethane® 2103-80AE fibers under polarized and unpolarized light are shown in Figure 2.14.

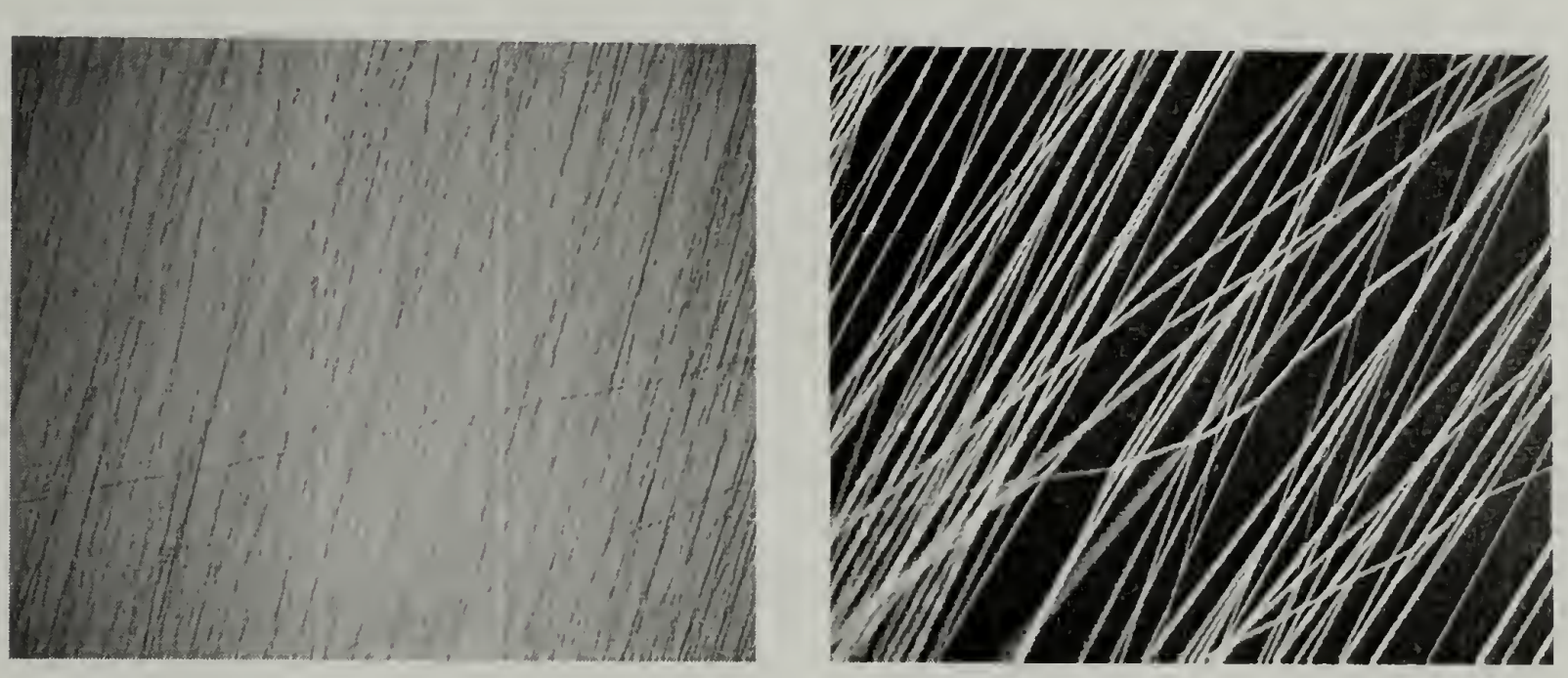

Figure 2.14 – Electrospun Pellethane® 2103-80AE fibers (100X magnification): (a) unpolarized light; (b) crossed polars.

Quantitatively, the molecular orientation in electrospun fibers is studied by polarized IR spectroscopy. To isolate the effect of molecular orientation in the electrospun fibers, a unidirectional aligned fiber mat is prepared by electrospinning

Pellethane® 2103-80AE solution onto a rotating mandrel. Solution concentration for electrospinning aligned fiber mats was altered slightly to optimize fiber morphology. As seen in Figure 2.15, electrospining the 7% Pellethane® 2103-80AE solution from the syringe onto a rotating drum results in a mat that has aligned fibers, but also has the bead-on-string morphology discussed previously.

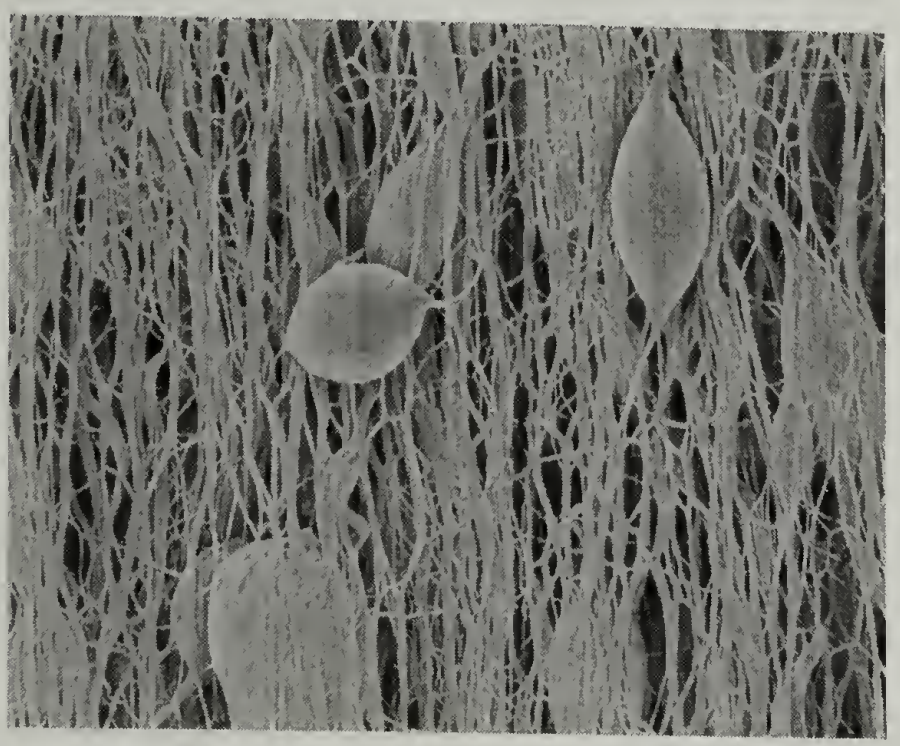

Figure 2.15 – Electrospun Pellethane® 2103-80AE: from 7% wt. in DMF/THF (3:1) onto a rotating target.

To produce an aligned fiber mat free of bead defects, and with fiber morphology similar to those achieved for the isotropic fiber mats, the spinning solution concentration was increased to 12% by weight and DMF used as the single solvent. The fiber morphologies achieved with the more concentrated spinning solution are illustrated in micrographs in Figures 2.16-18.

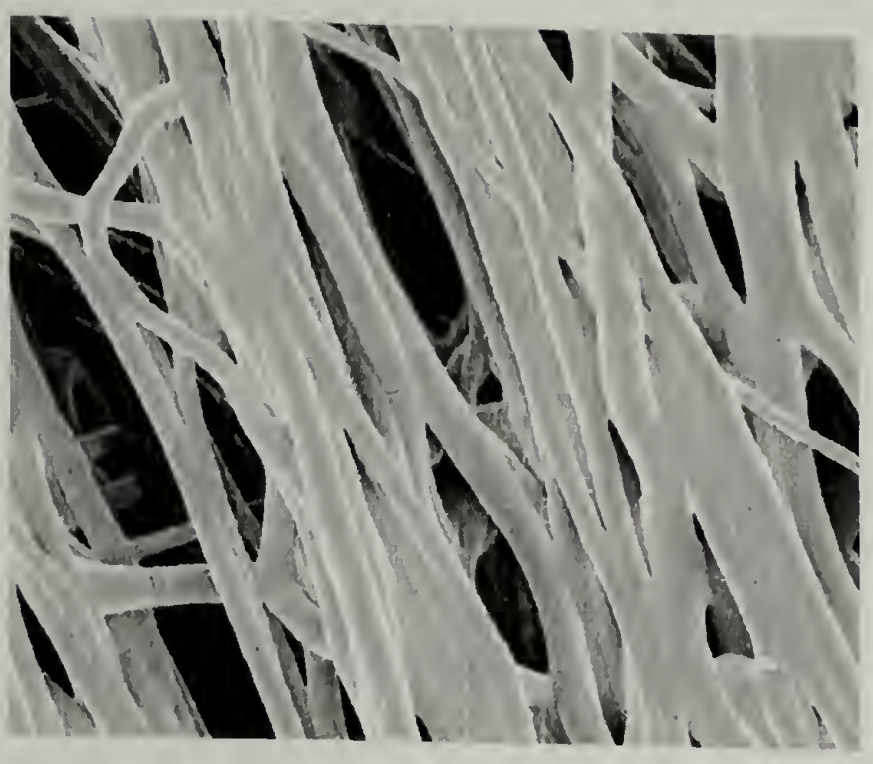

Figure 2.16 – Electrospun Pellethane® 2103-80AE: collected onto a target rotating at 6.14 m/s.

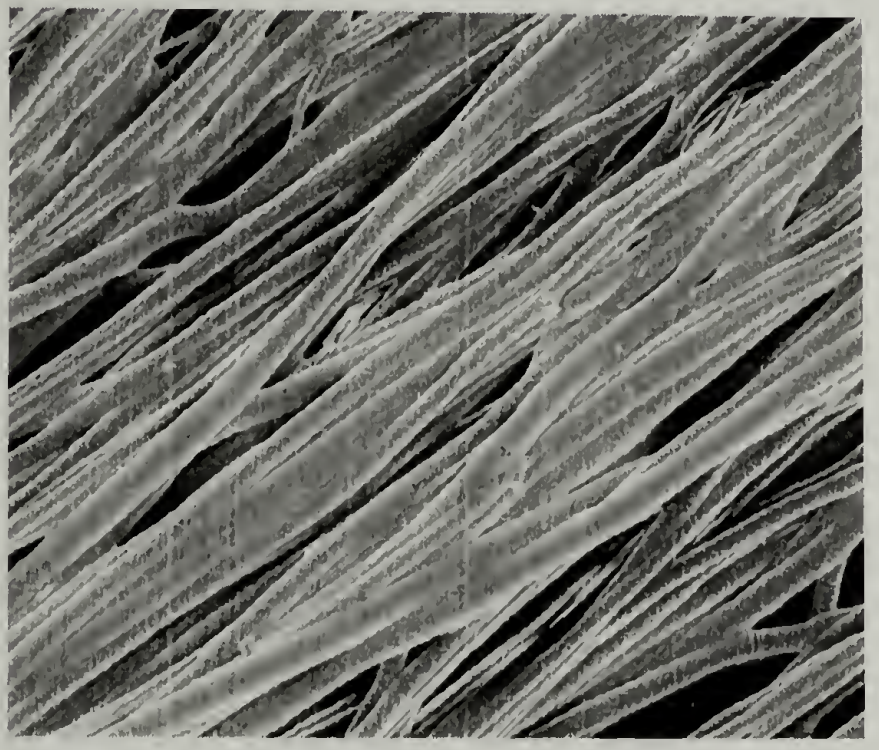

Figure 2.17 – Electrospun Pellethane® 2103-80AE: collected onto a target rotating at 8.61 m/s.

Figure 2.18 – Electrospun Pellethane® 2103-80AE; collected onto a target rotating at 9.84 m/s.

The above images also illustrate the observed similarities among the aligned fiber mats collected onto the rotating target at a variety of rotational speeds. Qualitatively, the fiber alignment appears very much the same for all three collection speeds. The difference in molecular orientation among the three collection speeds will be shown in dichroism results. Although the alignment of electrospun fibers is not perfect, it is sufficient to study the molecular orientation in the fibers. Because of this imperfect alignment of electrospun fibers, the orientation functions ultimately computed for the electrospun mats will be relatively conservative values.

An orientation function is calculated by analyzing the N-H stretching peak at 3320 cm^{-1} as described by Cooper et al.[76] This stretching vibration is located in the urethane linkage, and characterizes the orientation of the hard domains in the polyurethane. Assuming that the molecules in the electrospun fibers are not perfectly oriented, they will have an average angle with the fiber direction, θ. The average angle, θ, and the fraction of perfectly oriented molecules are related by the following equation

$$f = [3\langle\cos^2\theta\rangle - 1] / 2 \qquad 2.1$$

called Herman's orientation function.[77] Theoretically, the value of f can range from one, for perfectly oriented molecules, to zero for an isotropic material. If molecular orientation is perfectly orthogonal ($\theta = 90^\circ$) to the fiber direction, f is equal to $-\frac{1}{2}$. An orientation function can also be calculated using the dichroic ratios from IR absorption. The dichroic ratio for a particular absorption band is defined by

$$D = A_{\parallel} / A_{\perp} \qquad 2.2$$

where $A_{\parallel}$ and $A_{\perp}$ represent the peak absorbance of infrared radiation polarized parallel and perpendicular to the fiber direction, respectively. The orientation function is then defined by

$$f = [(D_0 + 2)/(D_0 - 1)][(D - 1)/(D + 2)] \qquad 2.3$$

in which D_0 is the dichroic ratio for perfect alignment. It is related to the transition moment direction (of a particular vibration) α by the expression

$$D_0 = 2 \cot^2 \alpha \qquad 2.4$$

According to Fraser[78], the N-H vibration lies essentially in the NH bond direction, which is 90° relative to the main chain direction (fiber direction), and $\alpha = 90^\circ$ is a

reasonable value. If molecular orientation exists in the fibers, there will be greater absorption when light is polarized perpendicular to the principle fiber direction than for parallel-polarized light. The absolute value of the orientation function is not of primary concern. More important is the relative value of *f* for the oriented electrospun fibers compared to the bulk. Simply, a degree of molecular orientation in the electrospun fibers, that does not exist in the bulk, may account for the higher stress in the electrospun material relative to the bulk, between 60% strain to break of the electrospun mat.

Figures 2.19-2.21 are IR absorption spectra for each of the aligned fiber mats prepared at different rotational collection speeds.

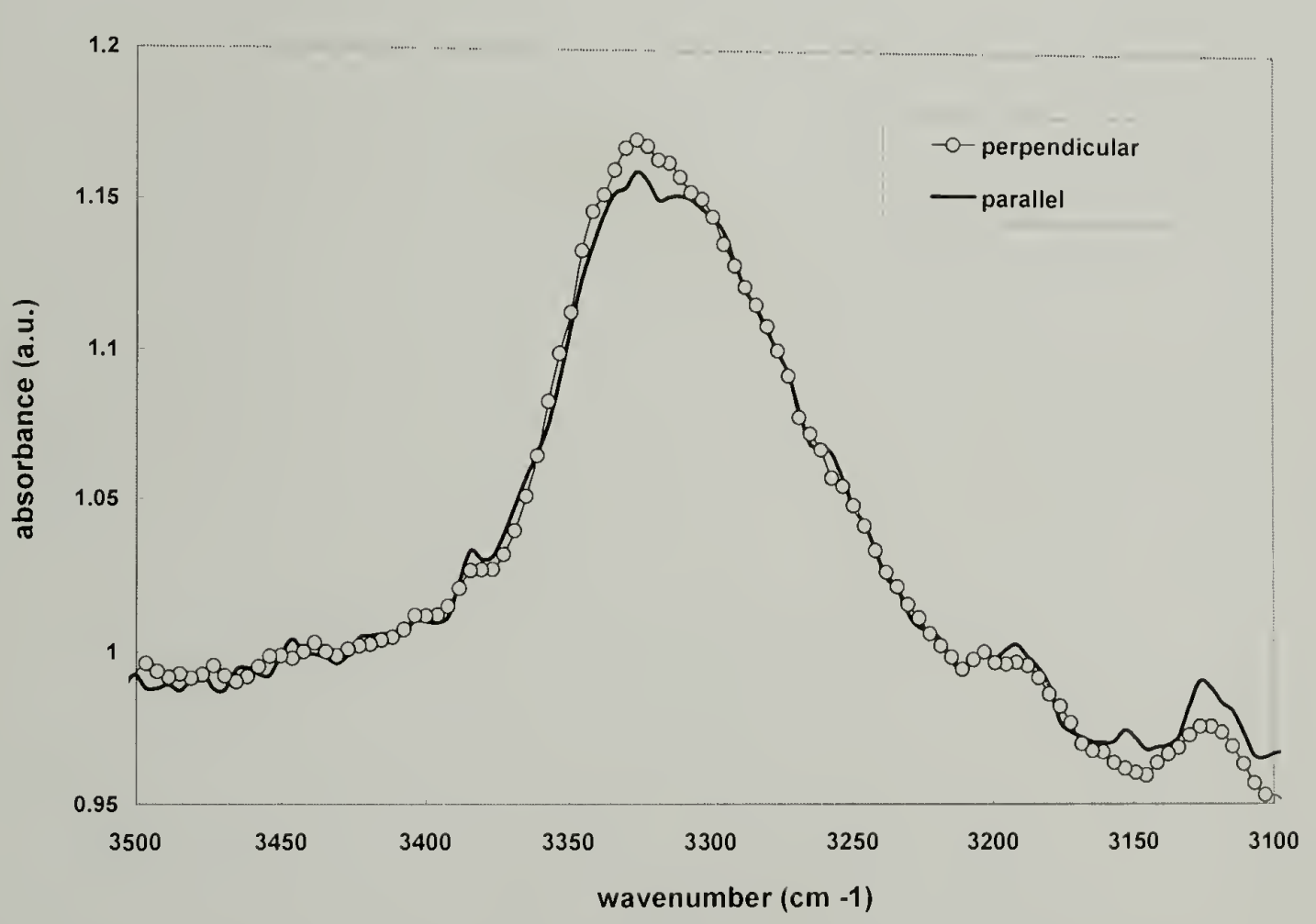

Figure 2.19 – IR spectra for electrospun fiber mat collected at 6.14 m/s.

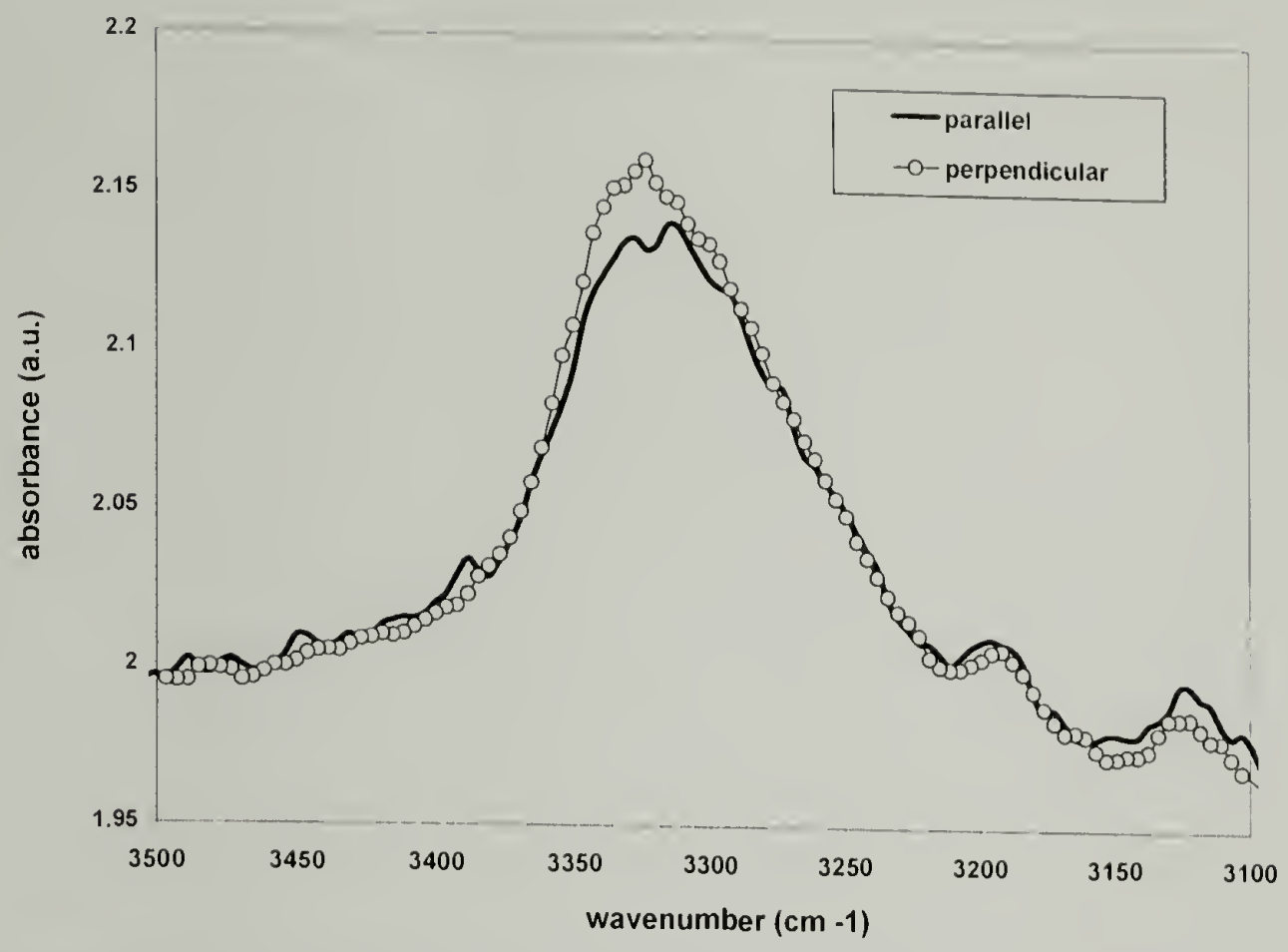

Figure 2.20 – IR spectra for electrospun fiber mat collected at 8.61 m/s.

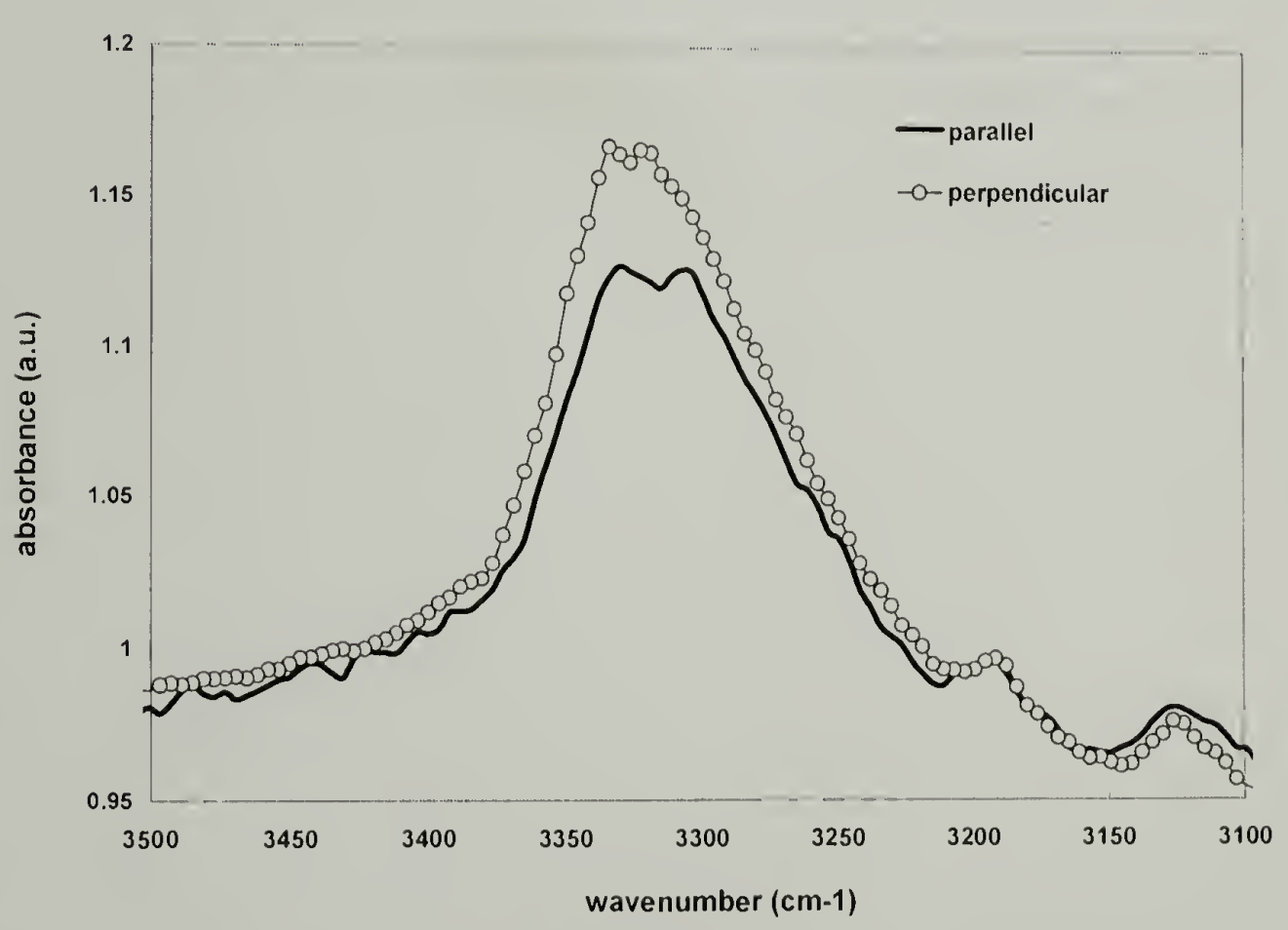

Figure 2.21 – IR spectra for eleetrospun fiber mat eollected at 9.84 m/s.

The difference between the absorption of parallel and perpendicular polarized light increases as the collection speed of the target increases. This is an expected result if we assume that higher rotational speed of the target result in more perfectly aligned fiber mats. The IR spectra for the fiber mat collected at speed of 9.81 m/s is used as the basis for comparing the molecular orientation of electrospun Pellethane® 2103-80AE fibers to the bulk material. The IR spectra of both the isotropic electrospun mat and the bulk polyurethane are shown in Figures 2.22 and 2.23, respectively.

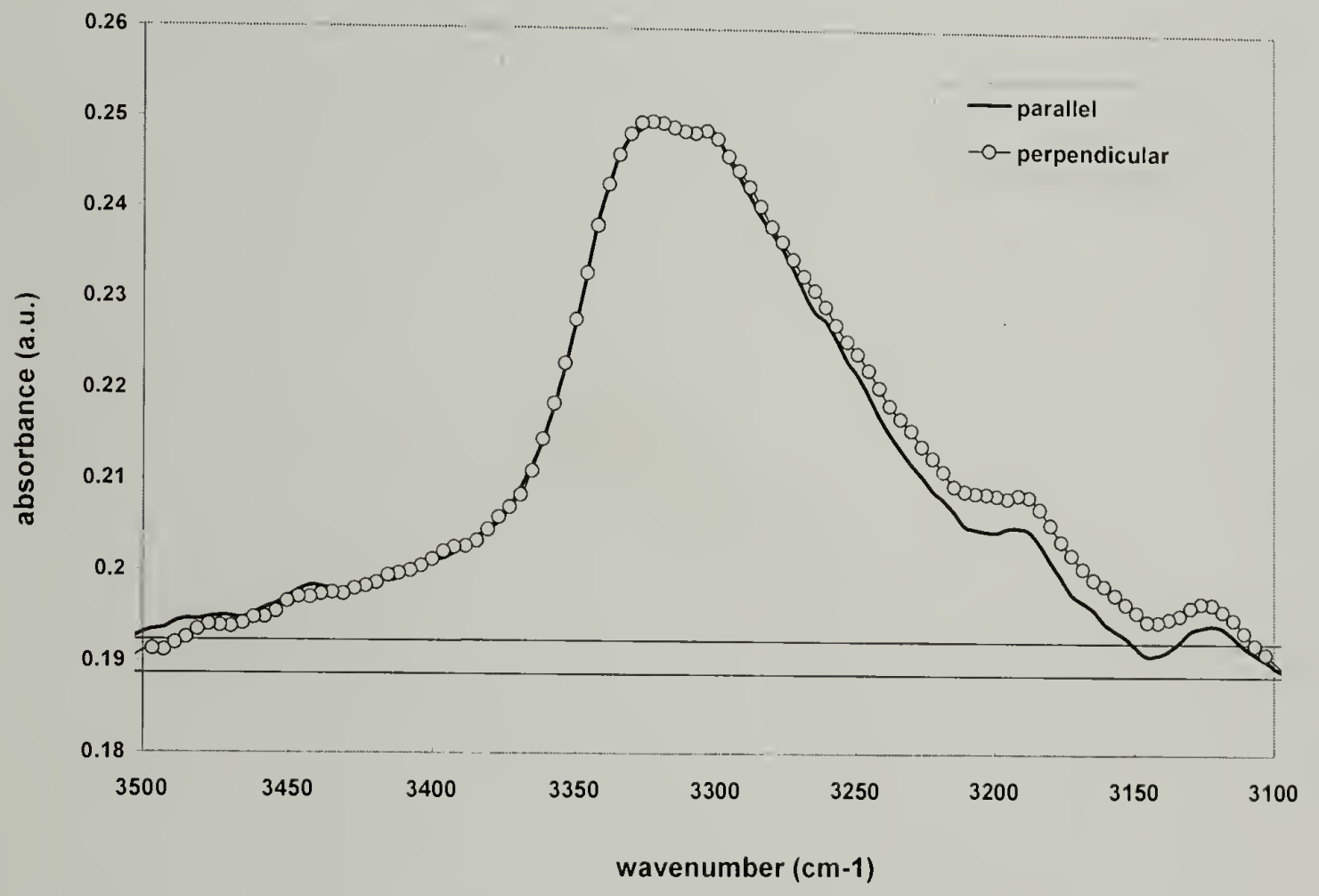

Figure 2.22 – IR spectra for isotropic electrospun Pellethane® 2103-80AE fiber mat.

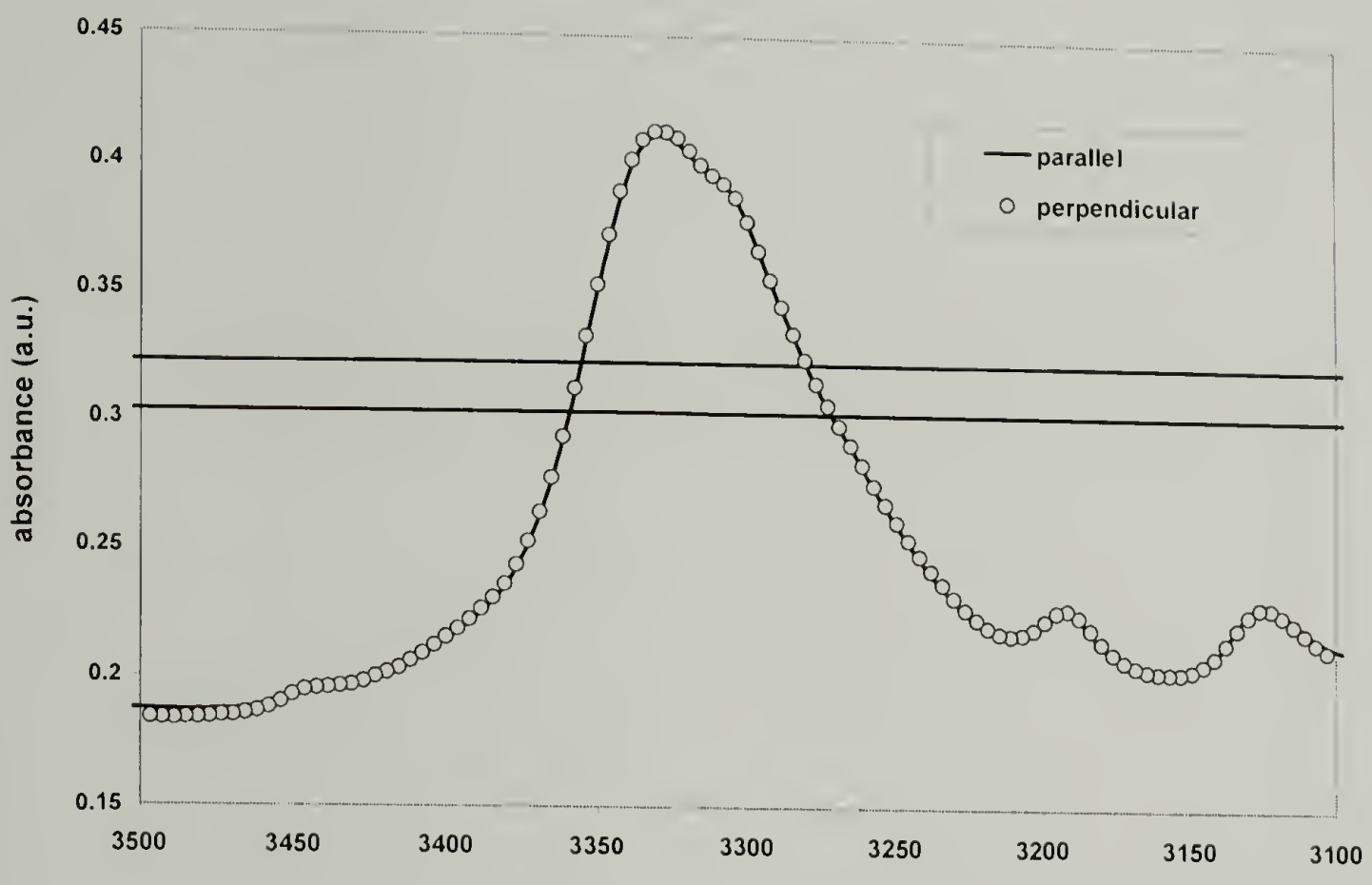

Figure 2.23 – IR spectra of bulk Pellethane® 2103-80AE.

The spectrum for aligned PU fibers shows higher peak absorbance at 3320 cm^{-1} for perpendicular polarized than for parallel polarized light. For the isotropic electrospun mat and the bulk film, there is no difference in peak absorbence between parallel and perpendicular polarized radiation at 3320 cm^{-1}. Dichroic ratios and orientation function values for each sample are presented in Table 1. The computed orientation function values for unoriented electrospun and bulk PU are both essentially zero. The orientation function for aligned electrospun PU is small, but not zero, and an order of magnitude larger than the *f* value for the PU film. These results indicate that

some degree of molecular orientation is induced by the process of electrospinning, and must be a contributing factor to the "stiffer" stress-strain response, and premature failure of the electrospun polyurethane.

	IR Absorbance @ 3320cm^{-1} (arbitrary units)		Orientation function (f)
	Parallel	Perpendicular	
PU film	0.404	0.405	0.002
Isotropic espun PU	0.249	0.249	0.000
Oricnted espun PU	1.122	1.164	0.025

Table 2.1 – IR absorbance and oricntation function values for electrospun (aligned and isotropic) and bulk Pellethane® 2103-80AE.

2.7 Hysteresis and permanent set

Although thermal analysis and x-ray diffraction indicate essentially no change in the electrospun polyurethane relative to the bulk, the small changes in molecular orientation elucidated by IR dichroism of the hard urethane chain segments may, at least in part, account for the change in mechanical response of the electrospun material. More telling information is gained from cyclic tensile strain experiments of the electrospun and bulk material. In separate studies, Falabella[79] and West et al.[80] showed hysteresis in the orientation function of the hard domains in segmented thermoplastic polyurethane elastomers, suggesting that the persistence or hard domain orientation after

the unloading of the material is due to plastic deformation of hard segments. The hysteresis of the orientation function of urethane segments also manifests itself as mechanical hysteresis and permanent set in the material. For electrospun and bulk Pellethane® 2103-80AE, the cyclic strain curves for samples stretched up to 150% strain are shown in Figures 2.24 and 2.25, respectively.

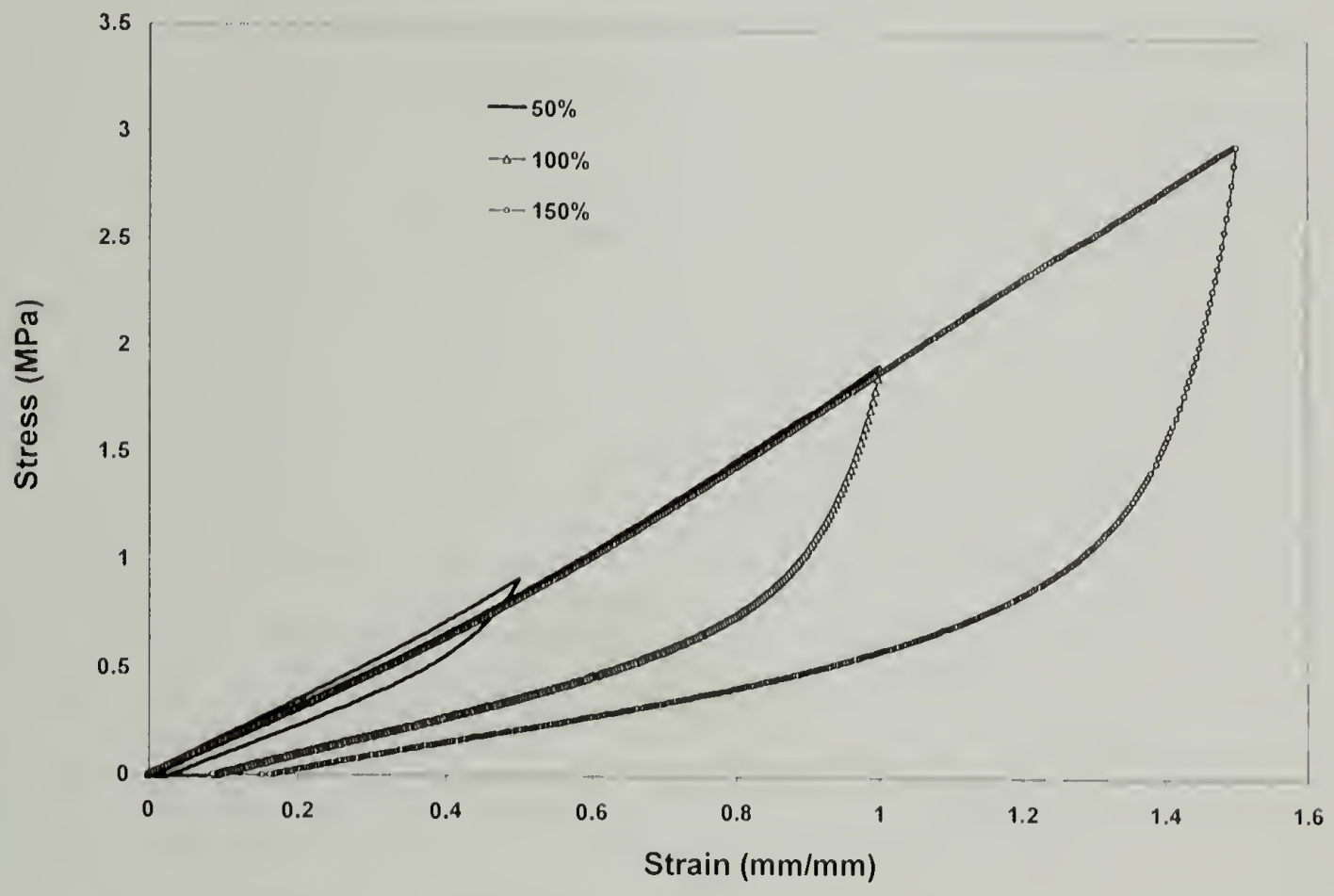

Figure 2.24 – Cyclic stress-strain curves for electrospun Pellethane® 2103-80AE.

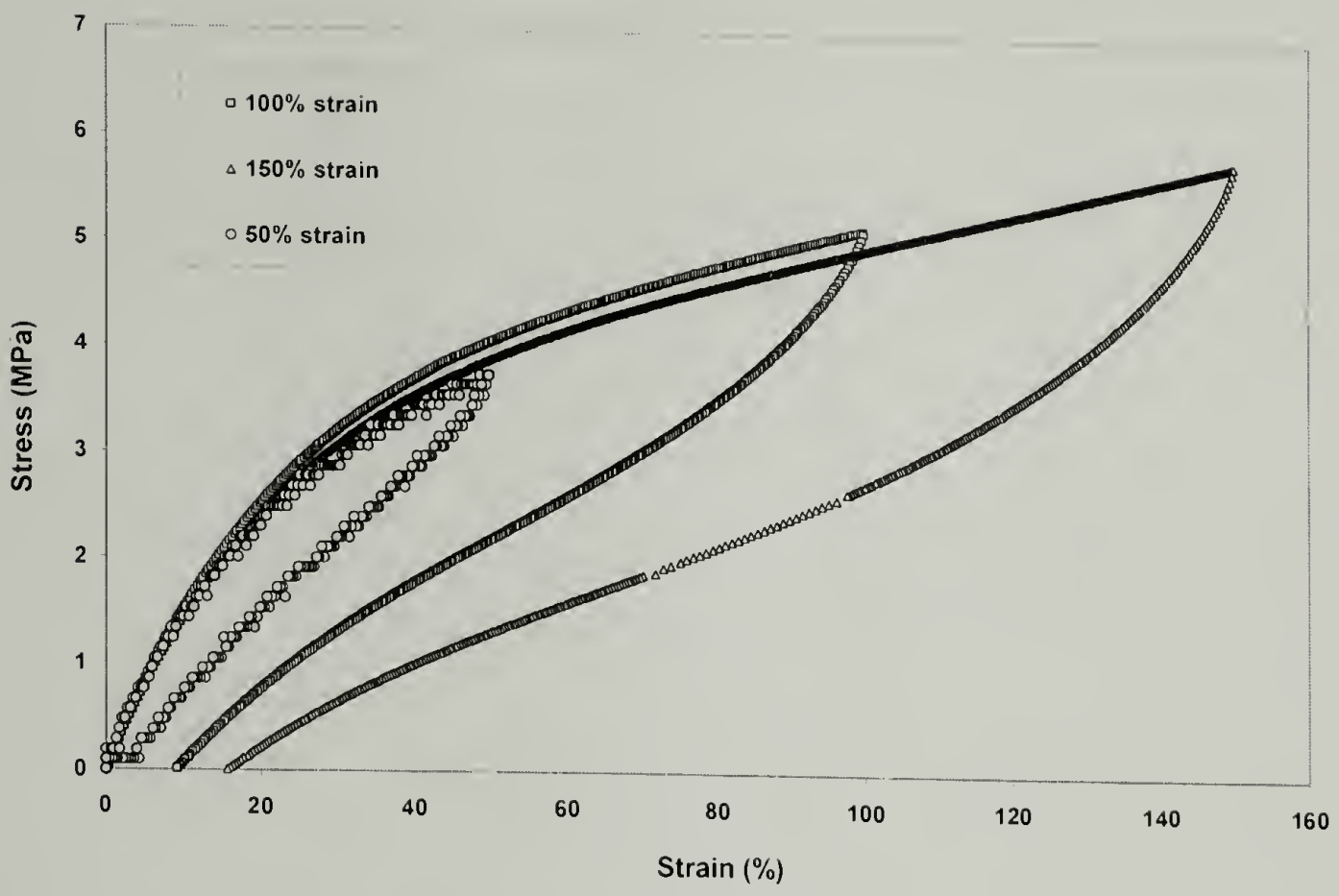

Figure 2.25 – Cyclic stress-strain curves for bulk Pellethane® 2103-80AE.

A maximum strain of 150% was chosen to be sure that any permanent set in the electrospun materials was not attributable to other effects such as gross damage of fibers, or debonding of fibers at junction points. Based on the micrograph shown in Figure 2.26 of electrospun Pellethane® 2103-80AE taken to 200% strain, it appears that no obvious damage is present in the material.

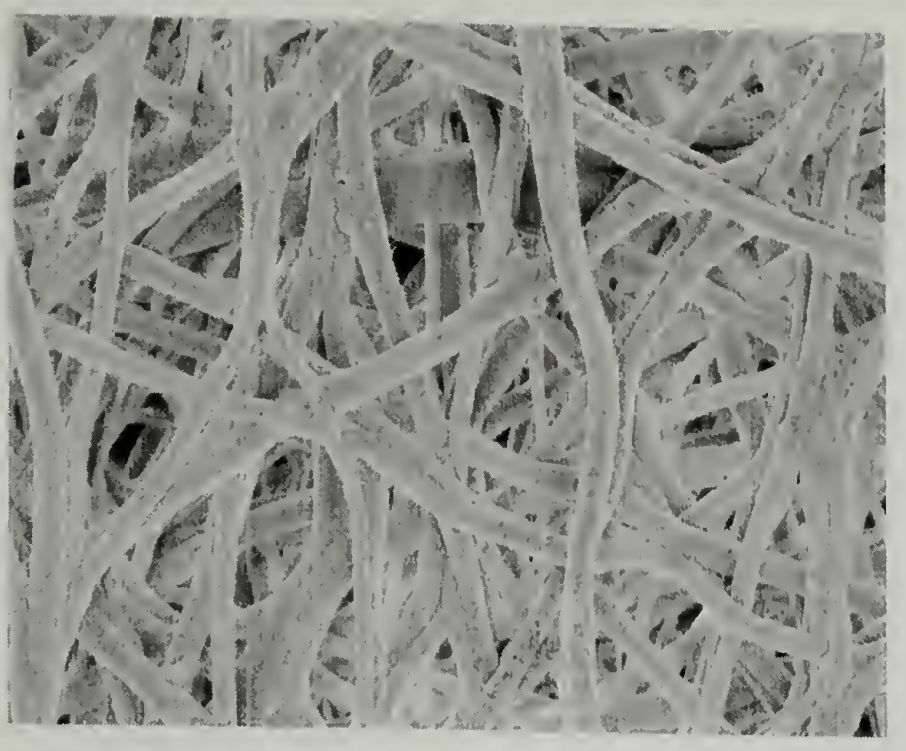

Figure 2.26 – Electrospun Pellethane® 2103-80AE, strained 200% in tension.

At first comparison of the cyclic loading/unloading curves for each material up to 150% strain, it appears the results are of little consequence, as the permanent set in each being approximately the same. Table 2.2 displays the permanent set for each materials as a function of applied tensile strain.

	Permanent set (%)		
Tensile Strain	50%	100%	150%
Pellethane 2103-80AE	3	9	15.5
Electrospun Pellethane 2103-80AE	3	9	16.5

Table 2.2 – Permanent set in Pellethane® 2103-80AE (bulk and electrospun) as a functioin of applied tensile strain.

The hysteresis curves for both materials appear to be the result of strain-induced crystallization. However, thermal analysis by differential scanning calorimetry conducted after the materials were subjected to cyclic strain show no melting endotherms to indicate the existence of crystals in either the electrospun or bulk material after cyclic strain. The DSC heating scans for the electrospun and bulk materials strained to 200% are shown in Figure 2.27

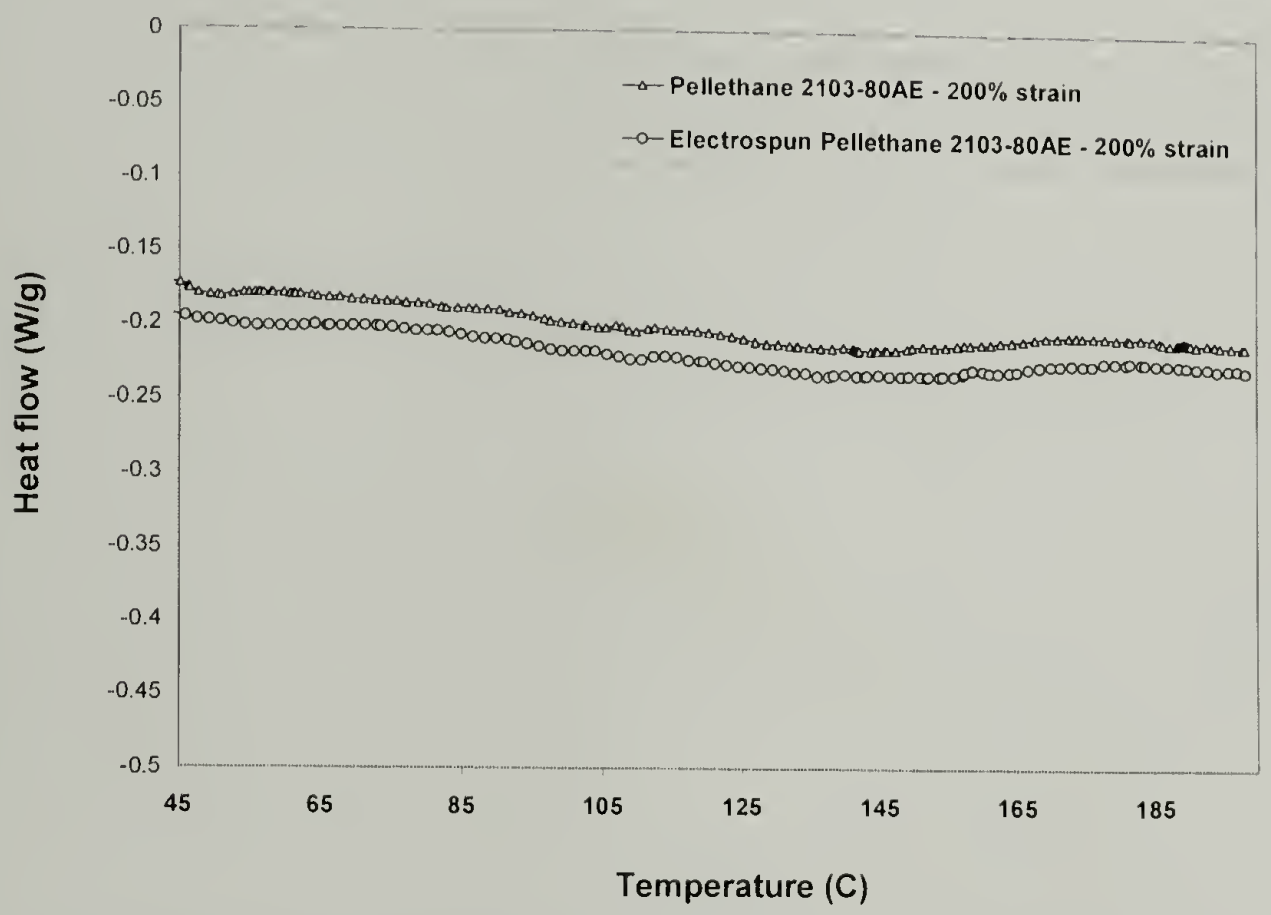

Figure 2.27 – DSC heating scans for Pellethane® 2103-80AE (bulk and electrospun) strained to 200%.

The permanent set in each material at 150% strain is approximately equal. Assuming the permanent set is due to plastic deformation of hard urethane segments, the result is actually significant. If one considers the composite theory of average strain in a two-component system presented by Christensen[81] and treats the electrospun mat as a composite material made of fibers (matrix) and voids (inclusions), the ratio of the

strains experienced by each of the components in the composite is a function of the shear moduli of the respective components, and the volume fraction of inclusions, given in the following expression

$$(\mu-\mu_m) / (\mu_i-\mu_m) = c \langle c_i \rangle / \langle c \rangle \qquad 2.5$$

where the variables are defined as:

μ = shear modulus of the composite material

μ_m = shear modulus of the matrix material

μ_i = shear modulus of the inclusions

c = volume fraction of the inclusion (V_i/V)

$\langle c_i \rangle$ = average shear strain in the inclusion

$\langle c \rangle$ = average shear strain in the composite

Without actually computing a ratio of relative strains, the fact that the electrospun material is predominantly composed of voids ($\approx$ 70%), and has a shear modulus assumed to be zero, qualitatively it is apparent that the strain experienced by the matrix phase (fibers) is less than the applied strain to the sample. Therefore, the result is significant in that the electrospun material has the same amount of permanent set as the bulk material at relatively smaller strain. This result suggests that connectivity of hard domains in the electrospun material is more prevalent and load is more efficiently transferred to the hard domains than in the bulk material. This efficient load transfer is also a reasonable explanation for the higher stress in the electrospun material than in the bulk in uniaxial tension from approximately 50% to 250% strain.

A clearer illustration of the effect of electrospinning on the change in molecular scale morphology or distribution of hard/soft segment domains in the thermoplastic polyurethanes is the mechanical response of aligned electrospun fiber mats of Pellethane® 2103-80AE. As discussed earlier, the stress-strain response of the isotropic electrospun fiber mats is not only a result of slight molecular scale differences between the electrospun and bulk materials, but also by the connectivity of the electrospun fibers at junction points throughout the fiber mat. In the aligned electrospun fiber mats, the effect of fiber connectivity is less influential on the overall mechanical response. In an aligned mat, the mechanical response is a truer reflection of inherent properties of the electrospun fibers, and more clearly demonstrates the effects of the electrospinning process on the material at the molecular level. The stress-strain curves shown in Figure 2.28 compare the response of aligned electrsopun Pellethane® 2103-80AE (morphology shown in Figure 2.28, and IR dichroism measured in Figure 2.21) to bulk Pellethane® 2103-80AE.

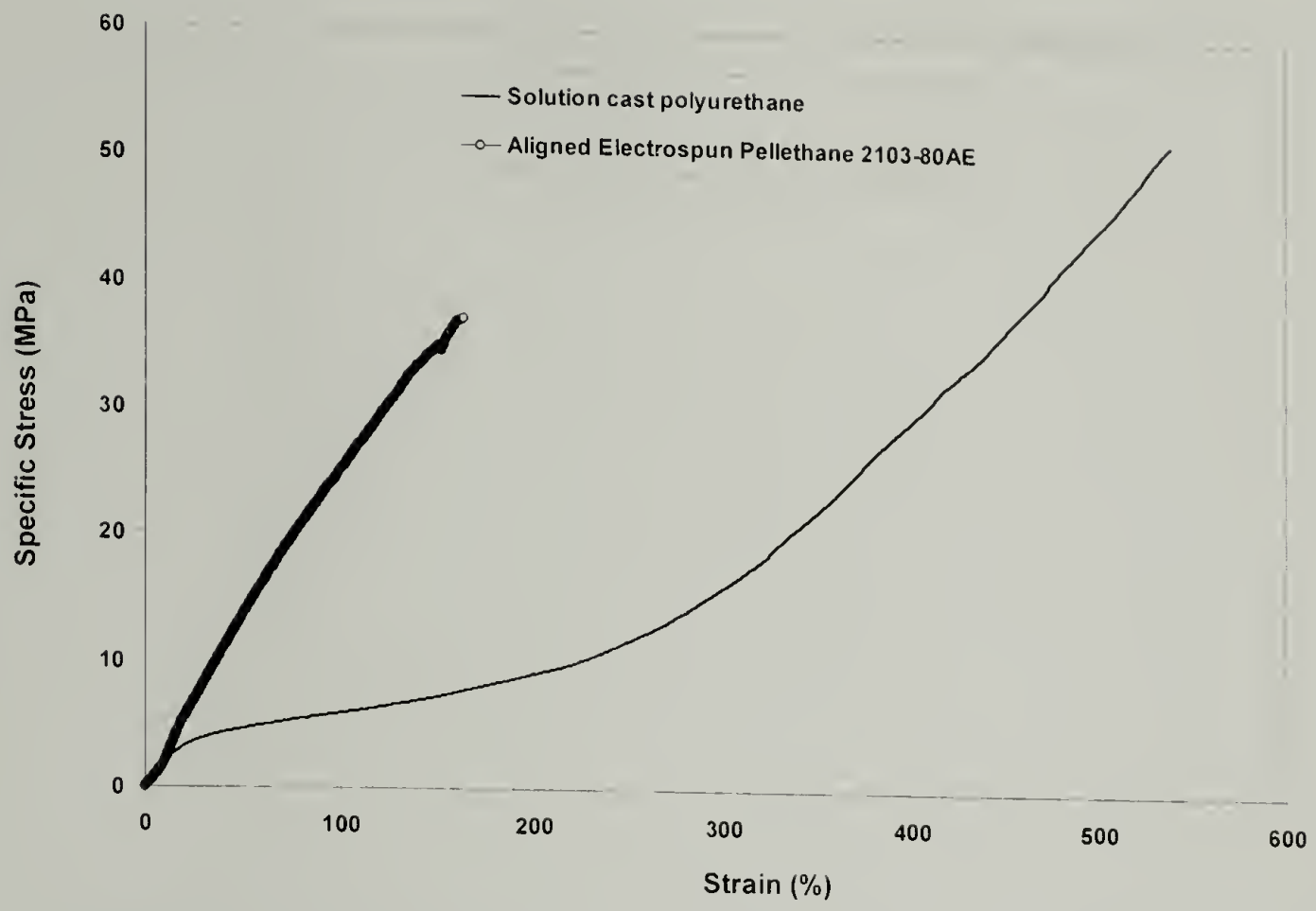

Figure 2.28 – Stress-strain curves for aligned electrospun fiber mat and bulk Pellethane® 2103-80AE.

The response of the aligned fiber mat more clearly illustrates that the small increase in molecular orientation measured from IR dichroism experiments, as well as perhaps more efficient cooperation of hard urethane chain segments in the polymer, results in a material with a characteristically stiffer response than the bulk.

2.8 Mechanical behavior of electrospun glassy polymers

To further illustrate the morphology change and increased cooperation among hard chain segments in electrospun thermoplastic polyurethanes, an attempt was made to electrospin and test mechanical properties of glassy homopolymer systems that would presumably show no effects of molecular scale change as a result of electrospinning. The assumption is that amorphous polymers such as polycarbonate, polystyrene, and poly(methyl methacrylate) would show no difference in mechanical

response between bulk and electrospun forms. All three of these glassy polymers were electrospun, but no mechanical properties were obtained in this study. In all three electrospun systems, the fiber mats produced have little or no mechanical integrity. By simple observation, electrospun mats of PC, PS and PMMA are looser and more three-dimensional in texture, less film-like than the two-dimensional morphology of the electrospun polyurethanes. Conventional tensile test specimens of the electrospun glassy polymers are more difficult to prepare than the electrospun PU's. The lack of mechanical integrity appears to be due to poor inter-fiber adhesion among electrospun glassy polymer fibers. Electrospun poly(methyl methacrylate) will be discussed in detail. Figure 2.29 shows a scanning electron micrograph of typical PMMA fibers electrospun from solution.

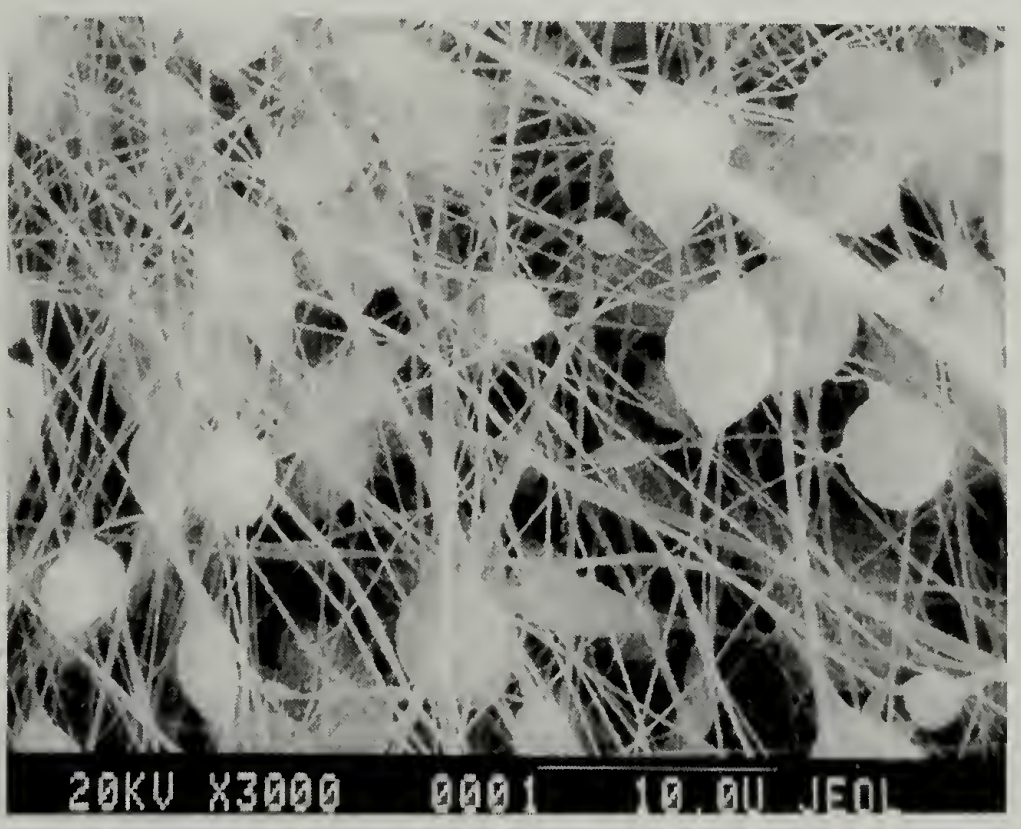

Figure 2.29 – Electrospun poly (methyl methacrylate).

The lack of inter-fiber adhesion is not obvious from the micrographs, however the material is not testable in a typical tensile test as were the electrospun polyurethanes, discussed earlier. In order to have a material that was more film-like in texture, the electrospun PMMA mats were subjected to a post treatment with heat and very light pressure in a heated press. The goal was to maintain the fibrous morphology of the material, yet promote fiber adhesion at juncture points by the application of heat and pressure. This concept was successful in the sense that post-treatment resulted in fiber mats that were more consolidated and macroscopically appeared to be films. The morphologies of electrospun PMMA post-treated at two different conditions are illustrated in Figure 2.30a and 2.30b.

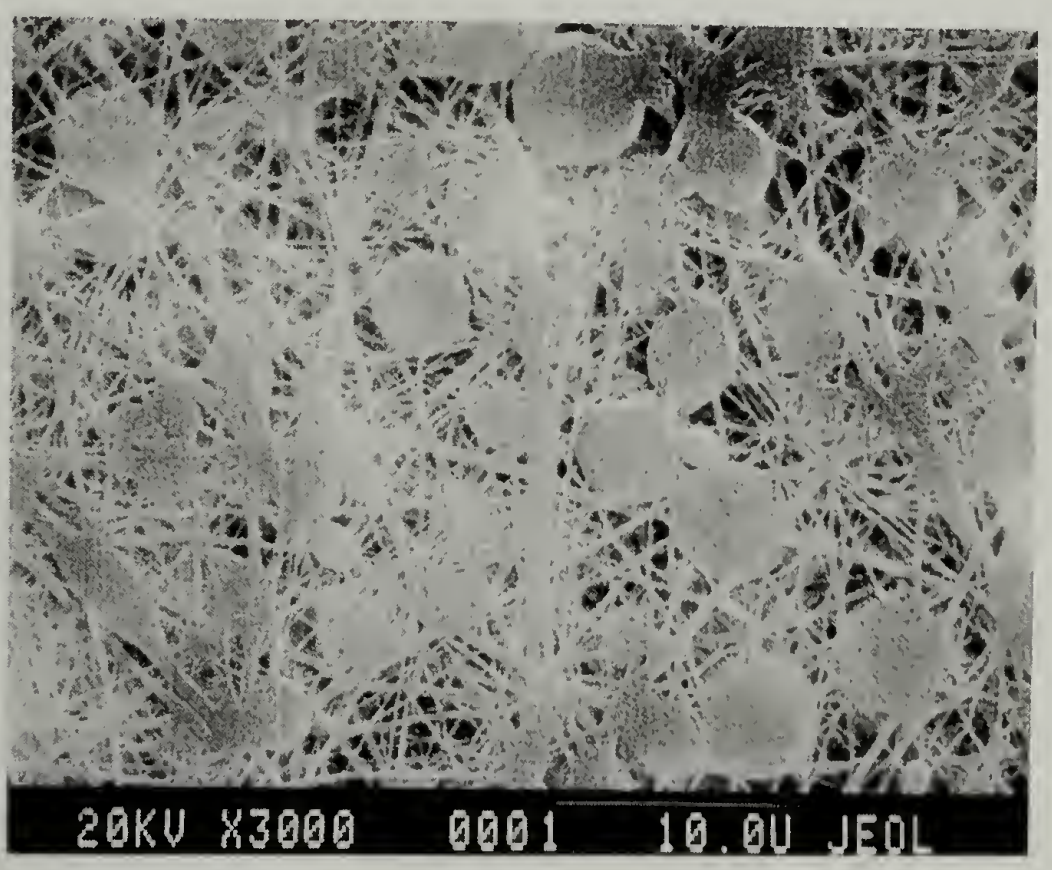

(a)

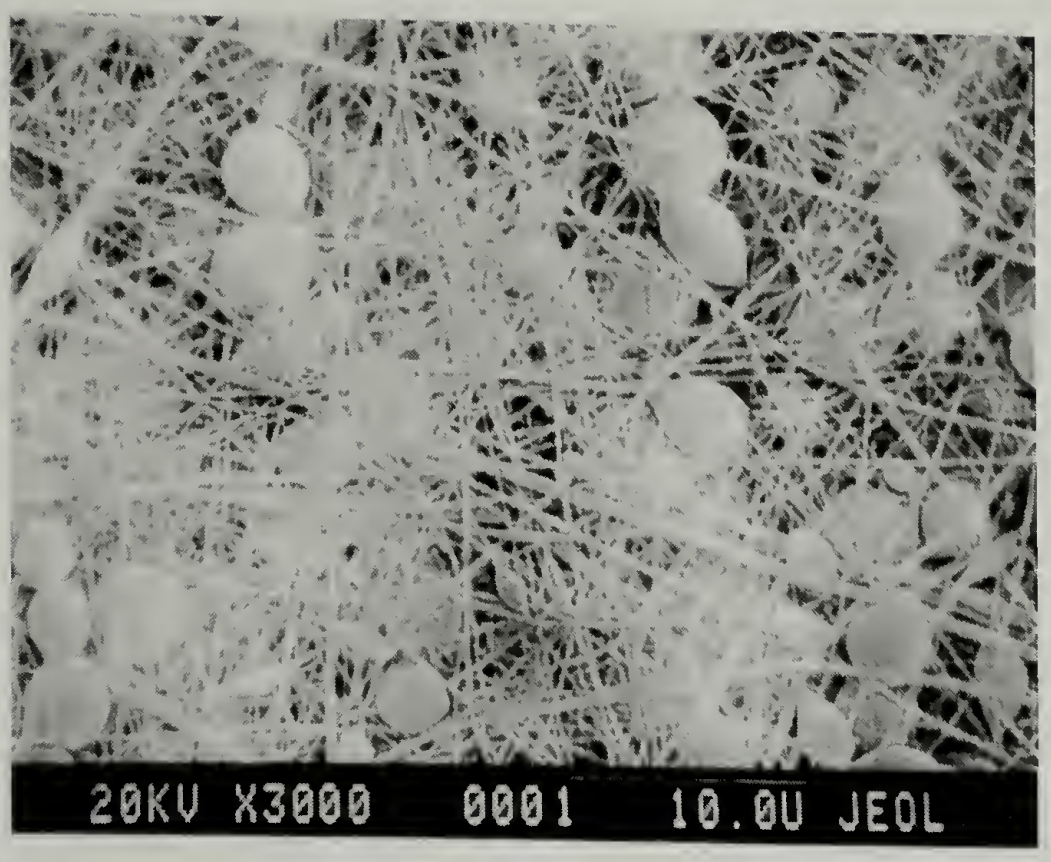

(b)

Figure 2.30 – Post-treated electrospun PMMA: (a) 100°C for 1 minute with light pressure; (b) 75°C for 2 minutes with light pressure.

Microscopically, the desired effect was achieved. Macroscopically and mechanically, however, the post-treated fiber mats were extremely brittle and were still untestable by conventional means, as the samples fractured immediately upon any attempt to mount into tensile testing grips.

Another attempt was made to test electrospun PMMA by electrospinning aligned PMMA fibers. As discussed earlier, the mechanical strength of aligned fiber mats is less dependent on the bonding of fibers at junction points, and more reflective of the true mechanical behavior of the electrospun material. Aligned electrsopun fiber mats of PMMA were prepared and are shown in Figure 2.31. However, even the aligned electrospun PMMA mats have essentially no mechanical strength. It appears that the lack of mechanical strength of the aligned PMMA mat is due to the discontinuous nature of the electrospun fibers. In Figure 2.31, many fiber ends can be seen in the

micrograph, and as for the isotropic electrospun PMMA mat, the aligned mat has no strength and is also untestable by conventional means.

Figure 2.31 – Aligned electrospun PMMA fibers.

2.9 Conclusions

Uniaxial tensile tests of electrospun thermoplastic polyurethanes show their mechanical behavior to be fundamentally different from their bulk analogs. The ultimate tensile strength of the electrospun materials is similar to the bulk, however the strain to failure is much lower as a results of cracks in the electrospun fibers acting as points of stress-concentration and leading to premature failure of the material. The source of the unique stress-strain response of the electrospun materials is not obvious based on conventional characterization techniques. The polyurethanes studied are not crystalline materials, therefore thermal analysis such as differential scanning calorimetry, as well as x-ray diffraction techniques provide no insight to possible

morphological changes in the material that occur as a result of the electrospinning process. IR dichroism experiments indicate slight molecular orientation in electrospun fibers, and cyclic strain experiments suggest that hard chain segments may be organized in the electrospun material more efficiently to carry load, than in the bulk. This is also evident in the mechanical response of aligned electrospun fiber mats, which are stiffer yet than the isotropic electrospun mats, and depend less on fiber bonding for their strength. While there are no obvious molecular scale differences between the electrospun and bulk materials, the nature of the mechanical behavior of the isotropic electrospun materials appears to be attributable to the adhesion at junction points among fibers making up the mats, and strain-induced orientation of fibers in the isotropic mats. The necessity of fiber-fiber adhesion in the production of good fiber mat properties is further illustrated by the lack of mechanical integrity of electrospun glassy polymers, such as poly(methyl methacrylate), that appear to have very little adhesion among the fibers that comprise the electrospun mats.

CHAPTER 3

MECHANICAL MODELING OF ELECTROSPUN POLYURETHANE MATS

3.1 Introduction

The mechanical properties of nonwoven materials have been studied for the past 40 years. Theoretical models have been constructed from information of fiber tensile properties and fiber web structures to predict mechanical behavior of nonwoven fabrics.[82-85] More recently, computer simulation techniques have been used to create models[86-87] of nonwovens and the finite element method has been used to predict mechanical properties of nonwoven geotextiles.[88]

Theoretical analysis of the mechanics of a material structure may be based on either a consideration of the forces involved—resolving and summing them—or on a consideration of the energy relations. In this chapter, both approaches will be taken to describe mechanics and mechanical properties of nonwoven electrospun fiber mats. Considerations of forces will be used to construct a theoretical stress-strain curve for an isotropic electrospun polyurethane fiber mat. The energy method will be employed more simply to predict the tensile modulus of isotropic electrospun polyurethane fiber mats, based on the measured tensile modulus of aligned fiber mats of the same materials, respectively.

The mechanical stress-strain response of an isotropic electrospun polyurethane fiber mat is modeled based on the stress-strain response of a mat of aligned electrospun fibers of the same material. Simple relationships are used in the modeling which take

into account the effect of applied strain on the isotropic electrospun mat, such as uniaxial stain, fiber orientation and rotation, and fiber buckling. Each of these events imparts a stress in the material that is dependent on the angle of a particular load-bearing element relative to the direction of applied strain. The sum of the axial components of the forces of all load-bearing elements at a particular strain, divided by the cross-sectional area, will constitute one coordinate (stress,strain) point on the model stress-strain curve. A series of coordinates at determined increments of strain from 0% to break (for the isotropic material) will construct the model stress-strain curve. The model stress-strain curve for the isotropic electrospun material is constructed based on the mechanical behavior of the oriented electrospun material, rather than from the bulk, as a result of the data presented in Chapter 2 that shows the stress-strain behavior of the electrospun material to be fundamentally different from the bulk.

Other modeling in this chapter is empirical in nature, and attempts to relate the tensile strength of isotropic electrospun polyurethanes to the strength of their bulk analogs. This is done through a simple rule of mixtures, treating the electrospun materials as two-component systems made up of the electrospun fibers as the matrix phase, and void volume as the included phase.

3.2 Results and Discussion

3.2.1 Modeling Stress-Strain Behavior of Isotropic Electrospun Mat

Electrospun polyurethane fiber mats were shown to have fundamentally different stress-strain response than their bulk analogs. To model this response, the starting point is the stress-strain response of an aligned fiber mat of the same material. Some

assumptions are made about both the oriented and the isotropic electrospun materials. As discussed in Chapter 2, the oriented fiber mats are prepared from a more concentrated polymer solution than are the isotropic mats, in order to produce an aligned mat free of defects, such as beads. The first assumption is that the stress-strain response of the randomly oriented fibers in the isotropic fiber mat is the same as the response of the fibers in the aligned fiber mat. Based on this assumption, the isotropic fiber mat is modeled as a random collection of fibers, whose individual properties are determined by testing an aligned mat of the same fibers.

When an isotropic fiber mat experiences uniaxial tensile strain, three main events occur in terms of individual fiber response. Fibers in the mat oriented parallel to the direction of applied strain will be stretched uniaxially, with an imposed strain equal to the applied strain. Fibers oriented at some angle with respect to the direction of applied strain, will undergo a combination of rotation and uniaxial strain, the amount of imposed strain determined by the angle of orientation. Fibers oriented approximately perpendicular to the direction of applied strain will buckle. These situations are illustrated schematically in Figure 3.1.

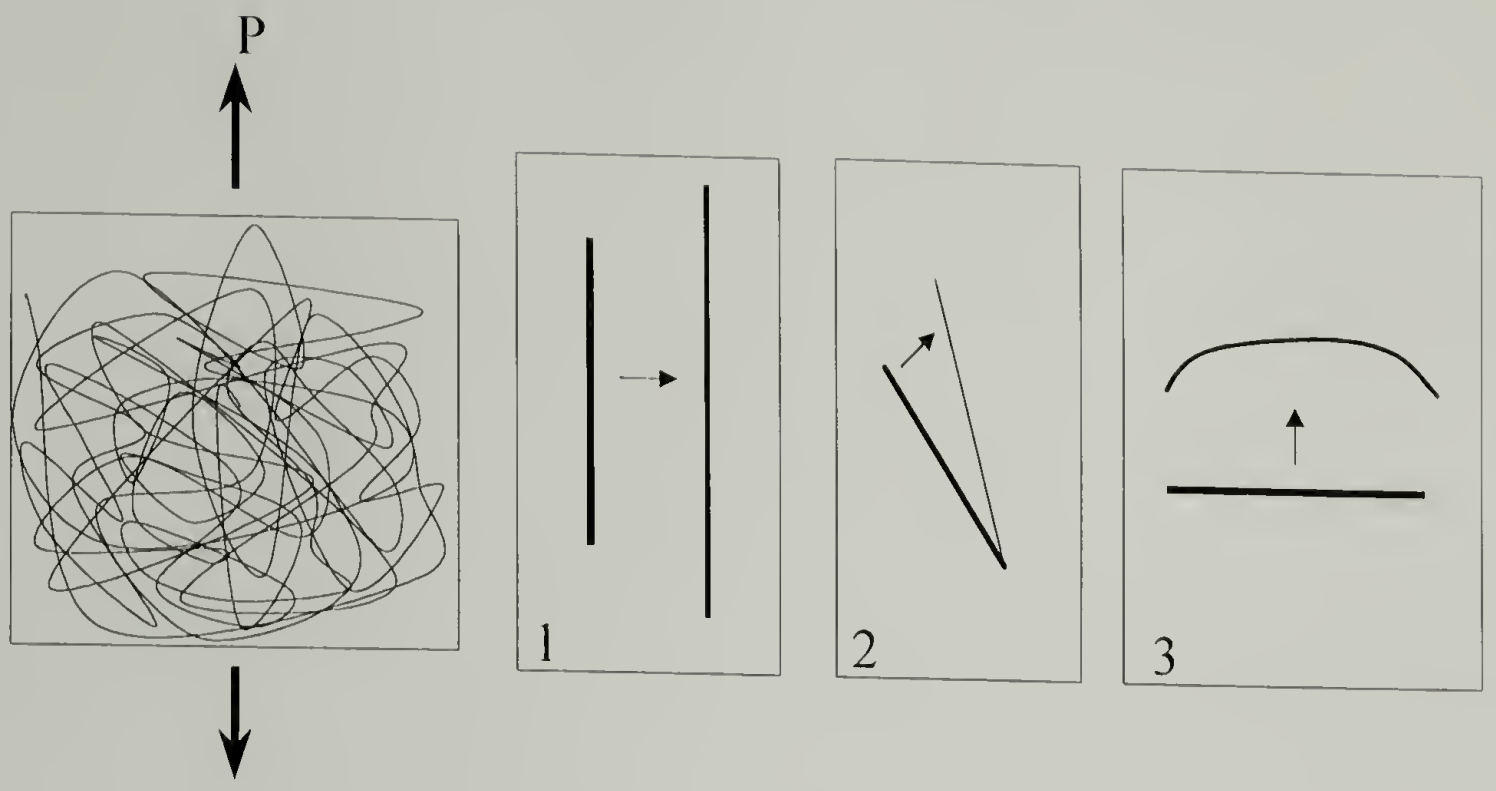

Figure 3.1 – Behavior of fibers in an isotropic electrospun mat under uniaxial tension: (1) uniaxial stretch, (2) rotation and stretch, (3) buckling.

The phenomenon of fiber buckling is illustrated experimentally in Figure 3.2, which shows an isotropic electrospun mat with an applied tensile strain of approximately 70%.

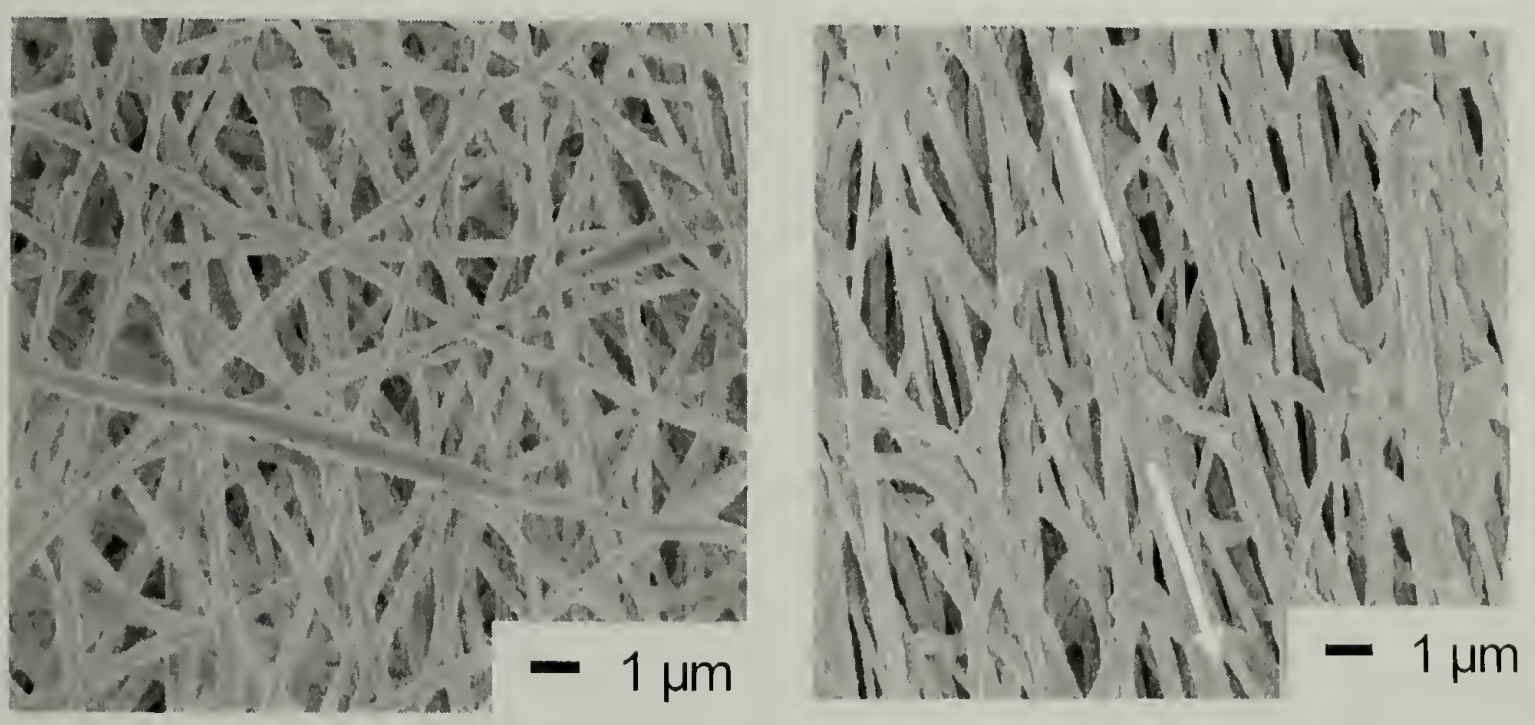

(a) (b)

Figure 3.2 – Electrospun polyurethane: (a) 0% strain ; (b) approximately 75 % strain. (arrows indicate the direction of applied strain)

Each of the events represented in Figure 3.1 contributes a stress in the material. Assuming the fibers in the electrospun mat to be long elements of high aspect ratio, fiber buckling is considered to contribute zero to the total stress in the sample. The fibers oriented in the direction of applied strain will contribute a force equal to the force in the aligned fiber mat at that particular strain, while the fibers oriented at some angle relative to the direction of applied strain will contribute a force proportional to the cosine of the angle relative to strain. The calculation of the contributions of stress from various fiber elements is given below. When the isotropic mat is strained, a fraction of the material is bearing load while some material is not contributing to the total force. To determine at what angle fiber elements begin to contribute to the stress in the material, a critical angle is determined. All fiber elements below the critical angle contribute to the total stress in the isotropic mat, while fiber elements oriented at angles larger than the critical angle are assumed not to contribute to the total stress in the material, and ignored. There is a unique critical angle for every value of applied strain, determined by a simple relationship that describes the change in length of a single fiber element in a mat of electrospun fibers.

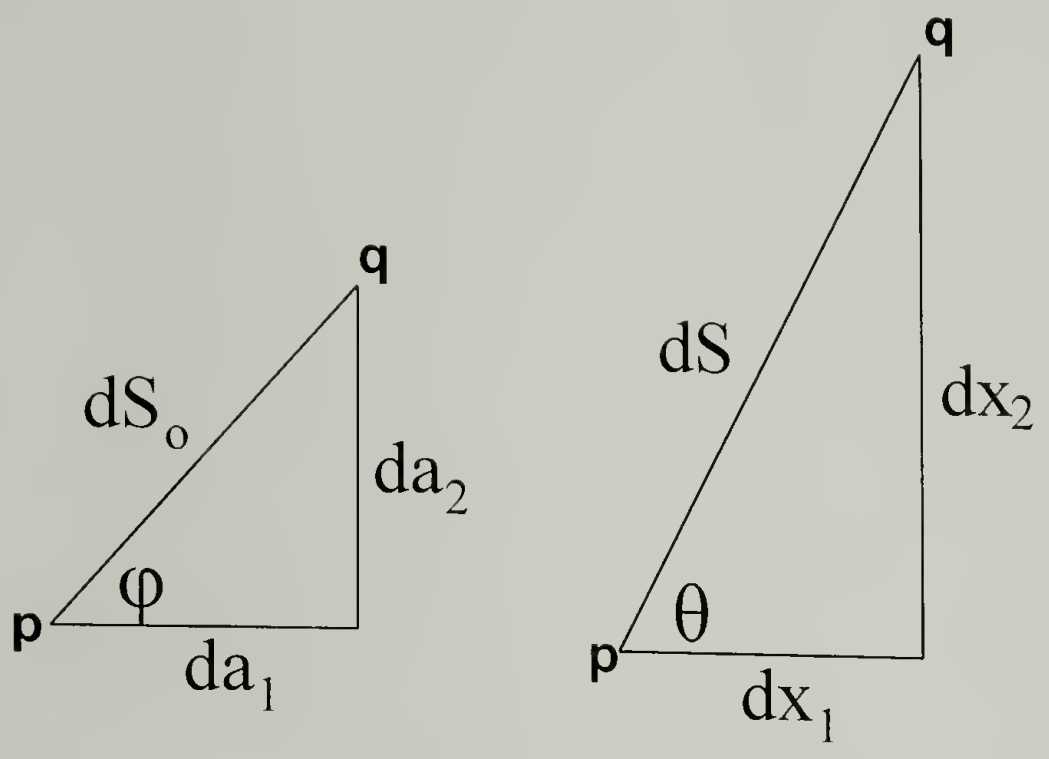

Figure 3.3 – Representation of a fiber element undergoing deformation.

The terms in the representation in Figure 3.3 are defined as:

dS_o = the original length of the fiber element

dS = deformed length of the fiber element

da_i (i =1,2) = horizontal and vertical components of the original element length

dx_i (i =1,2) = horizontal and vertical component of the deformed element length

a_i = coordinates in original, undeformed state

x_i = coordinates in deformed state

p,q = represent two arbitrary points on a fiber element

The length of the element in the undeformed state is

$$dS_o^2 = da_1^2 + da_2^2 + da_3^2 \tag{3.1}$$

and in the deformed state

$$dS^2 = dx_1^2 + dx_2^2 + dx_3^2 \tag{3.2}$$

which for principle directions can be expressed as

$$dS^2 = \lambda_1^2\, da_1^2 + \lambda_2^2\, da_2^2 + \lambda_3^2\, da_3^2 \tag{3.3}$$

where λ_i (i = 1,2,3) are the stretch ratios applied to the system. If equation 3.3 is divided by the undeformed length, dS_o^2,

$$dS^2/dS_o^2 = \lambda_1^2\, da_1^2/dS_o^2 + \lambda_2^2\, da_2^2/dS_o^2 + \lambda_3^2\, da_3^2/dS_o^2$$

$$\Lambda^2 = dS^2/dS_o^2 = \lambda_1^2 \cos^2(dS_o,a_1) + \lambda_2^2 \cos^2(dS_o,a_2) + \lambda_3^2 \cos^2(dS_o,a_3)$$

$$\Lambda^2 = \lambda_1^2 \cos^2(\varphi) + \lambda_2^2 \cos^2(\alpha) + \lambda_3^2 \cos^2(\beta) \tag{3.4}$$

where Λ^2 is the ratio of the deformed fiber element length to the undeformed length of the fiber element. The electrospun mats are relatively thin and two-dimensional in nature, with virtually all fibers lying in the plane of the mat, i.e. $\cos^2(\beta)$ is equal to zero. Equation 3.4 is simplified by assuming that rotation of fibers through the thickness of the mat is negligible, and becomes

$$\Lambda^2 = \lambda_1^2 \cos^2\varphi + \lambda_2^2 \sin^2\varphi \tag{3.5}$$

For large strains and assuming constant volume in the system,

$$\lambda_1\lambda_2\lambda_3 = V/V_o$$

$$\lambda_2 = \lambda_3$$

$$\lambda_1\lambda_2^2 = V/V_o = 1$$

$$\lambda_2^2 = 1/\lambda_1 \tag{3.6}$$

Substituting equation 3.6 into equation 3.5 and simplifying the expression to have a single trigonometric function, cosine,

$$\Lambda^2 = \lambda_1^2 \cos^2(\varphi) + (1/\lambda_1)(1-\cos^2\varphi)$$

$$\Lambda^2 = (\lambda_1^2 - 1/\lambda_1)\cos^2\varphi + 1/\lambda_1 \qquad (3.7)$$

in which Λ^2 represents the ratio of deformed to undeformed distance between points p and q. When Λ^2 is less than one, a fiber element between points p and q will buckle; when Λ^2 is equal to one, a fiber will rotate only and undergo no change in length; neither event contributing to the stress in the material. When Λ^2 is greater than one, a fiber element will undergo rotation as well as a finite amount of uniaxial strain. By setting equation 3.7 equal to one, the critical angle, φ_{crit}, can be determined.

$$\cos^2(\varphi_{crit}) = (1- 1/\lambda_1) / (\lambda_1^2 - 1/\lambda_1) \qquad (3.8)$$

Each strain has a unique critical angle (φ_{crit}). Figure 3.4 shows the relationship between stretch ratio (λ_1) and the critical angle (φ_{crit}).

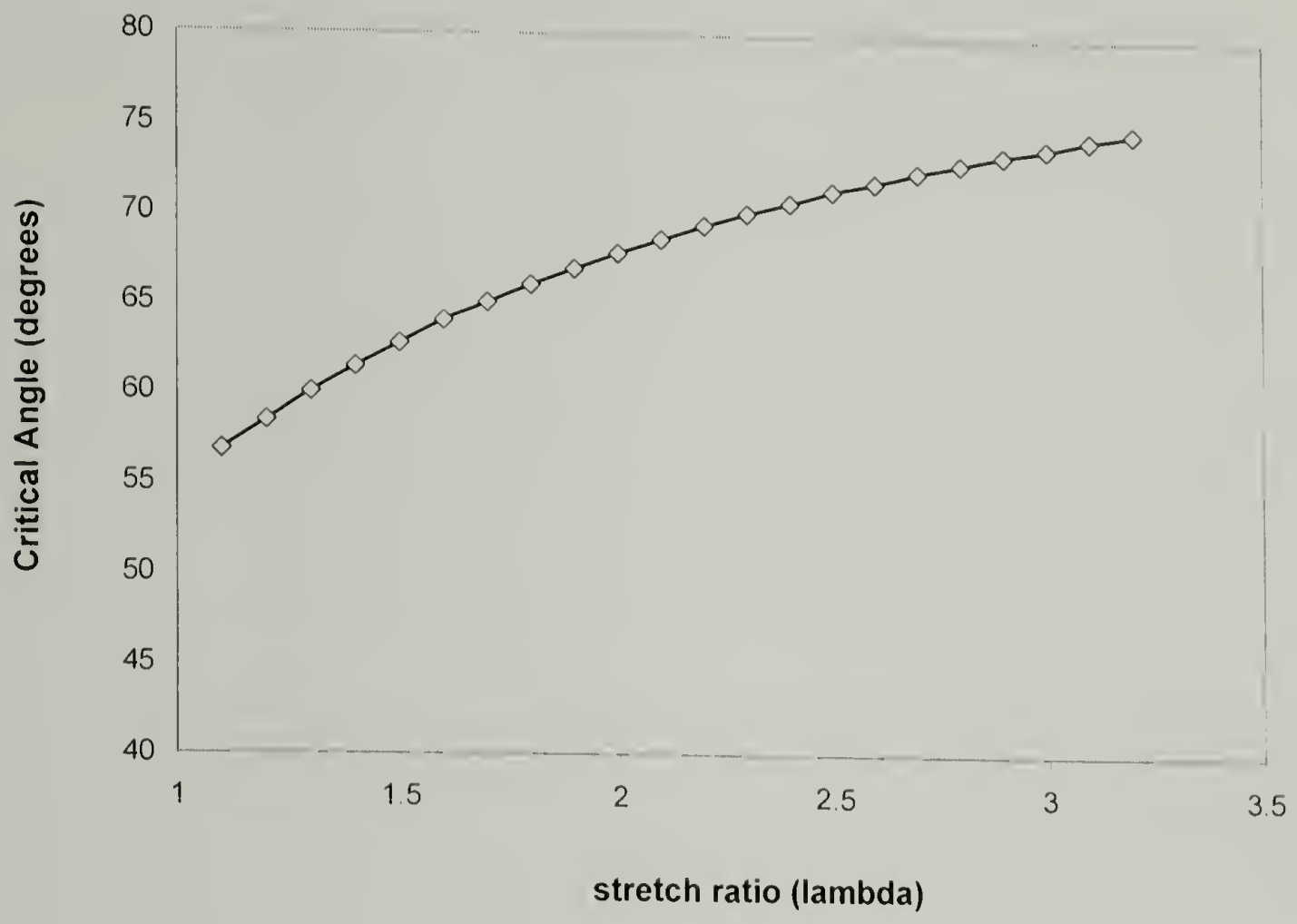

Figure 3.4 – Critical angle versus stretch ratio for a randomly oriented fiber.

At a given strain, fibers oriented at angles greater than φ_{crit}, relative to the direction of applied strain, are ignored; fibers oriented at angles between φ_{crit} and φ equal to $\pi/2$ are considered to contribute to the total stress in the material. When φ_{crit} is determined for a given deformation of the sample, the forces experienced by the fiber elements from φ_{crit} to φ equal to $\pi/2$ are determined and summed. The strain in the randomly oriented fiber elements is computed in five degree increments, assuming that all elements within that increment experience homogeneous affine deformation. Determination of the total stress in an isotropic electrospun mat at a given applied strain is carried out by summing the forces in all load-bearing fiber elements and dividing by a cross-sectional area.

Begin by considering an idealized representation of the isotropic fiber mat, shown in Figure 3.5.

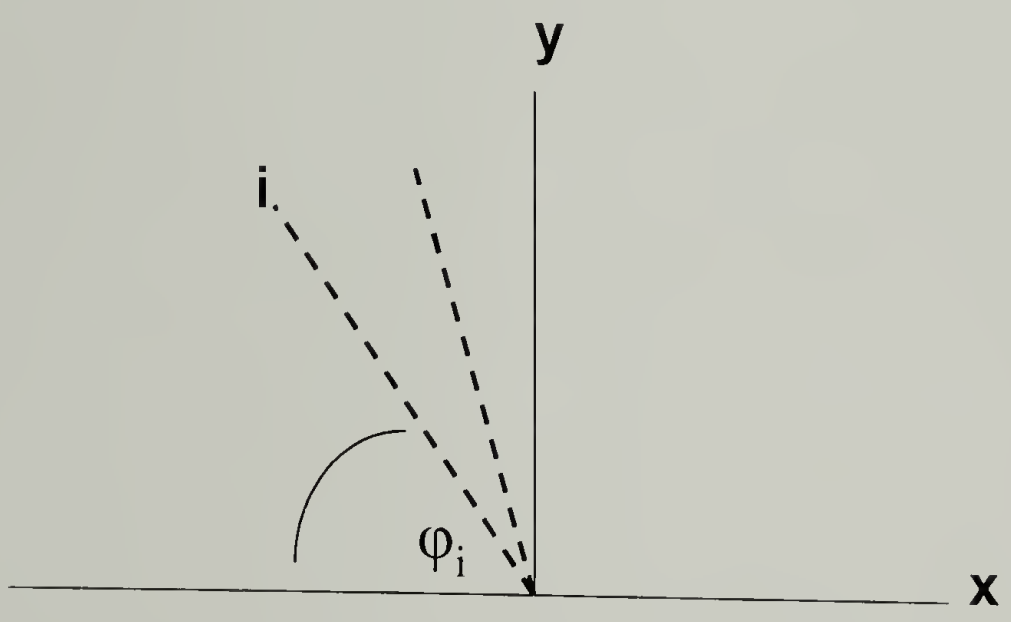

Figure 3.5 – Representation of randomly oriented fiber elements in an isotropic electrospun fiber mat.

In Figure 3.5, the dashed lines represent the randomly oriented fibers in the electrospun mat, strain is applied in the y-direction, and i represents the i^{th} fiber element in the material. The axial component of force in the i^{th} fiber element is given by

$$f_i(\varphi) = A_o\, \sigma_i(\varphi) \cos(\varphi) \qquad 3.9$$

where

$f_i(\varphi)$ = the axial component of the force in the i^{th} fiber element at angle φ

A_o = cross-sectional area of the i^{th} fiber element

$\sigma_i(\varphi)$ = stress in the i^{th} fiber element at angle φ

φ = angle of orientation of the i^{th} fiber element, relative to the direction of applied strain

The sum of the axial forces in all fiber elements at a given strain is

$$\Sigma f_i = \int_{\varphi crit}^{\pi/2} A_o \, \sigma(\varphi) \cos(\varphi) \, N(\varphi) \, d\varphi \qquad 3.10$$

in which,

$N(\varphi)\, d\varphi$ = the number of fiber elements between a given angle φ and $\varphi + d\varphi$

The total number of fiber elements in the material in which forces are to be summed, can be expressed in the following way

$$N_{TOT} = \int_{0}^{\pi/2} N(\varphi) \, d\varphi = N_o(\pi/2)$$

$$2 \, N_{TOT} / \pi \; = \; N_o = N(\varphi) \qquad 3.11$$

where

N_{TOT} = total number of fiber elements

N_o = number of fiber elements at a given angle φ (assuming a random distribution of fibers)

Subsituting the result in equation 3.11 into equation 3.10, the sum of forces in the i^{th} elements can be expressed

$$\Sigma f_i = (2A_o N_{TOT} / \pi) \int_{\varphi crit}^{\pi/2} \sigma(\varphi) \cos(\varphi)\, d\varphi \qquad 3.12$$

Equation 3.12 gives the total force in the isotropic electrospun material, at one applied strain. The force in each individual element at a particular strain is determined by the force in the aligned fiber mat at that strain. Therefore, in computing a stress in the isotropic electrospun material, not only is the total force to be divided by a cross-sectional area, but also the difference in the density, i.e. the load bearing cross-sectional area, between isotropic and aligned electrospun mats must be considered.

The average stress in the isotropic electrospun mat, σ', is equal to the sum of the forces in the material, divided by the cross-sectional area of total load-bearing elements

$$\sigma' = \Sigma f_i / \text{Area} = (2A_o N_{TOT} / Rt\, \pi) \int_{\varphi crit}^{\pi/2} \sigma(\varphi) \cos(\varphi)\, d\varphi \qquad 3.13$$

Rt in the equation above is the area over which forces are summed.

The prefactor term in equation 3.13, can be expressed as a ratio of volumes in the following way

$$2\, A_o N_{TOT} / (Rt)\, (\pi) = 2\, R\, A_o N_{TOT} / R^2\, t\, \pi = 2\, V_f / 4\, V_{TOT} \qquad 3.14$$

where

R = radius (length) of the i^{th} fiber element

t = thickness of the fiber mat

V_f = volume of all fiber elements

V_{TOT} = total volume occupied by the fiber mat

Equation 3.13 simplifies to the following expression when equation 3.14 is substituted

$$\sigma' = \tfrac{1}{2} V_f / V_{TOT} \int_{\varphi_{crit}}^{\pi/2} \sigma(\varphi) \cos(\varphi)\, d\varphi \qquad 3.15$$

The ratio of the volumes, V_f and V_{TOT} , can be expressed in terms of densities of the individual fibers and the isotropic electrospun fiber mat by the following simple relationships. Density, ρ, is equal to mass divided by volume

$$\rho = \text{mass} / \text{volume} \qquad 3.17$$

and the density of a fiber and the density of a fiber mat can expressed, respectively, as

$$\rho_{fiber} = M_o / V_f \qquad 3.18$$

$$\rho_{iso} = M_o / V_{TOT} \qquad 3.19$$

M_o = mass of fibers, which is the same for both

The V_f / V_{TOT} term in equation 3.15 can then be expressed as a density ratio, $\rho_{iso} / \rho_{fiber}$.

The results for the stress-strain modeling of the isotropic electrospun mat are shown in Figure 3.4, compared with the stress-strain curves of the aligned and isotropic electrospun mats.

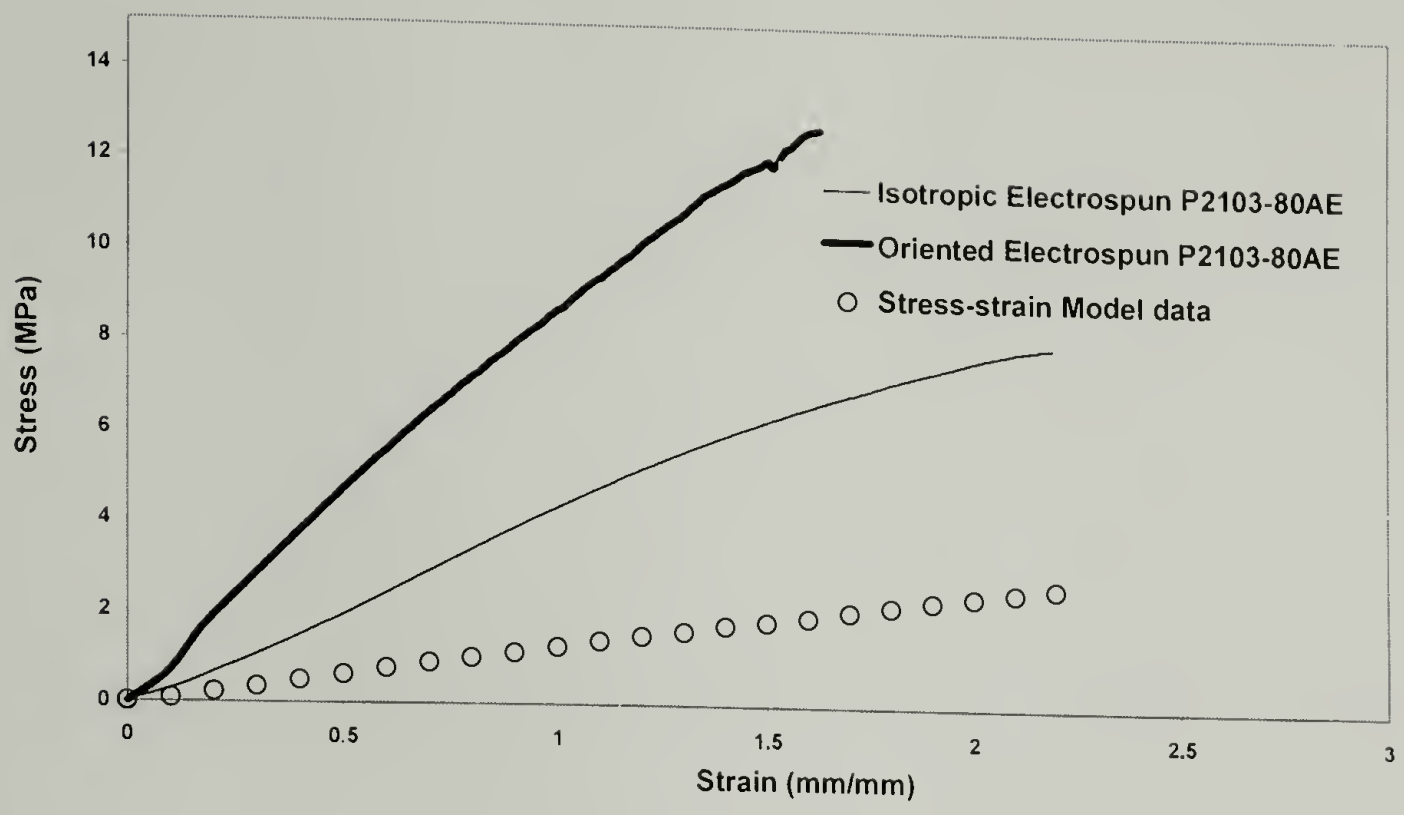

Figure 3.6 – Model stress-strain curve plotted with experimental stress-strain data for aligned and isotropic electrospun Pellethane® 2103-80AE.

The strain at break is larger for the isotropic mat than the aligned fiber mat. In order to have model data points beyond the strain at break for the aligned fiber mat, a trend-line was applied to the stress-strain curve of the aligned fiber mat. Points beyond the experimental curve were extrapolated with the equation given in Figure 3.5, illustrating the extension of the stress-strain curve with the second order polynomial equation, generated by graphical software.

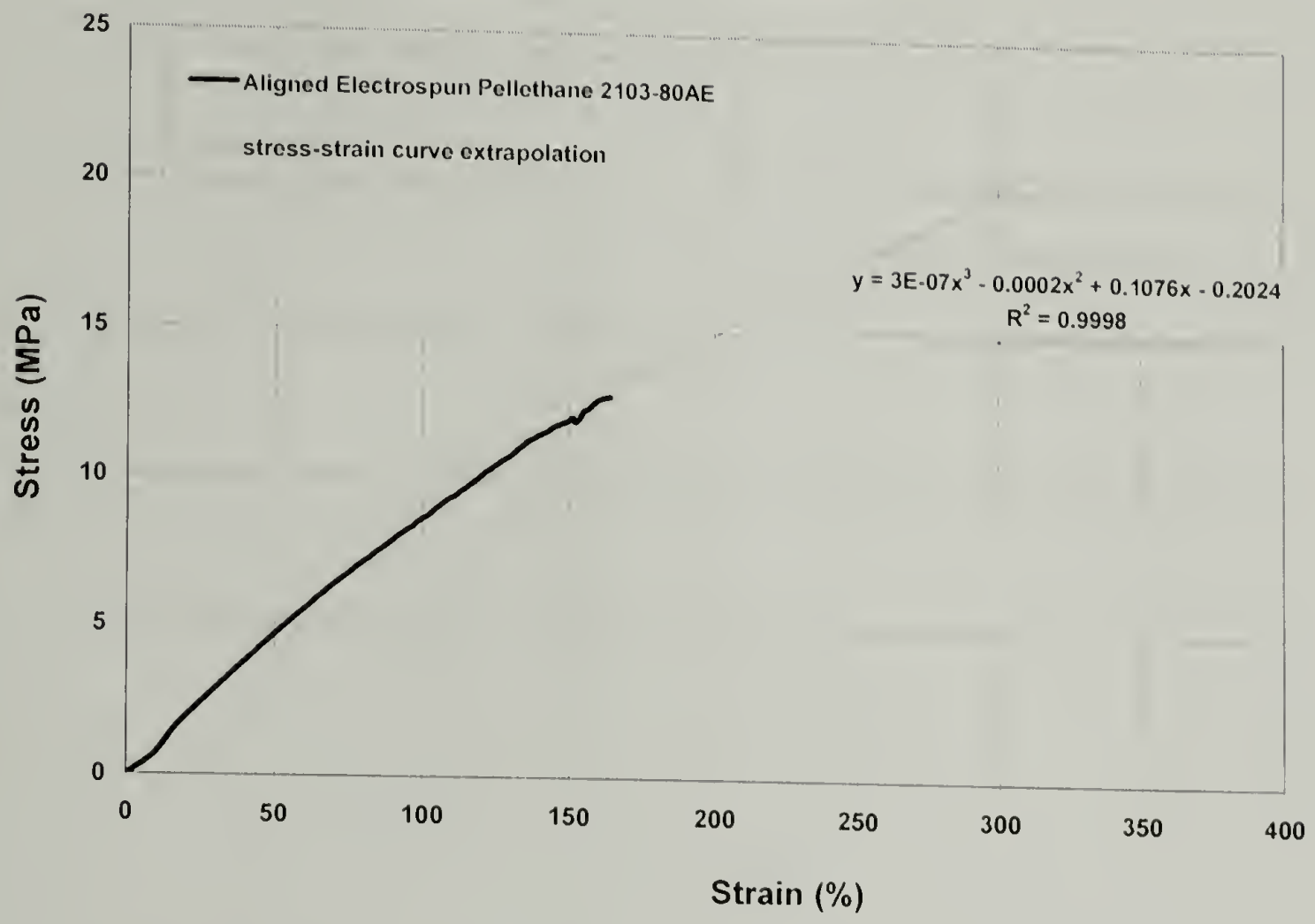

Figure 3.7 – Stress-strain curve for aligned electrospun Pellethane® 2103-80AE fiber mat with extrapolated polynomial trendline.

The shape of the model stress-strain curve appears to be representative of the experimental curve. However, the model data fall well below the experimental stress-strain curve for the isotropic electrospun fiber mat, especially at higher strains. A possible explanation for this relatively poor agreement may be the assumption made about the orientation of fiber elements in the isotropic electrospun mat. The model assumes that the distribution of fiber orientation as a function of strain remains flat, meaning the probability of finding a fiber element at any orientation in the material is the same at 0% strain or 100% strain. At small strains, this assumption may be accurate.

At large strains, however, fibers in the mat become oriented in the direction of stretch, as illustrated in Figure 3.2, and the probability of finding a fiber element at any orientation is no longer equal at all angles. At larger strains, the number of fibers undergoing uniaxial stretch increases relative to the number of fibers undergoing a rotation and stretch. The model does not account for this change, and therefore underestimates the stress in the material at higher strains. In addition, at larger strains the junction points of the fibers likely play a more significant role in the stress in the material, which is also unaccounted for in the model. Overall, the shape of the model curve is somewhat accurate in replicating the stress-strain behavior of the isotropic electrospun mat, based on the stress-strain behavior of an aligned electrospun mat. The results indicate that the basis of the model captures at least some of the physical character of the deformation of the isotropic electrospun mat, while quantitatively the model falls short by not accounting for the changing morphology and orientation of the fiber mat when strain is applied.

3.2.2 Empirical Model for Tensile Strength

The electrospun form of some thermoplastic polyurethanes has been shown to have fundamentally different stress-strain response compared to their bulk analogs. This response has been modeled in the previous section. The ultimate tensile strength of electrospun mats is modeled empirically to establish a relationship between the strength of the bulk starting materials and an electrospun mat of the same material. A simple empirical model established for composite materials is applied to electrospun systems to predict tensile strength of electrospun materials based on the void content of

the electrospun fiber mats. The following relationships were described by Christensen[81] for composite systems consisting of a matrix phase and inclusions:

$$\langle\sigma\rangle = (1 - c)\langle\sigma_m\rangle + c\langle\sigma_i\rangle \tag{3.11}$$

in which $\langle\sigma\rangle$ is referred to the average stress in the composite, $\langle\sigma_m\rangle$ is the average stress in the matrix phase, $\langle\sigma_i\rangle$ is the average stress in the included phase, and c is the volume fraction of inclusions. The individual average stresses written in terms of the modulus of each phase are

$$\langle\sigma\rangle = E\langle\varepsilon\rangle \tag{3.12}$$

$$\langle\sigma_m\rangle = E_m\langle\varepsilon_m\rangle \tag{3.13}$$

$$\langle\sigma_i\rangle = E_i\langle\varepsilon_i\rangle \tag{3.14}$$

E, E_m, and E_i are the moduli of the composite, matrix, and included phase, respectively. In the electrospun fiber mats, the included phase consists of voids, and therefore is assumed to have a modulus of zero, reducing equation 3.11 further to

$$\langle\sigma\rangle = (1 - c)\langle\sigma_m\rangle \tag{3.15}$$

which simply expresses the average stress in the composite material (i.e. the electrospun fiber mat) as the average stress in the matrix phase multiplied by the volume fraction of matrix phase in the composite. The volume fraction of inclusions is determined by the ratio of the density of the electrospun mat to the density of the bulk material

$$c = \rho_{electrospun} / \rho_{bulk} \tag{3.16}$$

In order to evaluate this model and determine if density is the determining component of the tensile strength of electrospun polyurethane mats, electrospun mats of varying densities are prepared. Producing mats of different densities is achieved by electrospinning a range of solutions that differ in polymer concentration and solvent composition. Two polyurethanes, Pellethane® 2103-80AE and Pellethane® 2363-55DE are tested and compared with the model. The relationship between fiber mat density and spinning solution concentration of each polymer system is presented graphically in Figure 3.6 and tabulated in Table 3.1.

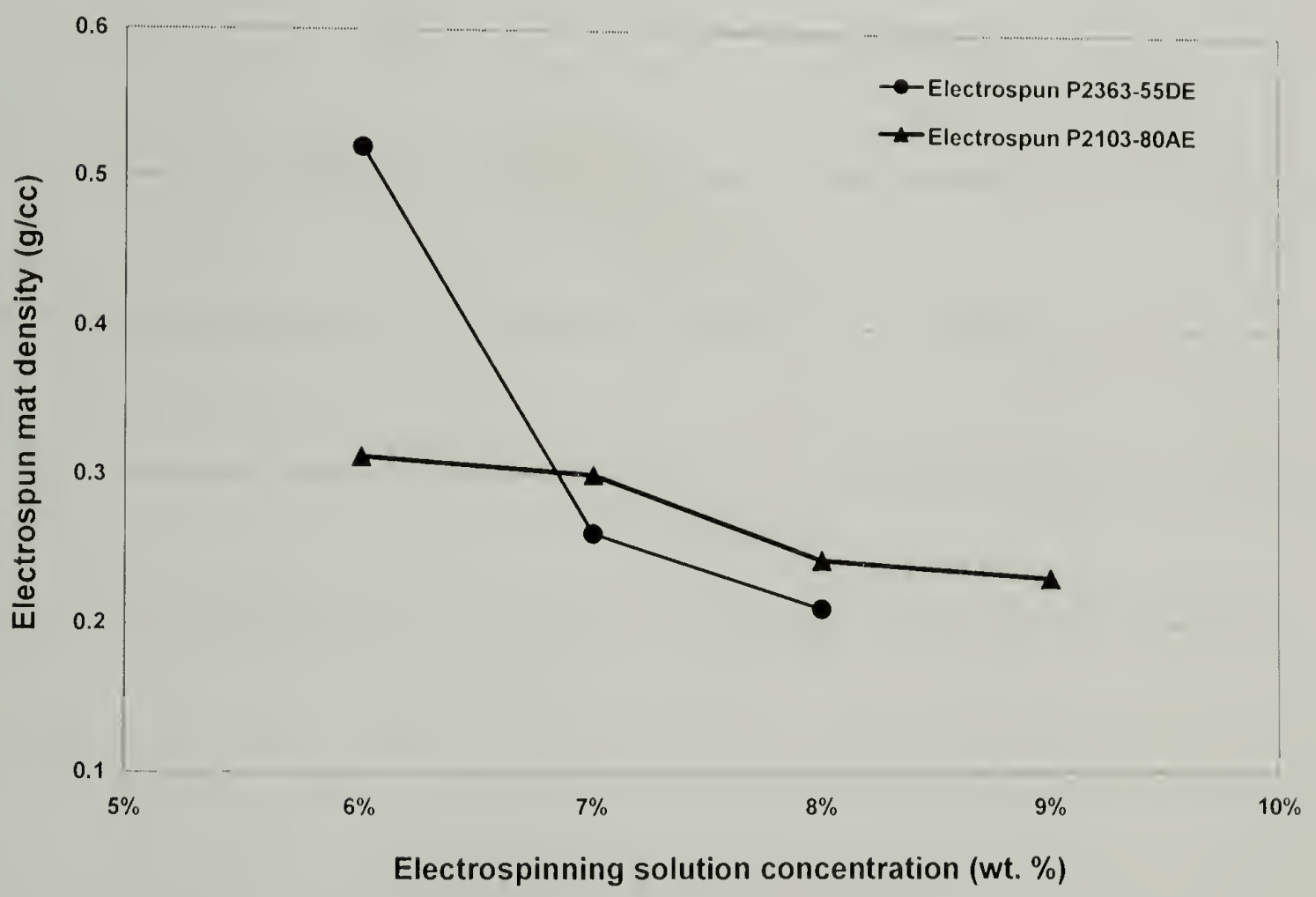

Figure 3.8 – Relationship between electrospinning solution concentration and resulting fiber mat density for Pellethane® 2103-80AE and Pellethane® 2363-55DE.

Polymer	Spinning solution concentration (wt. %)	Electrospun fiber mat density (g/cc)
Pellethane® 2103-80AE	6 %	0.312
	7 %	0.30
	8 %	0.243
	9 %	0.231
Pellethane® 2363-55DE	6 %	0.52
	7 %	0.26
	8 %	0.21

Table 3.1 – Spinning solution concentration and fiber mat density for Pellethane® 2103-80AE and Pellethane® 2363-55DE.

The modeling results for the tensile strength of electrospun polyurethane mats are illustrated in Figures 3.9 and 3.10 for Pellethane® 2363-55DE and Pellethane® 2103-80AE, respectively. In Figure 3.11, the data for each electrospun material has been normalized by the density and strength of their respective bulk analogs, and plotted on a common curve.

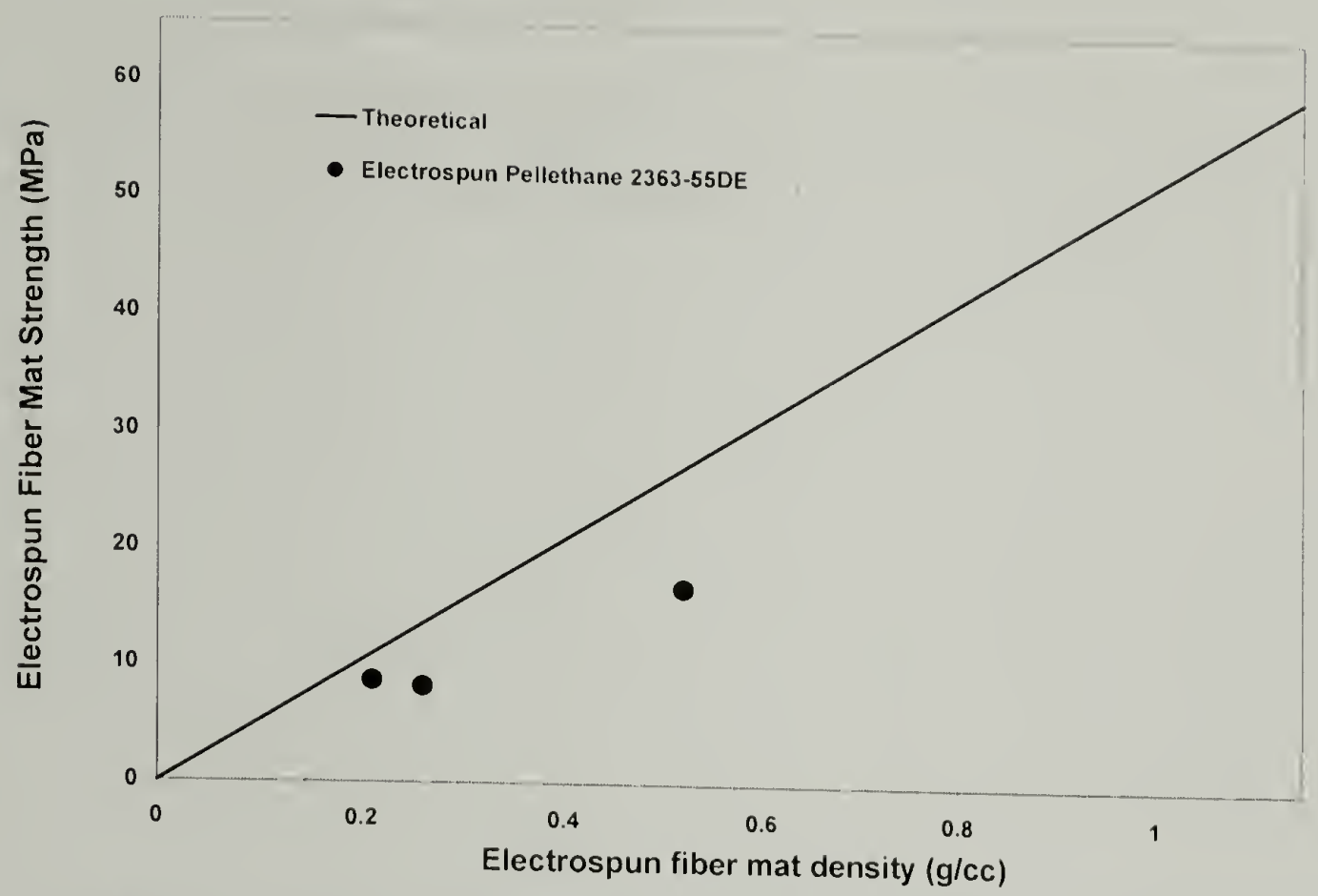

Figure 3.9 – Composite strength model and experimental data for electrospun Pellethane® 2363-55DE.

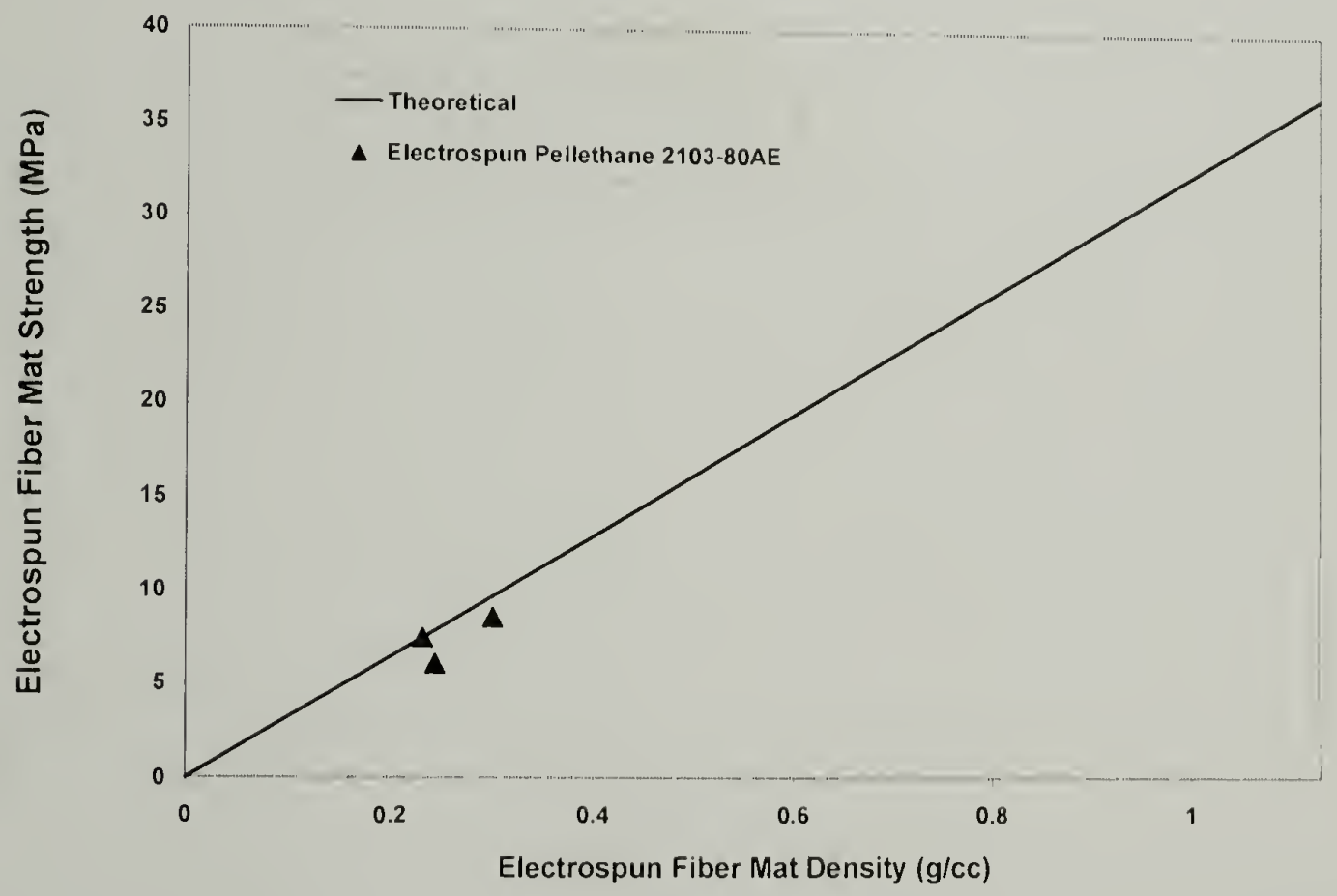

Figure 3.10 – Composite strength model and experimental data for electrospun Pellethane® 2103-80AE.

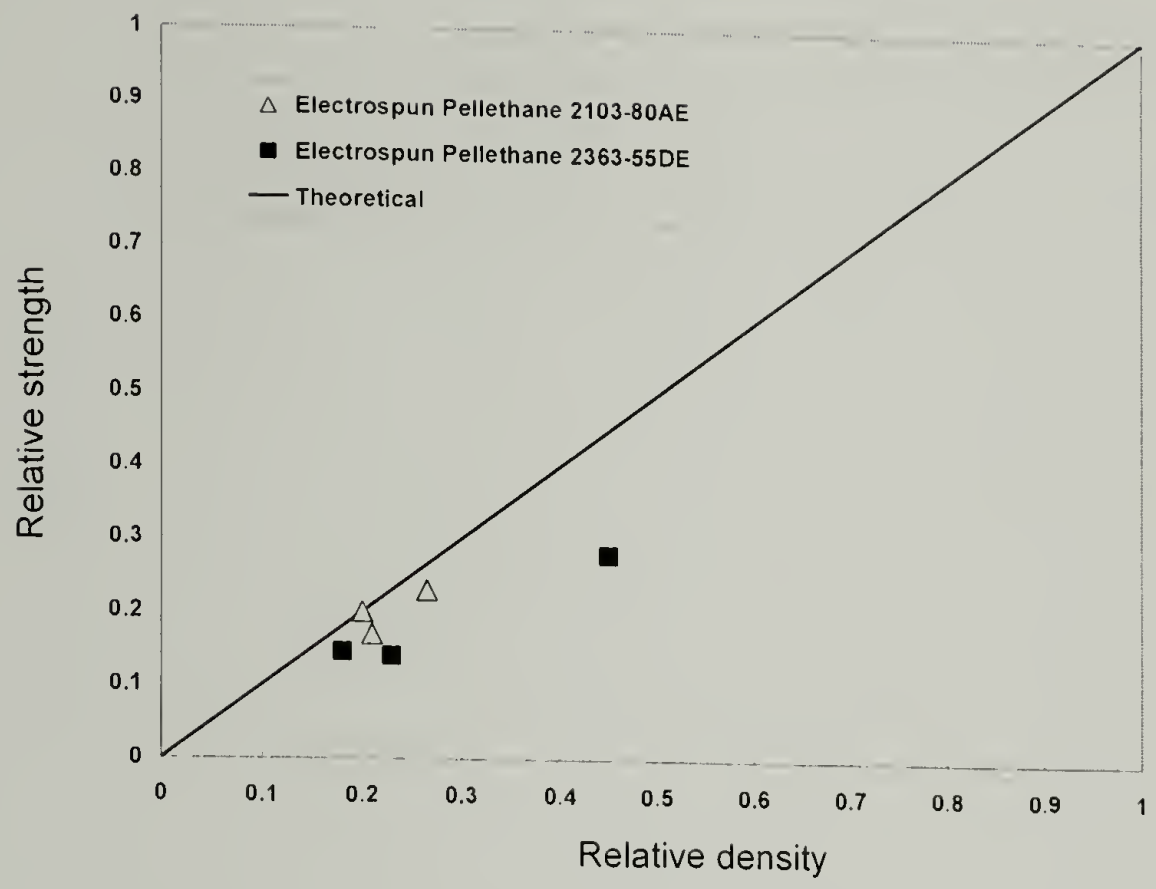

Figure 3.11 – Normalized composite strength model curve with experimental data (Pellethane® 2103-80AE and Pellethane® 2363-55DE).

There is a reasonable fit between the experimental data and the theoretical curves. Th result is interesting: a simple empirical relationship that specifies no details about the shape or size of inclusions in a two-component system, appears to have fairly good agreement with the experimental results for two electrospun materials. The fit of the data from the Pellethane® 2103-80AE appears to be slightly better than the fit for the electrospun Pellethane® 2363-55DE. Pellethane® 2363-55DE data points all fall below the theoretical line. This is possibly a consequence of the morphological phenomenon discussed in Chapter 2 of cracks in electrospun fibers. As illustrated in electron micrographs, the Pellethane® 2363-55DE electrospun fibers show a larger abundance of cracks than the Pellethane® 2103-80AE electrospun fibers. However, the

range of density and strength over with the Pellethane® 2103-80AE system is measured, is more limited than for the Pellethane® 2363-55DE. The densities of the various Pellethane® 2103-80AE fiber mats are very near one another; there is more distinction in the densities of the various electrospun Pellethane® 2363-55DE fiber mats. Overall, however, the range of all the experimental data is limited. When optimum electrospinning solution conditions are identified for a particular system in order to produce defect-free fibers, the range of solutions from which other defect-free fiber mats can be electrospun is limited to little more than 1-2% wt. above and below the optimum concentration. When polymer concentration is reduced, the bead-on-string morphology becomes prevalent as a result of more solvent being present in the electrospinning jet, increasing the surface tension of the jet, and promoting coalescence of the jet into regularly spaced spherical beads along the fiber as a result of instabilities discussed in Chapter 1. When polymer concentration is increased, a point is reached at which viscosity of the solution is so high that mass transport of solution to the electrospinning pipette tip becomes difficult. Additionally, at higher polymer concentrations, the electrospinning jet tends to dry quickly, due to rapid solvent evaporation, and often the electrospinning process is interrupted by a solidification of the Taylor cone.

3.2.3 Energy Method for Modeling Elastic Tensile Modulus

The tensile modulus of the two electrospun polyurethane systems is modeled by an energy method. Ultimately, the derived relationship takes into account only the relative densities of the isotropic and aligned electrospun mats of each material.

When a material is deformed elastically, the deformation ratio, λ, can be expressed in terms of strain, ε.

$$\lambda = 1 + \varepsilon \tag{3.17}$$

Further, the average deformation can also be expressed in terms of the average strain in the material

$$\lambda' = 1 + \varepsilon' \tag{3.18}$$

where λ' is the average deformation and ε' is the average strain of a fiber element at some orientation.

Equation 3.7, derived earlier in this chapter for the deformation of a single fiber element can be expressed in terms of the average strain in the material by substituting equations 3.17 and 3.18 into equation 3.7, to arrive at the following equation for average strain in an element, as a function of its orientation relative to applied strain direction

$$\varepsilon'(\varphi) = \varepsilon_1 [(3 \cos^2\varphi - 1) / 2] \tag{3.19}$$

Strain energy density in a material is

$$U = \tfrac{1}{2} \sigma'\varepsilon' = E\varepsilon'^2 / 2 \tag{3.20}$$

Which written in terms of the average strain is

$$E_{aligned}\, \varepsilon'^2(\varphi) / 2 = (E_{aligned}\, \varepsilon_1^2 / 2) [(3 \cos^2\varphi - 1) / 2]^2 \tag{3.21}$$

where $E_{aligned}$ is the elastic modulus of the aligned electrospun fiber mat. The total strain energy in the system, integrated over the volume in cylindrical coordinates is

$$\int_0^{\pi/2} E_{aligned}/2\ \varepsilon'^2(\varphi)\, dzdrd\varphi = (E\varepsilon_1^2/2)\ (3tR^2\pi/4) \qquad 3.22$$

Multiplied by $V_{aligned}/V_{aligned}$ (volume of the aligned fiber mat),

$$\Psi = E_{aligned}\varepsilon_1^2/2\ (3/4)[tR^2\pi/V_{aligned}]V_{aligned} \qquad 3.23$$

The term in the equation, $tR^2\pi/V_{aligned}$, will be represented by c, a volume fraction. The derivative of the internal energy, with respect to ε_1 , is

$$d\Psi/d\varepsilon_1 = \sigma_1\ V_{aligned} = E_{aligned}/\varepsilon_1\ (3/4)\ c\ V_{aligned}$$

$$E_{isotropic}\ \varepsilon_1 = E_{aligned}\ \varepsilon_1\ (3/4)\ c$$

$$E_{isotropic} = \tfrac{3}{4}\ E_{aligned}\ c \qquad 3.24$$

Equation 3.24 expresses the modulus of the isotpropic electrospun material relative to the modulus of an aligned electrospun mat of the same material as a function of c, volume fraction, which will be defined as the relative densities of the two electrospun materials

$$c = \rho_{isotropic} / \rho_{aligned} \qquad 3.25$$

Tables 3.3 and 3.4 show the comparison between experimental and model modulus values for electrospun Pellethane® 2103-80AE and Pellethane® 2363-55DE, respectively. Agreement between model and experimental data is good for Pellethane® 2103-80AE, but poor for Pellethane® 2363-55DE. There do not appear to be obvious

reasons for the poor agreement for the latter system, but an anomaly in that system is the fact that the density of the aligned electrospun fiber mat is actually lower than any of the isotropic electrospun Pellethane® 2363-55DE fiber mats. This is an atypical result in terms of relative mat densities, but does not necessarily account for the poor fit. It simply illustrates the variability in the materials that are produced by electrospinning, and perhaps the difficulty in developing an empirical model which can accurately describe the mechanical properties of a variety of electrospun materials.

Electrospinning solution concentration (%wt)	Aligned mat density (g/cc)	Aligned mat modulus (Mpa)	Isotropic mat density (g/cc)	Isotropic mat modulus (Mpa)	Model isotropic mat modulus (MPa)
7	0.39	6.4	0.30	3.2	3.7
8	0.39	6.4	0.24	2.0	2.9
9	0.39	6.4	0.23	3.0	2.8

Table 3.2 – Energy model results for electrospun Pellethane® 2103-80AE.

Electrospinning solution concentration (%wt)	Aligned mat density (g/cc)	Aligned mat modulus (Mpa)	Isotropic mat density (g/cc)	Isotropic mat modulus (Mpa)	Model isotropic mat modulus (MPa)
6	0.18	4.5	0.52	17.5	9.75
7	0.18	4.5	0.26	8.9	4.8
8	0.18	4.5	0.21	11.2	3.9

Table 3.3 – Energy model results for electrospun Pellethane® 2363-55DE

3.3 Conclusions

The mechanical behavior and properties—tensile strength and modulus—of electrospun thermoplastic polyurethanes are modeled in this chapter. The stress-strain response of an isotropic mat of electrospun Pellethane® 2103-80AE was modeled based on the stress-strain response of an aligned electrospun fiber mat of the same polymer. Model stress-strain data were computed with simple relationships that resolve the axial components of the force in the isotropic material based on the applied strain and the relative orientation of fiber elements in the electrospun mat. At a given strain, a critical angle is defined that determines which fibers contribute to the total stress in the isotropic mat, and ignores those fibers that do not contribute to the stress. The model curve underestimates the experimental data, but has a similar shape to the experimental stress-strain curve for the isotropic electrospun mat.

Tensile strength and elastic modulus of two electrospun polyurethane systems are modeled empirically. The tensile strength of the isotropic electrospun mats is

modeled with respect to the tensile strength of their respective bulk analogs through a relationship that was developed for 2-phase composite materials with a matrix and an included phase.[81] The experimental data for both electrospun materials follow the general trend of the model, yet fall below the model curves, perhaps as a result of the existence of cracks in the electrospun fibers, which reduces the overall strength of the electrospun mat.

An energy method was used to model the tensile modulus of isotropic electrospun mats, based on the elastic modulus of their respective aligned electrospun fiber analogs. The relationship between the moduli of the two materials—isotropic and aligned fiber mats—is based simply on a density factor. Agreement between experimental data and model is good for one system, Pellethane® 2103-80AE, but poor for the Pellethane® 2363-55DE system.

Both empirical models presented are based on the densities of the electrospun materials, which presents a limitation. In both polymer systems, and generally for electrospun polymers, the range of solution concentrations that can be electrospun into fibers free of defects such as beads, is relatively narrow. While a trend is shown between solution concentration and density of electrospun materials, the range of densities obtainable is relatively narrow within a single material system.

CHAPTER 4

COLOR CHANGE OF ELECTROSPUN FIBER MATS

4.1 Introduction

Morphologically, electrospun fiber mats resemble natural and synthetic polymeric cellular structures, or foams. This point is illustrated in Figures 4.1 and 4.2. Figure 4.1 shows a commercial polyurethane foam and cancellous bone tissue. Figure 4.2 shows electrospun polyurethane fibers.

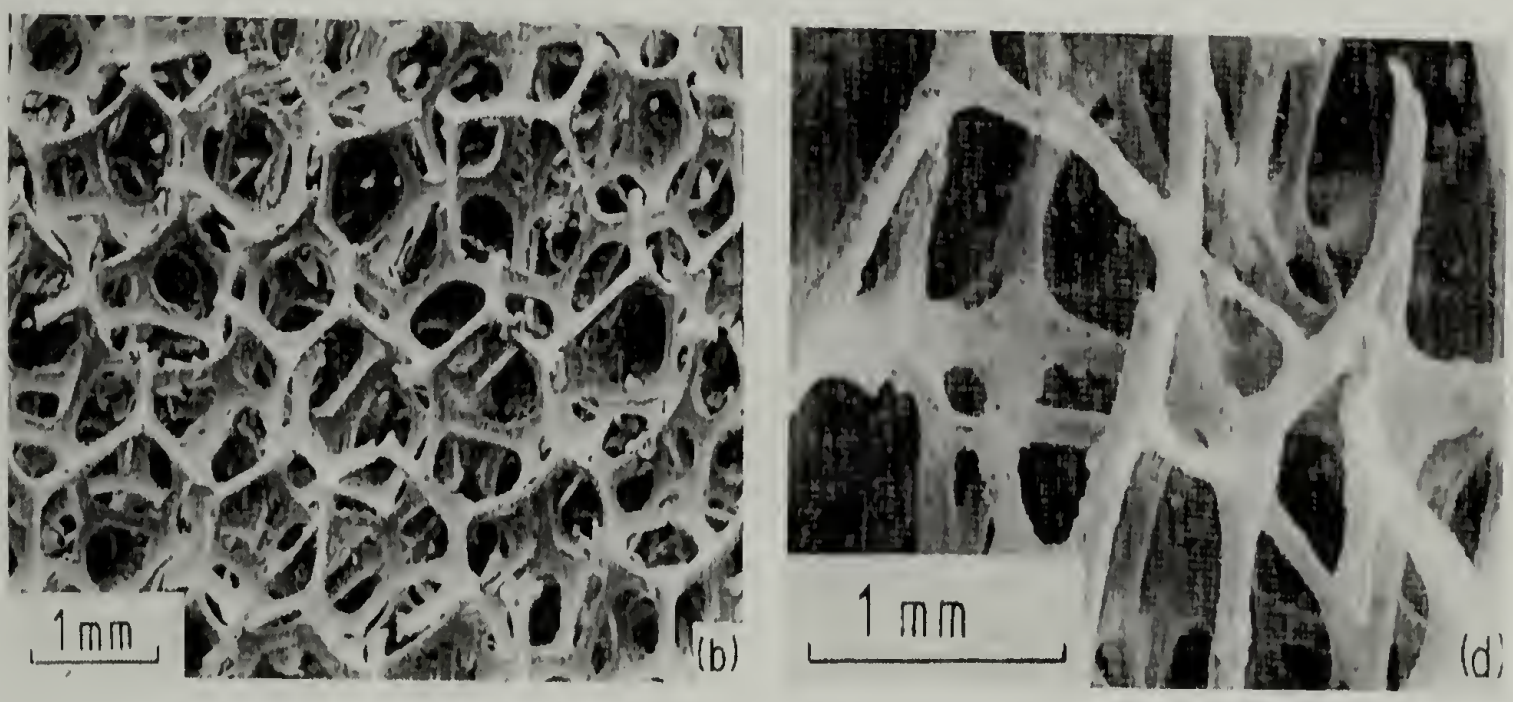

Figure 4.1 – Polyurethane foam (left) and cancellous bone (right).[89]

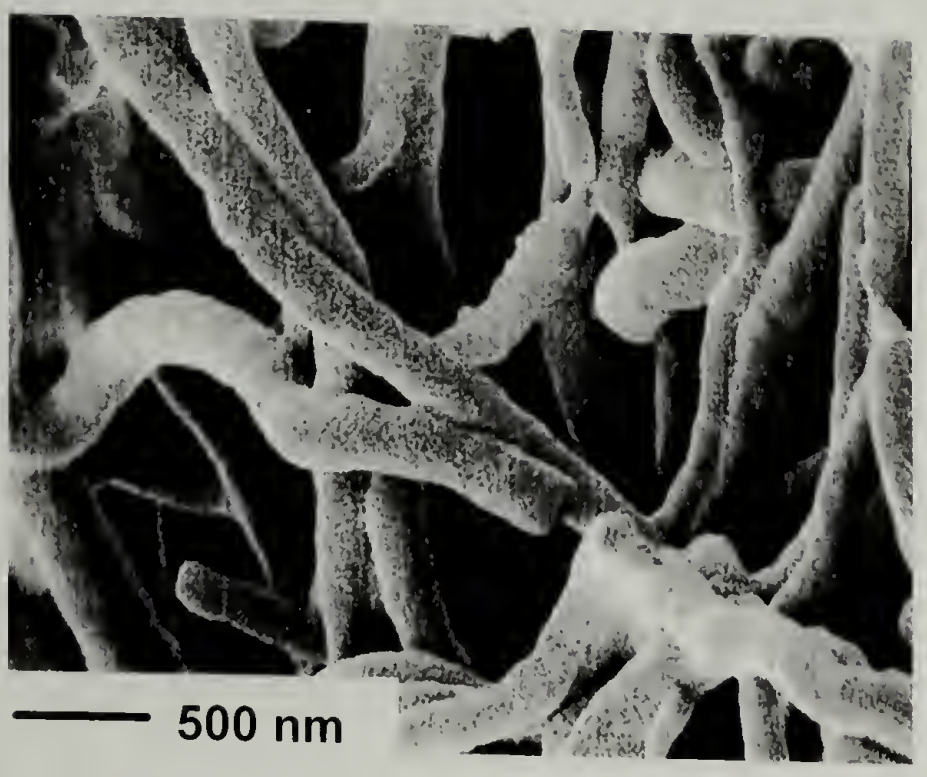

Figure 4.2 – Electrospun polyurethane.

In size, the electrospun fibers are many times smaller than the characteristic features of other common cellular materials. However, in terms of scattering visible light, foams and electrospun mats have similar characteristics such as high porosity and large surface area. In polymeric foams, the scattering of light is due to gas-solid interfaces, similar to gas-liquid interfaces in aqueous foams such as soapy water. The refractive-index mismatch at interfaces is large, resulting in many scattering events.[90] In electrospun fiber mats the number of scattering interfaces is even more numerous due to the extremely fine diameter of the fibers and large surface area of the material. This scattering gives electrospun samples their white opaque appearance.

When fiber mats are electrospun, their appearance is always white in color, irrespective of the polymer/solvent system. In this chapter, a study is made concerning the color of electrospun fiber mats when fillers of color are added to electrospinning solutions. Three different polymer solutions containing carbon black are electrospun to

make isotropic fiber mats. In each of the systems described, when fiber mats are prepared, the black spinning solutions produce white fiber mats. When these fiber mats are subsequently heated, their color changes from white to black at a characteristic temperature for the respective polymers. The electrospun carbon black-containing fiber mats are further demonstrated to be candidate materials for thermal imaging media.

4.2 Materials

Three polymer/solvent systems were investigated to demonstrate the phenomenon of color change produced by electrospinning. The concentrations and solvents for each system were chosen to optimize the electrospinning process and achieve maximum color change from solution to fiber mat.

The following polymer/solvent systems were prepared and electrospun:

1. polycarbonate (PC) with ≈ 2% carbon black (as received); 14% wt. polymer in tetrahydrofuran (THF) / N,N-dimethyl formamide (DMF) (1:1)
2. poly(ethylene oxide) (PEO); Mw ≅ 2,000,000 g/mol, 2%wt. polymer in water, with 5%wt.(of polymer) carbon black
3. poly(methyl methacrylate) (PMMA), M_w ≅ 120,000 g/mol, 15% wt. polymer in tetrahydrofuran/N,N-dimethyl formamide (1:1) with 1%wt.(of polymer) carbon black

PMMA, PEO, THF and DMF were received from Aldrich Chemical Company. Polycarbonate was provided by Motorola, Inc. All polymers and solvents were used

as-received. Carbon black was received from Cabot, in three sizes, characterized by their surface area—27, 119, and 130 m^2/gram.

4.3 Experimental

The polycarbonate solution was prepared by dissolving black PC (≈ 2% carbon black) pellets in an equal mixture of tetrahydrofuran and N,N-dimethylformamide. The PMMA and PEO solutions were prepared by dissolving neat polymer completely, followed by addition of carbon black and vigorous stirring for at least 24 hours to promote homogeneous dispersion of the carbon black in the solution. Ultimately, all solutions were homogeneously black in color when each was electrospun. Each solution was electrospun onto an aluminum weigh pan and allowed to dry at room temperature and pressure for at least 24 hours prior to subsequent experimentation. Electrospun mats were heated and observed on a Fisher-Johns (Fisher Scientific) melting point apparatus, at a heating rate of approximately 10°C/minute. When a visible color change was observed, the specimen was removed from the hot stage and the temperature recorded. All specimens were sputter coated with gold and examined with a JEOL 35-CF scanning electron microscope at 20 kV accelerating voltage. Differential scanning calorimetry experiments were performed on a DSC 2910 Differential Scanning Calorimeter (TA Instruments, Inc.) at a heating rate of 10°C/minute.

4.4 Results and Discussion

The electrospun polymers were chosen to demonstrate the reproducibility of the color change phenomenon among a variety of systems including amorphous and semicrystalline polymers, with organic and aqueous solvents; a solution of a polymer resin compounded with carbon black was compared to solutions prepared from neat polymers with carbon black post-added to solution. Each of the polymer solutions described in the materials section is black in color. When the solutions are electrospun, the resulting isotropic fiber mat is white, or nearly white, in color. The transmission of light through a foam of finite thickness increases as the average void size grows. In other words, as the number of scattering surfaces decreases, the static transmission of light increases and the amount of scattered light decreases. Therefore, maximum light scattering occurs when the number of gas-solid interfaces is maximized—very effectively achieved in electrospun mats by decreasing average fiber diameter which increases total surface area. In the case of an amorphous polymer, the bulk solid material has no gas-solid interfaces, and no crystals to scatter light, and the material is optically transparent. Conversely, the electrospun form of the same amorphous polymer has many gas-solid interfaces which scatter light. This relationship holds true for black, as well as translucent, polymers. In black electrospinning solutions, the carbon black filler absorbs all wavelengths of light. When a black solution is electrospun and a fibrous, porous mat is prepared, the scattering from numerous gas-solid interfaces precludes absorption of the light by the carbon black filler within individual electrospun fibers. An electrospun mat with fibrous morphology and average fiber diameters in the sub-micron size range is a necessary condition for a black solution to electrospin to a

white mat. Proof that carbon black particles are traveling with the electrospinning jet and residing within the collected electrospun fibers is seen when the fiber mats are heated. In each of the electrospun systems described, the fiber mats turn black in color when heated to a characteristic temperature. The following sections will relate the macroscopically observed color change upon heating experienced by each of the electrospun fiber mats with the underlying microscopic morphology change. It should be noted that all electron micrographs are black and white, and in no way are meant to represent the observed macroscopic color change in the electrospun materials. The observed color of the electrospun mats at all temperatures are noted in parenthesis in the figure captions.

4.4.1 Polycarbonate

Figure 4.3 shows the morphology and size of electrospun fibers spun from solutions of polycarbonate in an equal mixture of DMF and THF, with and without carbon black. A common feature of both systems is the bead-on-string morphology. The observed color of both electrospun materials is white, resulting from the light scattering produced by the porous, foam-like morphologies. When the mat electrospun from neat solution is heated, it becomes optically clear.

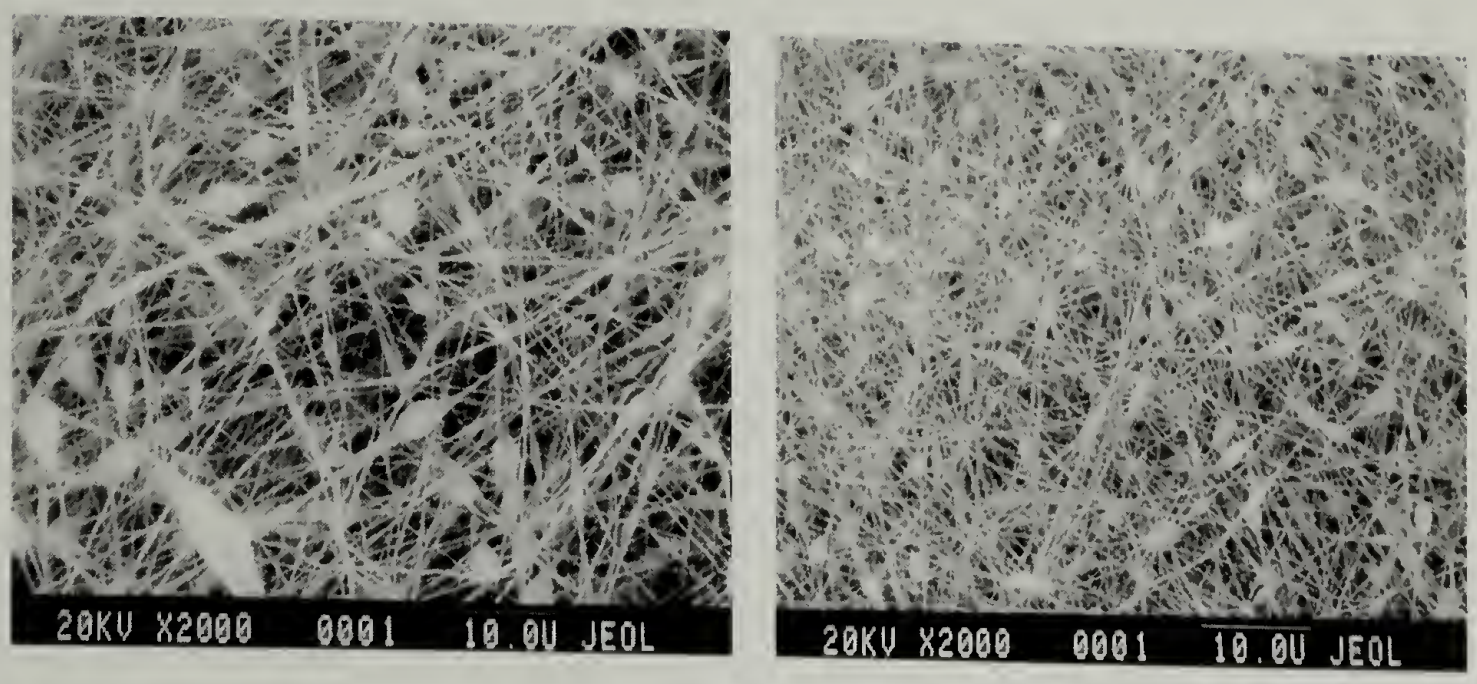

Figure 4.3 – Electrospun polycarbonate: no carbon black (left); with 2 % carbon black (right) (both fiber mats are white).

When the mat electrospun from the black solution is heated, it turns black in color. Figure 4.4 shows scanning electron micrographs of the morphology change of electrospun polycarbonate containing carbon black as the material is heated and changes color macroscopically. At 120°C, the morphology is essentially unchanged from the original morphology, and the color of the mat remains white. As the temperature is increased to 140°C, a slight coarsening of the electrospun fiber structure occurs. The beads that were lenticular in shape at room temperature become more spherical in shape. This coarsening results in a slight color change of the fiber mat from white to light gray. At 160°C, all fibers have essentially coalesced and the morphology is essentially a porous film. The slight porosity produces a small amount of scattered light, and the material appears dark gray in color. At 175°C, the material is completely coalesced into a film, with very few pores. The numerous surfaces and gas-solid interfaces that produced scattering no longer exist, and the material appears black in color.

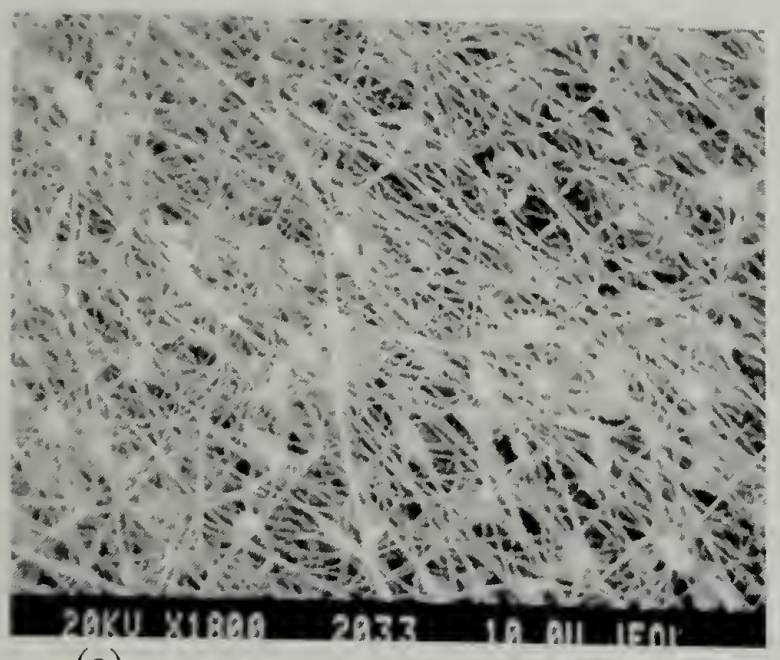

(a)

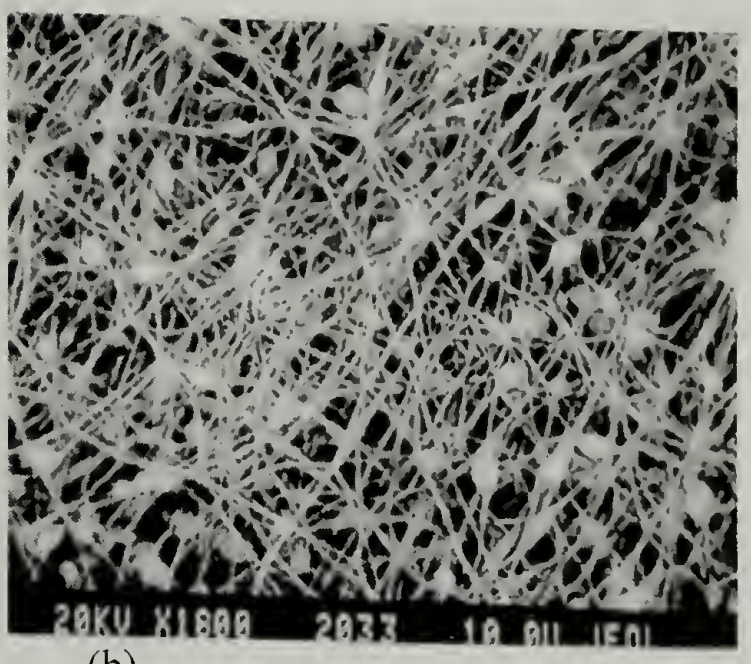

(b)

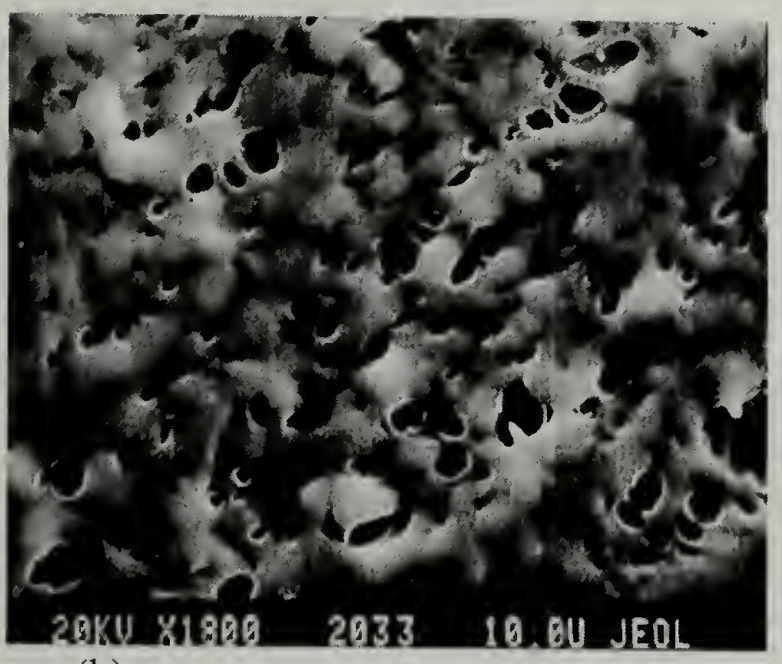

(b)

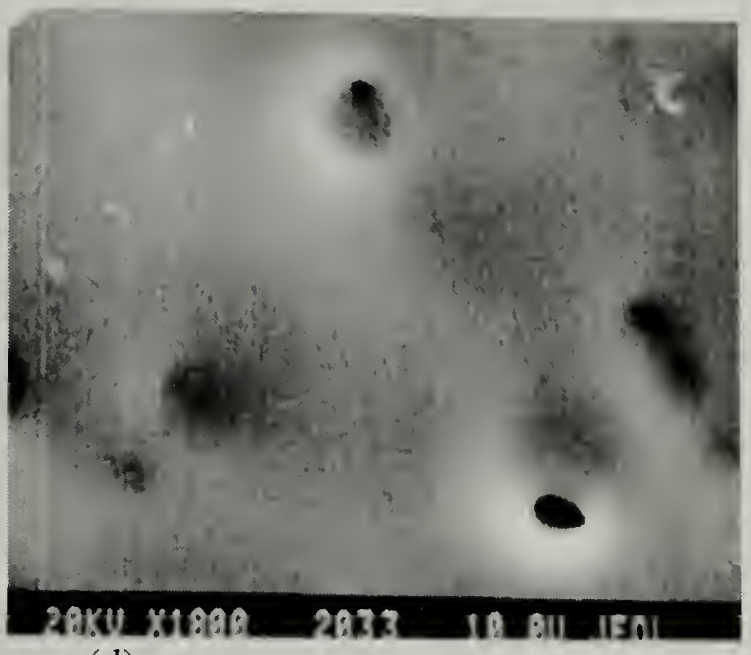

(d)

Figure 4.4 – Electrospun polycarbonate heated to (a) 120° C (white), (b) 140° C (light gray), (c) 160° C (dark gray), (d) 175° C (black).

As illustrated by the electron micrographs in Figure 4.4, the most significant change from fibrillar morphology to more film-like morphology occurs between 140° C and 160° C. This temperature range encompasses the glass transition temperature of the electrospun polycarbonate, as seen in differential scanning calorimetry. The DSC heating scan of the electrospun polycarbonate with carbon black is shown in Figure 4.5. The glass transition temperature (T_g) is observed at approximately 142° C. When the

electrospun material is heated to temperatures above its glass transition temperature, the material flows and leads to the gross coalescence of fibers into the porous film seen in Figure 4.4c.

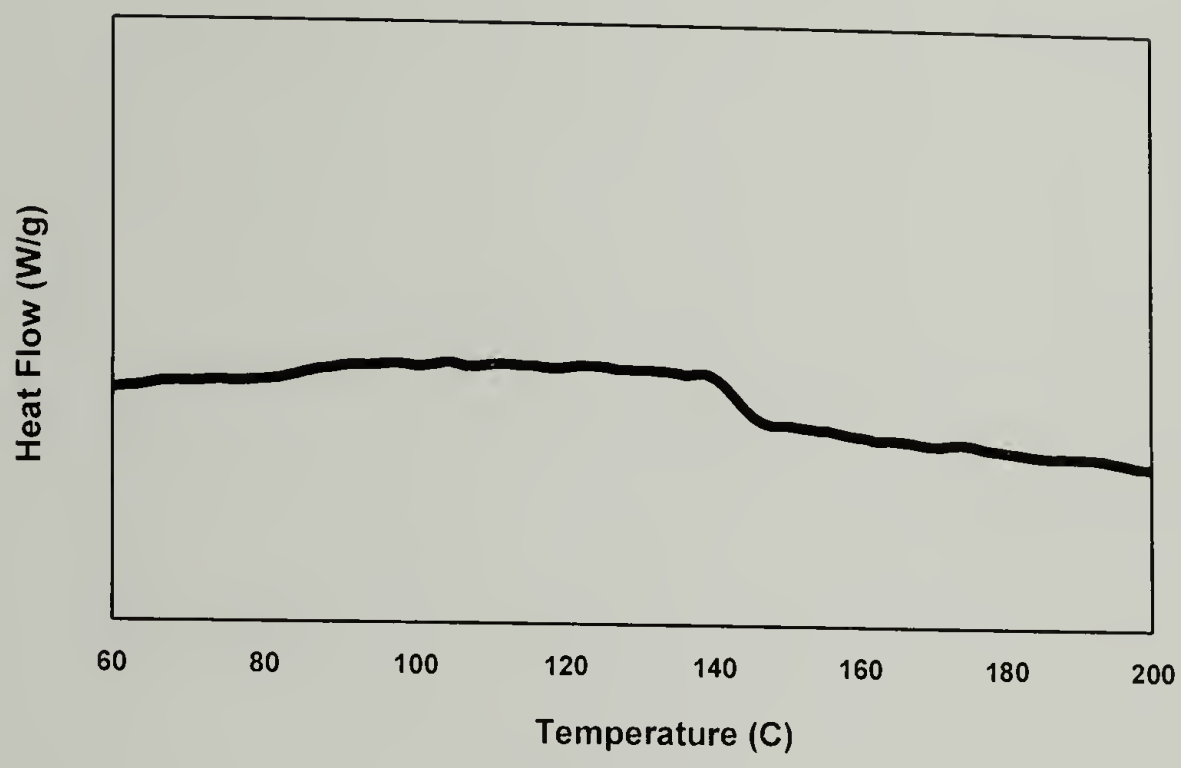

Figure 4.5 – DSC heating scan of electrospun polycarbonate with carbon black.

4.4.2 Poly(ethylene oxide)

Electrospun PEO/carbon black shows similar results to those seen for electrospun polycarbonate, as well as some notable differences including fiber morphology, color change temperature, and the progression of color change upon heating. Figure 4.6 is an electron micrograph that shows the morphology of electrospun PEO with carbon black. The density of beads in the electrospun material is high, and more populated than in the electrospun PC/carbon black system. However, the notable characteristic of the features seen in Figure 4.6 is that the fibers, as well as the numerous beads are less than 1.0 micron in size, and are typically in the range of 500 nanometers

and less. Although the occurance of beads is high, the size of the beads and electrospun fibers remains very small, and the surface area and number of scattering gas-solid interfaces remains very high. As a consequence, the electrospun fiber mat appears white in color. Figure 4.7 is a scanning electron micrographs showing the electrospun PEO/carbon black material after being heated to 65° C. The material shown in Figure 4.7 is black in color. The morphological change of electrospun PEO from fibrillar to film-like upon heating is relatively abrupt, in contrast to the PC/carbon black system. However, the microscopic and macroscopic observed changes are similar. The electrospun PEO/carbon black begins as a fibrous mat with numerous scatting surfaces and appears white in color. When heated, the material flows and fibers coalesce to form a material with a film-like morphology, which has a greatly reduced number of scattering surfaces, and appears black in color. The heated material is somewhat porous, and remnants of the fibrous morphology can be seen, but the film-like morphology is dominant and has far fewer scattering interfaces that the material prior to heating and coalescence.

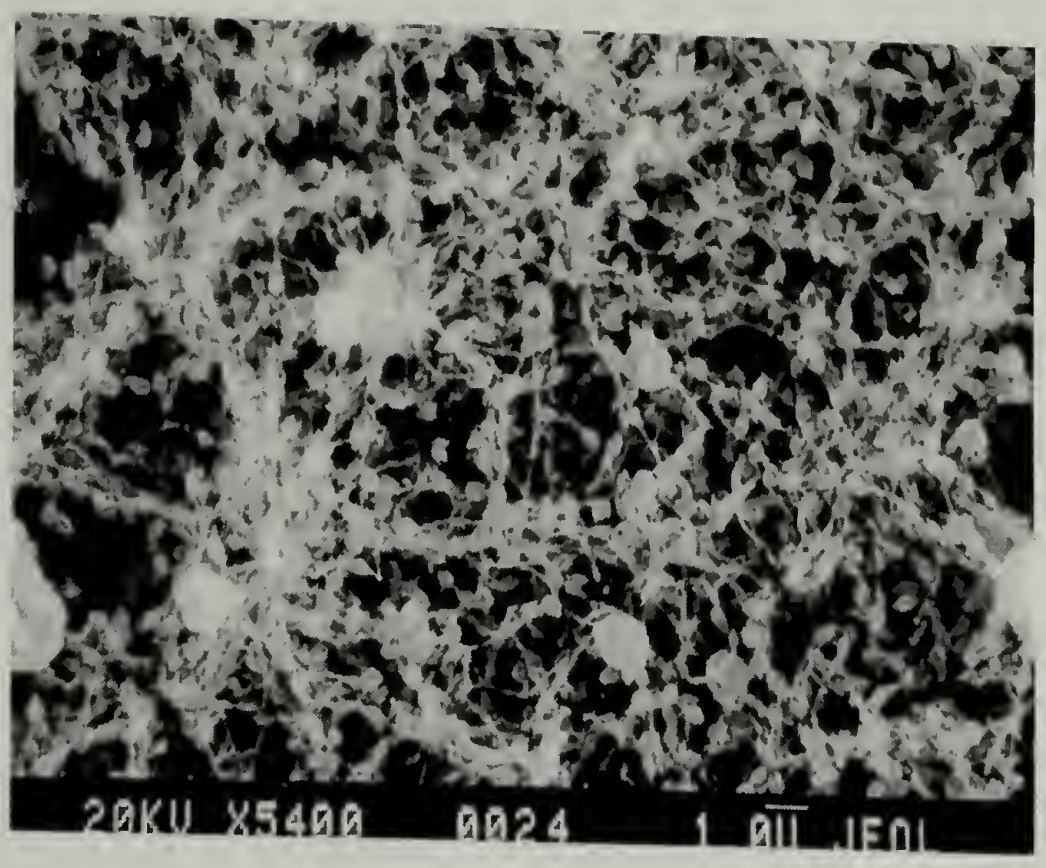

Figure 4.6 – Electrospun poly(ethylene oxide) with 5% carbon black; room temperature (white).

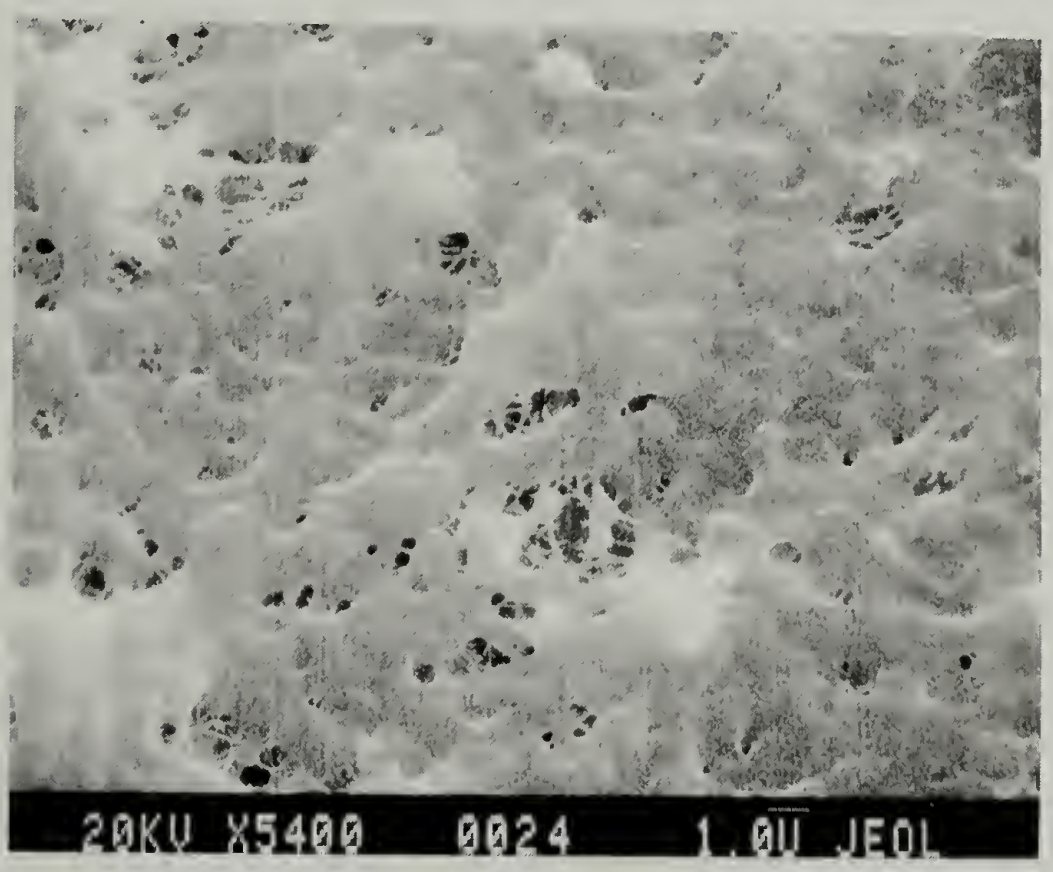

Figure 4.7 – Electrospun poly(ethyelene oxide) with 5% carbon black; 65° C (black).

The observed color change in the material from white to black corresponds to the melting transition of the material, as observed by differential scanning calorimetry.

The DSC heating sean of the eleetrospun PEO/earbon blaek is shown in Figure 4.8. The eolor change experieneed by the eleetrospun PEO/carbon blaek is abrupt from white to black, rather than passing through shades of gray, as is observed in the PC/carbon black system. This is perhaps a consequence of the thermal transition through whieh this color ehange eomes about. For electrospun PC, the material passes through a glass transition temperature, whieh promotes material flow, but temperatures higher than T_g are required to achieve full color change from white to black. For eleetrospun PEO, the thermal transition is erystalline melting, whieh is a true solid-liquid transition. As a result, the material flows at the onset of the melting transition. The eleetrospun fiber morphology is quickly lost in favor of the film-like morphology whieh eauses the color ehange of the eleetrospun material from white to blaek.

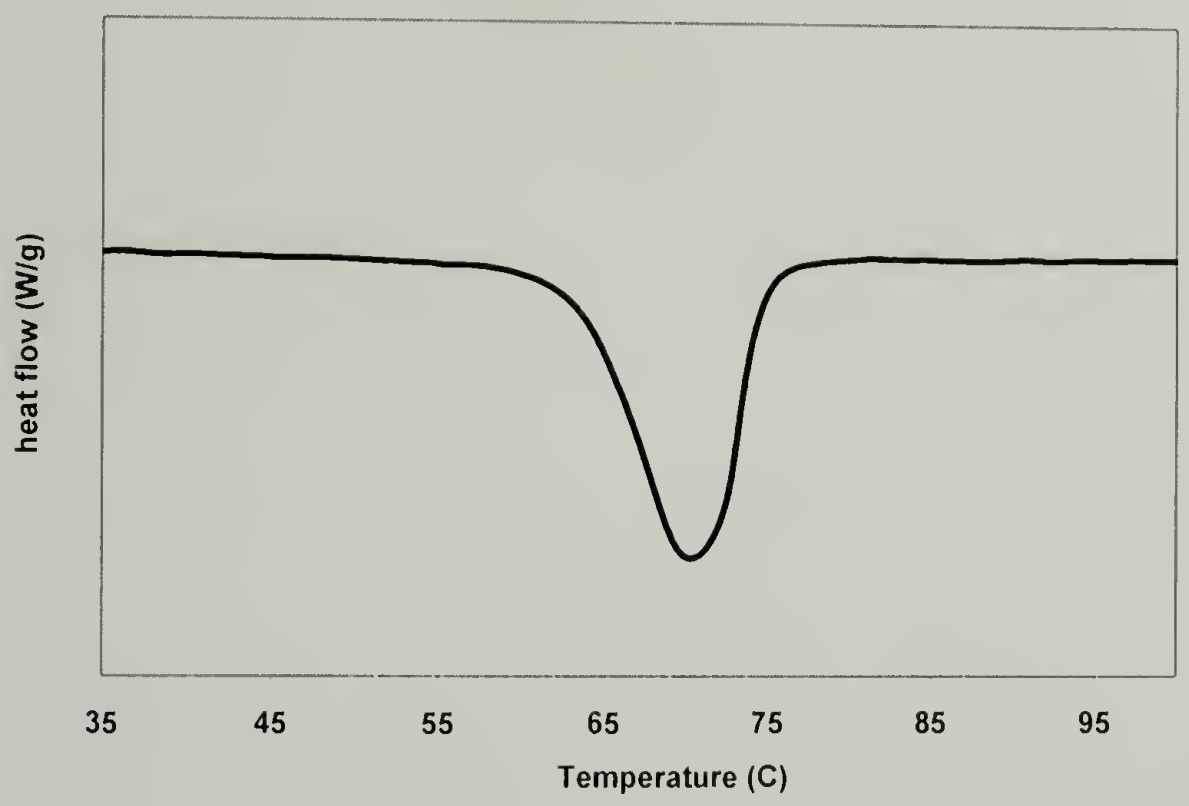

Figure 4.8 – DSC heating scan of eleetrospun PEO with 5% earbon black.

4.4.3 Poly(methyl methacrylate)

The third polymer studied is poly(methyl methacrylate). PMMA/carbon black was chosen to be a comparable amorphous system to PC/carbon black. In contrast to the precompounded PC/carbon black system, neat PMMA resin was dissolved in solution, followed by addition of carbon black to the solution prior to electrospinning. The initial results are similar to the other two previously described systems, in that the black spinning solution produces a white fiber mat when it is electrospun. The morphology of electrospun PMMA/carbon black is shown in the electron micrograph in Figure 4.9a. Electrospun PMMA/carbon black shows similarities to electrospun PC/carbon black. The bead-on-string morphology is prevalent in electrospun PMMA. A key difference between electrospun PC and PMMA is the fiber and bead size of each. A qualitative comparison of the two electrospun systems shows that the size of the electrospun fibers and beads of electrospun PMMA are typically larger than for electrospun PC. This size difference results in a slight difference in the color of electrospun PMMA, compared to electrospun PC and PEO. The color of the electrospun PMMA mat prior to heating is slightly off-white. This may be caused by the existence of beads which have diameters of at least 5 micrometers. These relatively large features reduce the overall effective surface area of the material, as well as present aggregates, containing carbon black, that apparently absorb some light and create the observed off-white appearance. A comparison of electrospun PMMA/carbon black and PC/carbon black is shown in Figure 4.9.

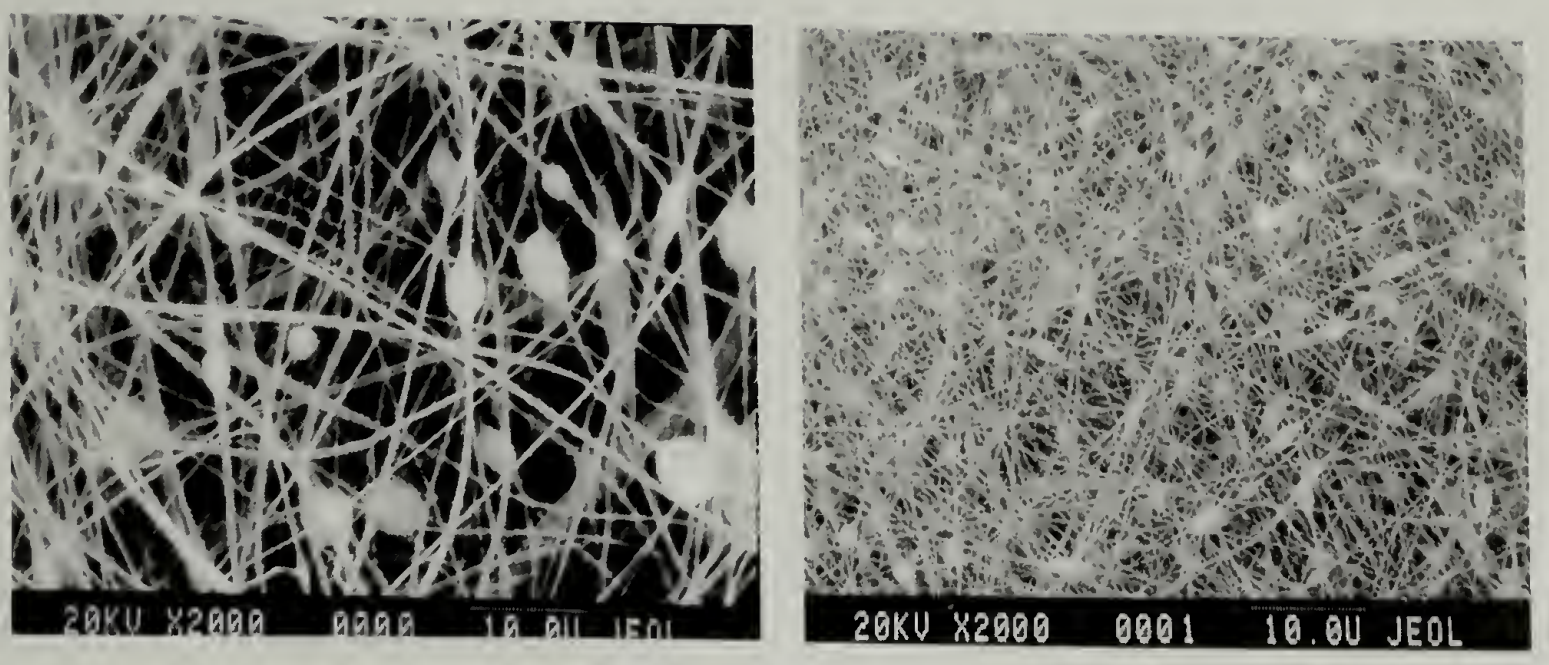

Figure 4.9 – Electrospun PMMA/carbon black (left) and electrospun PC/carbon black (right).

When the PMMA/carbon black fiber mat is heated, the result is again similar to the other systems. The progression of color change from white to black closely resembles that seen for the PC/carbon black system. The morphological change of the material when heated is illustrated in the series of electron micrographs in Figure 4.10. The color change of the white electrospun mat is gradual, through darkening shades of gray, and eventually becomes completely black at approximately 185° C.

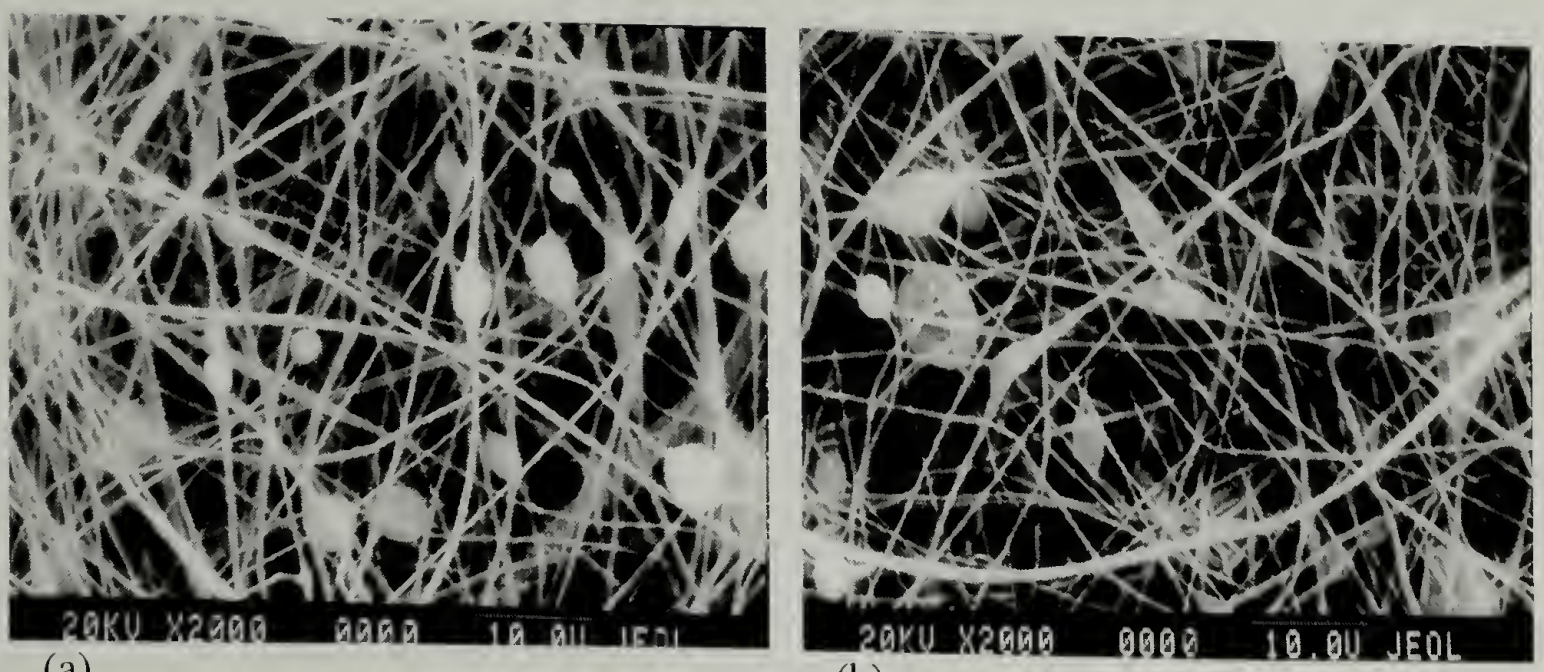

(a) (b)

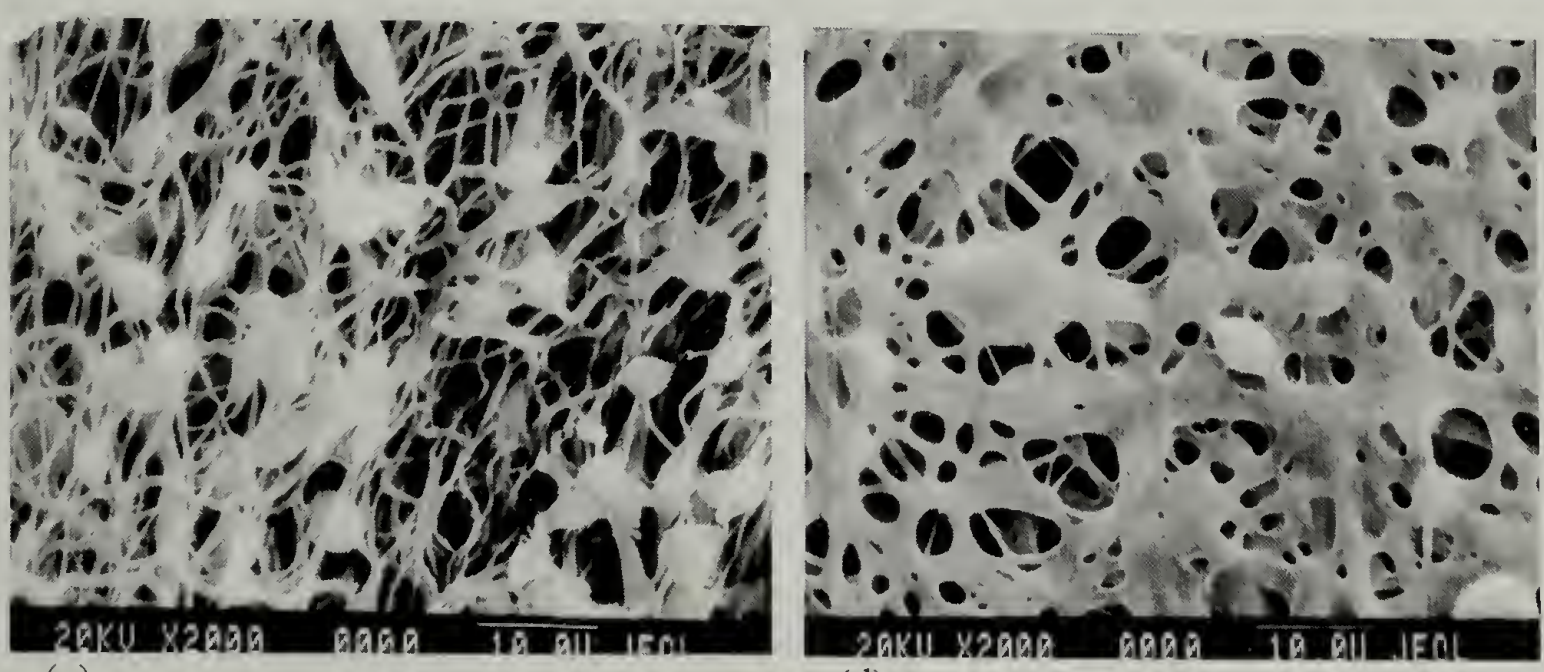

(c) (d)

Figure 4.10 – Electrospun PMMA with 1% carbon black: (a) room temperature (white), (b) 120° C (light gray), (c) 160° C (dark gray), (d) 185° C (black).

As the electrospun material is heated and changes from a fibrous morphology at room temperature to film-like at 185° C, the macroscopic color of the material changes from off-white to black. As described previously, the color change of the electrospun material from white to black is the result of gross material flow and coalescence of fibers into a film-like morphology. The number of scattering surfaces is greatly reduced with this morphology change, and diffuse light scattering is no longer dominant, but is replaced by absorption of the light by the carbon black in the film. The anomaly for the

electrospun PMMA/carbon black system is the temperature at which the most dramatic color change is observed. Differential scanning calorimetry—shown in Figure 4.11—indicates that the glass transition temperature of electrospun PMMA is the same as a typical bulk PMMA sample—100 - 105° C. Color change from white to black of the electrospun PMMA/carbon black does not begin, however, until approximately 120° C, and obvious morphological coarsening of the fiber mat does not occur until 160° C. The fiber mat does not become completely black until 185° C. As discussed previously, the observed color change is the effect of a morphological change from fibrous to film-like which results from material flow above T_g or T_m. The electrospun PMMA material used in this study has a relatively high molecular weight—approximately 120,000 g/mol—and well above the entanglement molecular weight for PMMA.[91-92] At this molecular weight, the PMMA above Tg is a rubbery material and does not undergo gross material flow. In addition, the amount of material used for the melting point observation studies was very small, further precluding any large scale material flow even when heated to above its glass transition temperature. Higher temperatures are required to promote flow and coalescence of the material from fiber mat to film like, and produce the observed color change from off-white to black.

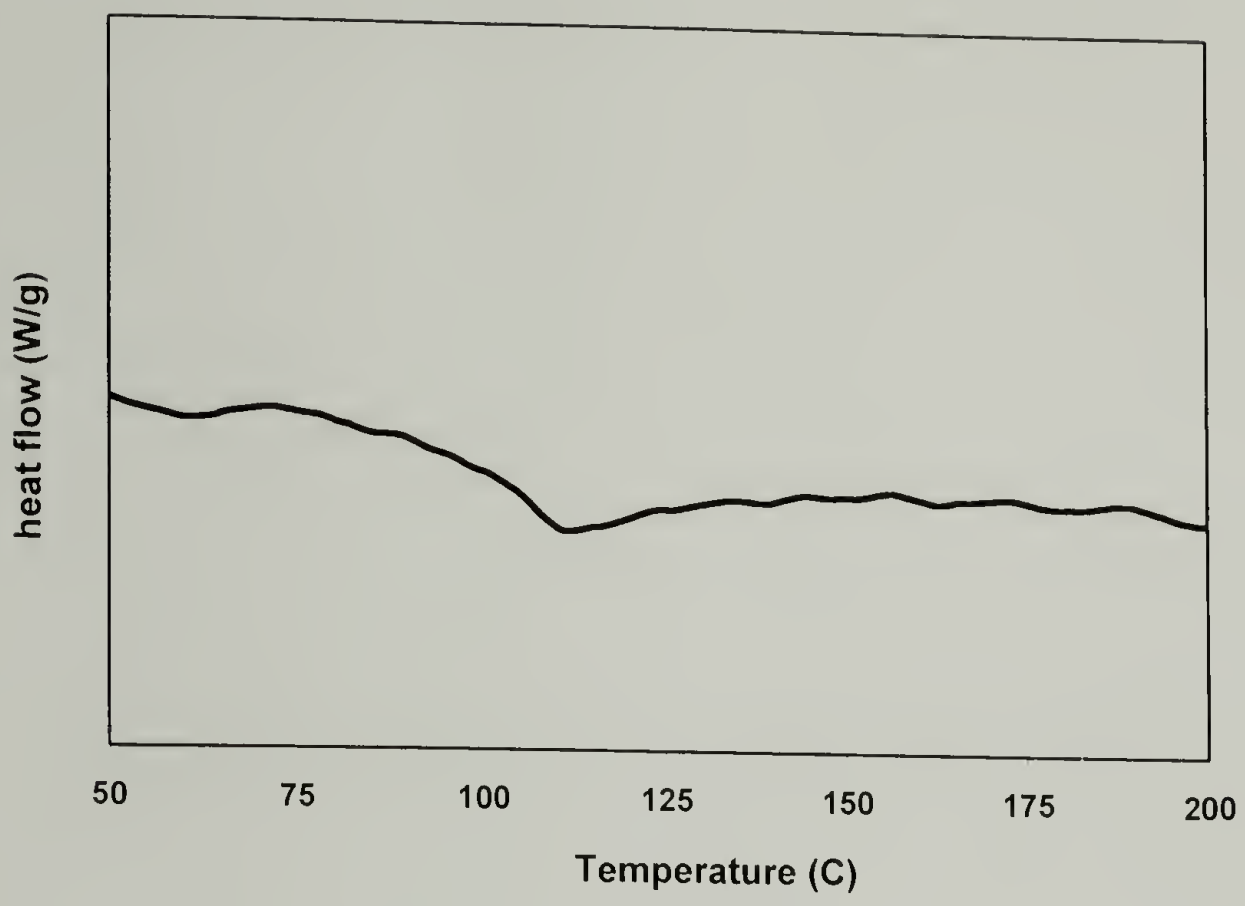

Figure 4.11 – DSC heating scan of electrospun PMMA with 1% carbon black.

In addition to nanoscale fibers, a morphological characteristic common to all three electrsopun systems is a bead-on-string morphology of the fibers. This morphological phenomenon has previously been observed and reported in the literature and reviewed in Chapter 1. In the context of eolor change, the size and number of the beads seen in the SEM mierographs for each system are important. The degree of "whiteness" of the electrospun fiber mats differs for eaeh system, and is dependent on the fiber and bead sizes. The eleetrospun PC/earbon black shows the smallest fibers and fewest beads, and consequently appears the whitest of all the electrospun fiber mats presented in this ehapter. The electrospun PEO/carbon black has many beads, but of small size—typieally less than 1 micron in diameter—and has a white fiber mat. The electrospun PMMA/carbon black has few beads, but relatively large fibers and has an

off-white appearance. The necessity of fibrillar morphology in order to achieve a color change from black solution to white mat is supported by an electrospun polyurethane/carbon black system. Figure 4.12 is an electron micrograph showing a polyurethane electrospun from 9.5% wt. in DMF with 1% carbon black. This electrospun material is black.

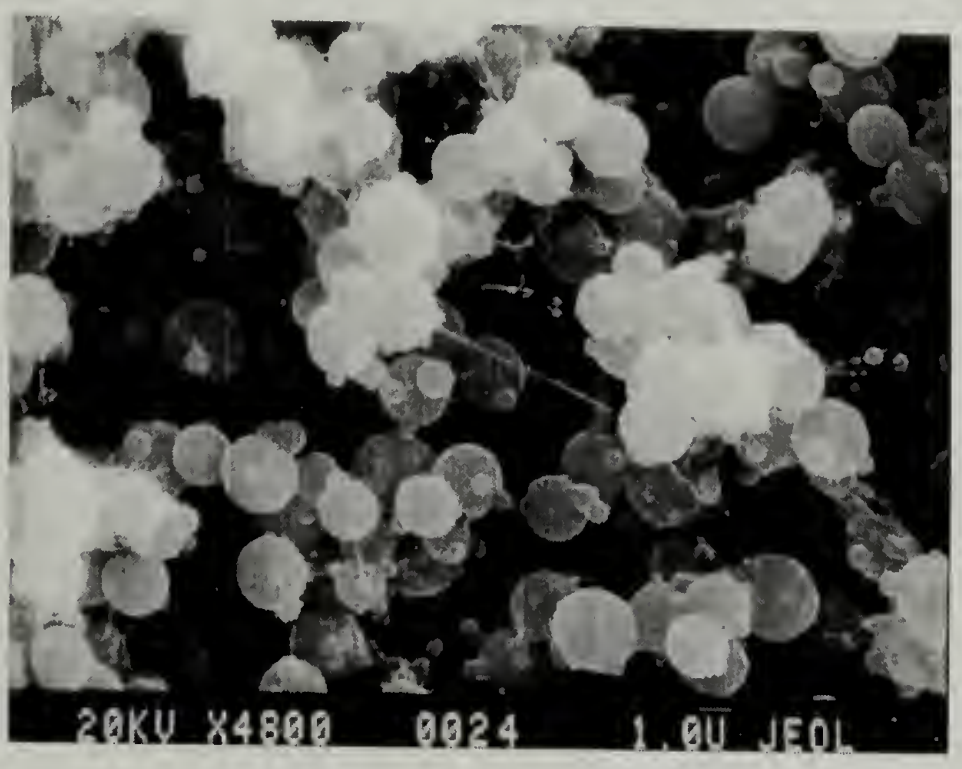

Figure 4.12 – Electrospun polyurethane with 1% carbon black; room temperature (black).

Spherical particles constitute the most significant morphology of the electrospun PU/carbon black, while few fibers are detectable in the micrograph. The size of the spheres is typically larger than 1.0 micrometer in diameter. The spinning solution is black, and the resulting electrospun material is black as well. The lack of fibrillar morphology and predominance of relatively large spherical particles reduces the number of scattering interfaces and results in a black, rather than white, electrospun mat.

4.5 Applications

Thermally induced color change materials are potentially useful for a simple application such as single use temperature sensors, owing to their selectivity of color change based on material-specific thermal transitions. Another, more advanced application which has been realized and demonstrated in collaboration with Eastman Kodak Company is the use of the electrospun materials as thermally imageable media. Taking advantage of the color change in some systems as a gradual progression from white to black through darkening shades of gray, the PC/carbon black system in particular was used to create a grayscale image by simple thermal scanning of an electrospun mat. The image shown in Figure 4.13 is electrospun PC/carbon black imaged with a laser by locally heating the electrospun mat at a number of mapped locations based on a digitally scanned imaged. The dark and light areas of the image indicate locations on the mat where relatively high and low energies were applied, respectively. Figure 4.14 is an optical micrograph showing the boundary between an area of imaged material and unimaged material. In the imaged area, wrinkles can be seen that result from shrinkage and coalescence of the fiber mat when it is locally heated.

Figure 4.13 – Thermally imaged electrospun PC/carbon black fiber mat (original image size is approximately 3x5 centimeters).

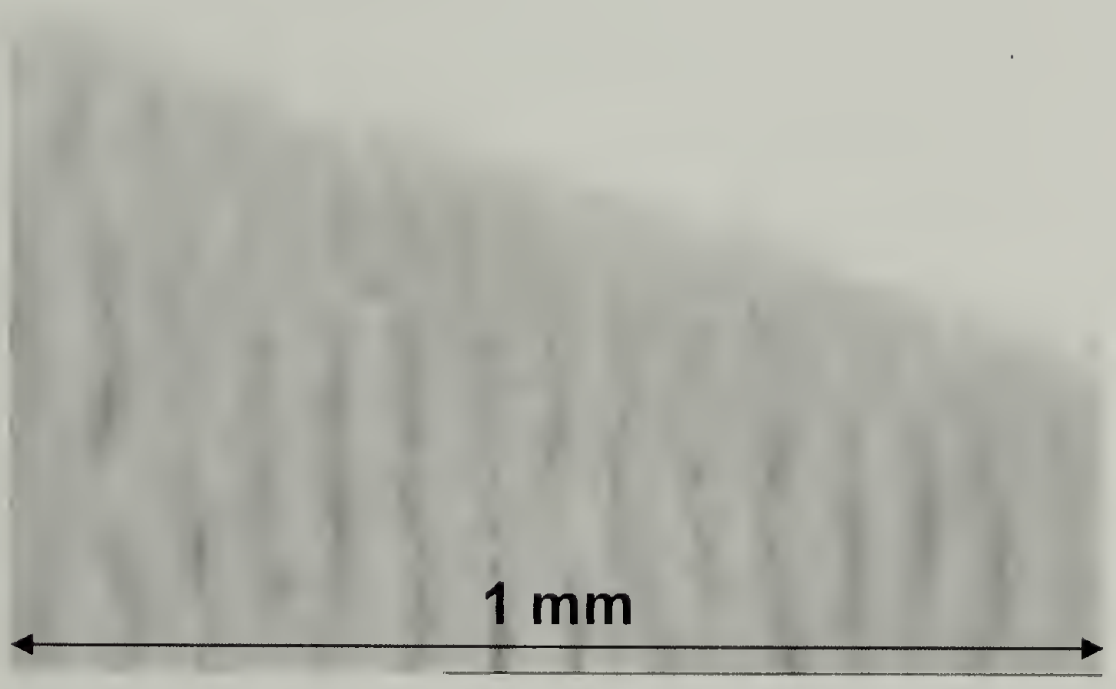

Figure 4.14 – Optical micrograph of thermally imaged electrospun mat (dark area has been imaged; light area has not been imaged).

4.6 Conclusions

In all three of the polymer/solvent systems studied in this chapter, a color change was produced by electrospinning a black solution to a white, or off-white, fiber mat. The white electrospun mats were subsequently heated and became black in color. The

results indicate that carbon black is still present in the electrospun fiber mats, and that the multiple light scattering events that result from the highly porous mats mask the presence of the carbon black. The key morphological characteristic common to all three systems—as seen in the room temperature micrographs—is a nonwoven isotropic fiber mat with fibers and beads of diameters less than 500 nanometers. Also consistent among the electrospun polymers is the microscopic morphological change accompanying the macroscopic color change of the fiber mat from white to black. In each system, color change occurs as a result of the transition from a fibrillar mat to a film-like material. By heating the electrospun fiber mats and eliminating the numerous gas-solid scattering interfaces, the number of light scattering events present in the fiber mats is greatly reduced and the mats become black due to the absorbance of light by the carbon black particles. In two of the three systems, the temperature at which color change occurs is coincident with a characteristic thermal transition temperature for that material—T_g for polycarbonate and T_m for poly(ethylene oxide). For electrospun PMMA/carbon black, color change is observed at temperatures well above the T_g for PMMA, in part due to the relatively high molecular weight of the PMMA.

CHAPTER 5

MELTING BEHAVIOR OF ELECTROSPUN LINEAR AROMATIC POLYESTERS: PET, PTT AND PBT

5.1 Introduction

The potential effect of electrospinning on molecular orientation has been speculated and the effect of electrospinning on the conformation of chains in semicrystalline polymers has been reported in the literature. Based on the size of an electrospinning jet relative to a conventional solution spun fiber, simple calculation suggests that an electrospinning jet potentially dries and solidifies roughly 10,000 times faster than would a conventional wet spun fiber. The rate of crystallization of an electrospun polymer fiber must also be affected relative to a conventional solution spinning process. Changes in degree of crystallinity or crystalline structure may be observable when electrospun polymers are compared to their bulk analogs. To determine if electrospinning influences crystallization, a family of polyesters—PET, PTT, and PBT—which are well studied and reported in the literature, have been electrospun. Relative crystallization rates, crystalline phases, and degree of crystallinity of this family of polymers have been extensively studied and reported. The aim of this chapter is to determine if electrospinning produces any change in the melting behavior of these polymers relative to their bulk analogs, or from solution cast bulk samples. Typically, this family of polyesters is processed from the melt. The study of electrospinning these polymers will include determining the optimum solution concentrations to produce cylindrical, defect-free fibers. Subsequently, thermal analysis will be used to compare electrospun forms to bulk pellets as well as solution cast films

to observe differences, if any, in melting behavior. Data from differential scanning calorimetry will be compared to studies presented in the literature of controlled crystallization of these polymers from the melt, and an attempt will be made to correlate reported observations in the literature and the results from electrospun fibers of PET, PTT and PBT. Similarities between the results for electrospun fibers and results reported in the literature for melt-crystallized polyesters may provide some insight to the rate of crystallization of fibers during the electrospinning process.

The crystallinity of a semicrystalline polymer has been shown to be affected by the electrospinning process. Differential scanning calorimetry of poly(ethylene oxide) electrospun from aqueous solution is compared with PEO powder and shown in Figure 5.1.

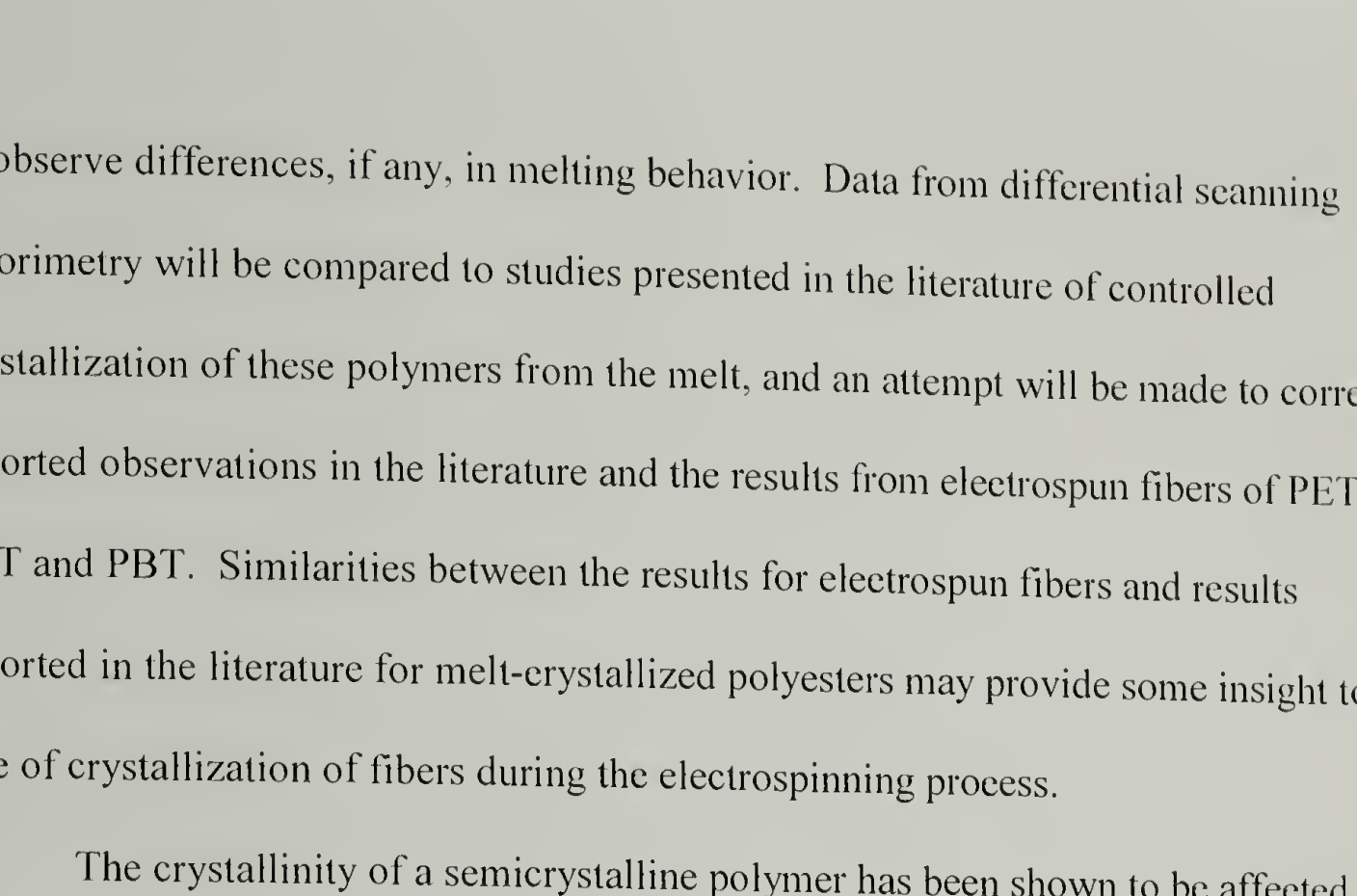

Figure 5.1 – DSC of powder and electrospun PEO.

The family of linear aromatic polyesters known as poly(ethylene terephthalate) (PET), poly(trimethylene terephthalate) (PTT), and poly(butylene terephthalate) (PBT) have been studied extensively and used in a number of engineering applications due to their excellent mechanical and thermal properties. The polymers are exactly analogous to one another, differing only by a single methylene unit each. The chemical structure of each is shown in Figure 5.2.

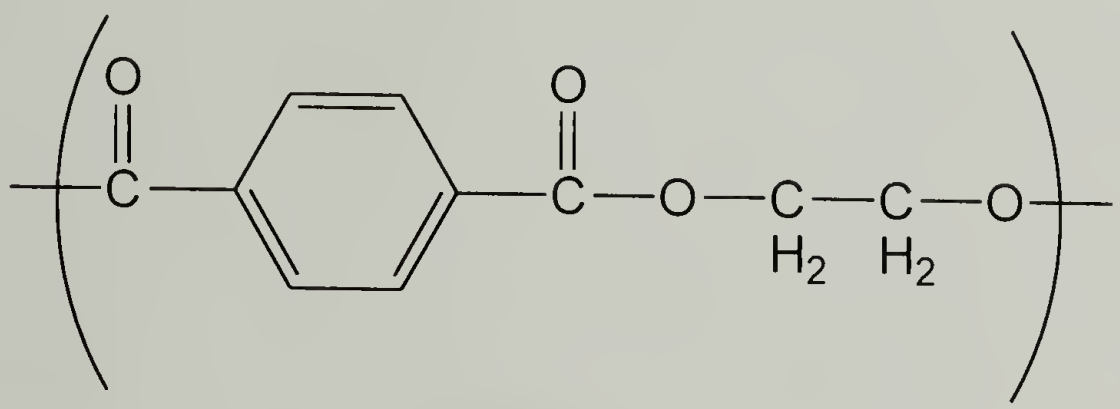

PET

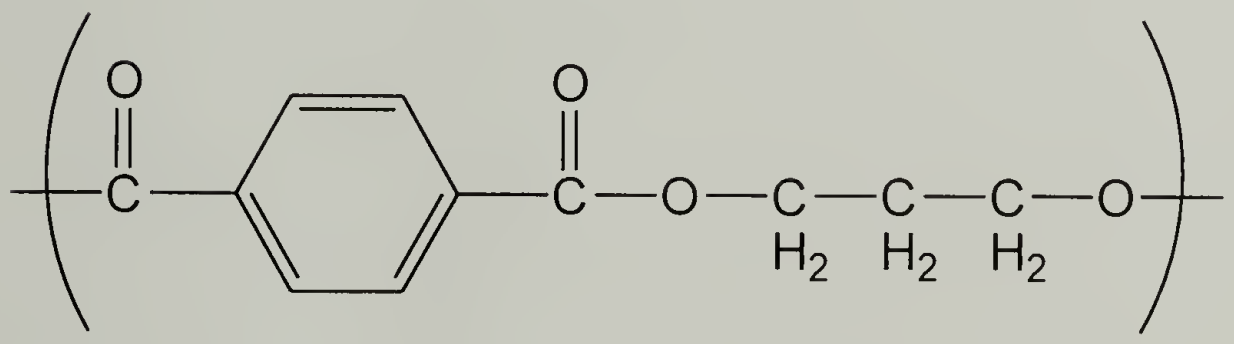

PTT

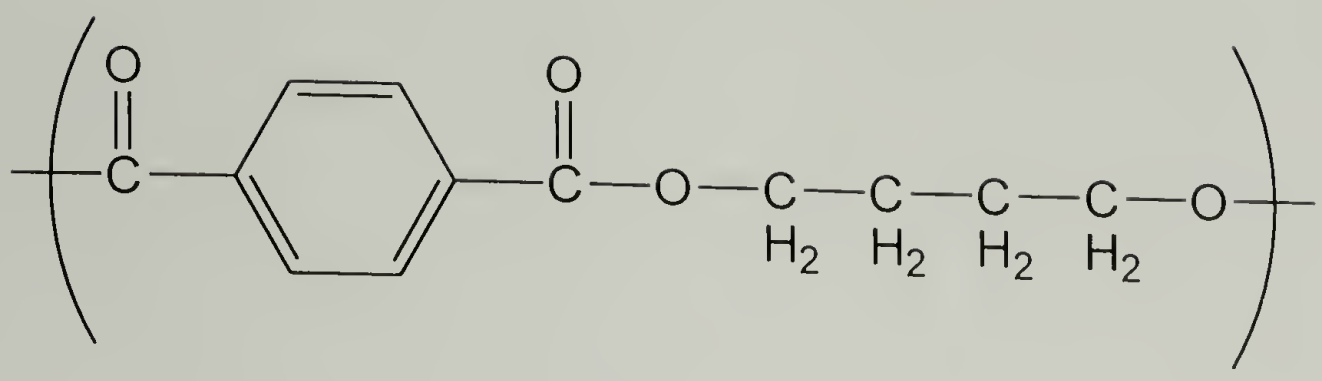

PBT

Figure 5.2 – Chemical structures of linear aromatic polyesters.

By increasing the number of methylene units, the chain flexibility for this family of polyesters goes as PET<PTT<PBT, and the relative crystallization rates of each at a given degree of undercooling follows exactly inverse to the chain stiffness. PBT has the highest crystallization rates with Avrami rate constant (k_a) being on the order of 10^{-2} to 10^{-1} min^{-n}, which is approximately an order of magnitude greater than PTT at 10^{-3} to 10^{-2} min^{-n}, which is about an order of magnitude greater than PET at 10^{-4} to 10^{-2} min^{-n}.[93] Relative crystallization rates of these three polymers are shown graphically in Figure 5.1, plotted as the reciprocal half-time of crystallization versus the degree of undercooling for each polymer. The degree of undercooling is the number of degrees in centrigrade below the equilibrium melting temperature of the respective polymer, at which crystallization is measured. The equilibrium melting temperature for PET, PTT, and PBT are 270° C, 244° C, and 235° C, respectively.[94]

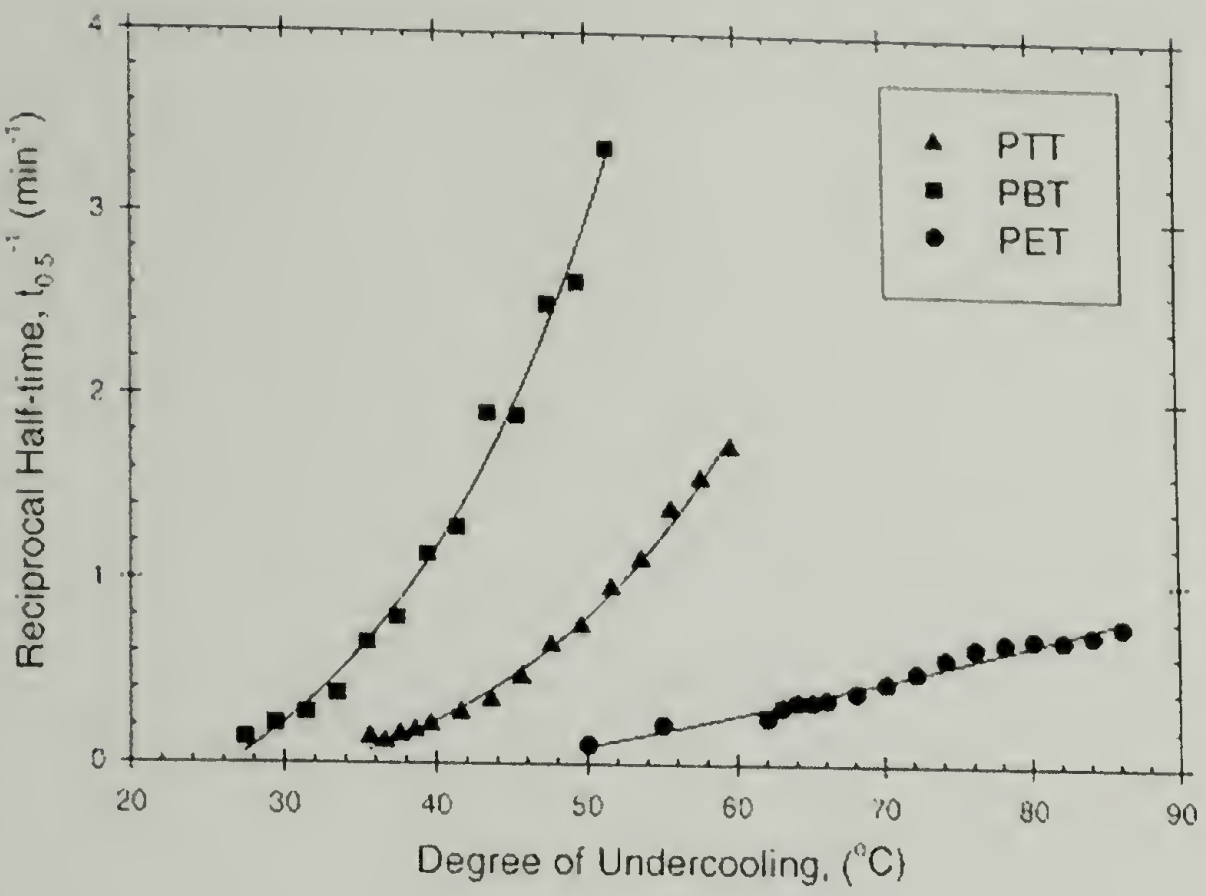

Figure 5.3 - Reciprocal half-time of crystallization as a function of degree of undercooling for PET, PTT, and PBT.[93]

5.1.1 Poly(ethylene terephthalate)

PET crystallized under isothermal conditions often shows double melting endotherms depending on the crystallization temperature and on the heating rate used in DSC analysis. This double melting behavior has been attributed by different authors[94-99] to partial melting of the crystallites formed at T_c (temperature of crystallization) followed by a rapid recrystallization during scanning. The dependence of melting temperature on the isothermal crystallization temperature has been ascribed to a change of crystallite thickness with the degree of undercooling.

5.1.2 Poly(trimethylene terephthalate)

Poly(trimethylene terephthalate) is the most recently introduced commercial polymer of this family of linear aromatic polyesters. It is currently developed by Shell

Chemical Company for fiber and engineering thermoplastic applications.[100-102] Compared with PET and PBT, relatively few studies have been made of the melting behavior of PTT. A recent report attributes the multiple melting endotherms observed for melt-crystallized PTT to the dual populations of lamellar stacks formed during primary crystallization and recrystallization during subsequent heating. Based on WAXD analysis, the crystal unit cell of PTT is shown to remain the same, independent of crystallization temperature.[103]

5.1.3 Poly(butylene terephthalate)

PBT is widely used in engineering applications for its good mechanical and thermal properties. Because of a crystallization rate much higher than PET, PBT is suitable for injection molding and extrusion, as well as matrices for glass fiber-reinforced composites.

For PBT that has been cooled at a constant rate from the melt, the DSC heating scan can show up to three separate melting endotherms, depending on the cooling rate. PBT can crystallize into two different types of spherulites, which has lead some authors to assign different melting peaks to each type of spherulite.[104-105] Although two melting endotherms are observable, there is only one crystal structure, the triclinic α-form, as determined by x-ray diffraction methods.[104] Others suggest that the multiple melting peaks may arise from melting and recrystallization taking place during heating in the DSC and are not indicative of the crystalline morphology at room temperature.[106-110]

In all systems, if double melting endotherms are caused by two crystalline spherulite morphologies or a bimodal distribution of crystallite sizes, melting will occur

without exothermic heat in the temperature range between the melting peaks. If the double melting peaks are caused by melt recrystallization, exothermic heat change should be observed in the temperature range between the melting peaks.

5.2 Experimental

5.2.1 Materials

Phenol and 1,1,2,2-tetrachloroethane were received from Aldrich Chemical Company and used without further purification

Polymers

1. Poly(ethylene terephthalate) in small pellet form received from Aldrich Chemical Co.
2. Poly(trimethylene terephthalate) in small pellet form received from Shell Oil Co.
3. Poly(butylene terephthalate) in small pellet form received from Eastman Kodak Co.

Electrospinning solutions:

20% wt. PET in phenol/tetrachloroethane (60/40)

10% wt. PTT in phenol/tetrachloroethane (60/40)

10% wt. PBT in phenol/tetrachloroethane (60/40)

All solutions were stirred vigorously and held at approximately 105°C until all polymer was visibly dissolved (approximately 30-45 minutes for each sample). Subsequently, solutions were allowed to continue to stir at room temperature for at least 24 hours prior to electrospinning.

Solution cast samples analyzed by DSC were cast into petri dishes from the same solutions as their respective fibers were electrospun, and dried in a vacuum at room temperature for at least one week prior to analysis.

5.2.2 Experimental procedures

Differential scanning calorimetry experiments were performed on a TA Instruments differential scanning calorimeter at a heating rate of 10°C/min for all samples. Morphological data was obtained from images taken using a JEOL 6320F field emission scanning electron microscope operating at an accelerating voltage of 5 kV.

5.3 Results and Discussion

5.3.1 Poly(ethylene terephthalate)

The DSC heating scans for electrospun PET and pellet are compared in Figure 5.1. The pellet shows a single melting endotherm at approximately 260°C, indicative of material that was crystallized at relatively small undercooling, or annealed subsequent to initial crystallization.

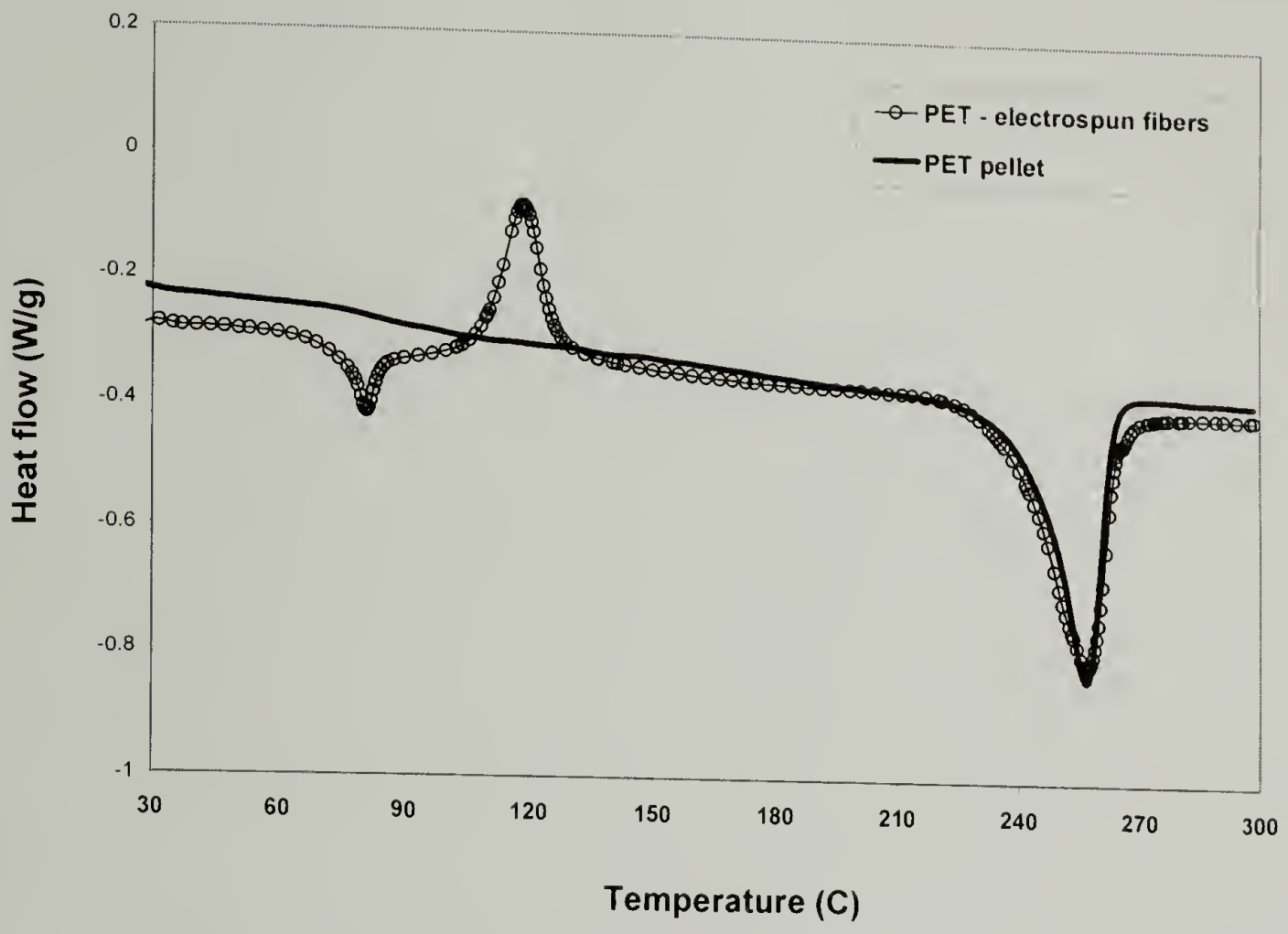

Figure 5.4 – DSC heating scans for PET pellet and electrospun PET fibers.

Electrospun PET in the first heating scan shows transitions similar to an isotropic amorphous PET film as shown by Lin and Koenig.[111] In their study, Lin and Koenig monitored the change in melting behavior of amorphous PET films as a function of annealing time and temperature. The DSC scan for PET annealed for 0 minutes, i.e. as received amorphous films, shows a glass transition at approximately 70° C, followed by a relatively large crystallization exotherm at 150° C, and ultimately followed by the true melting endotherm for crystalline PET at approximately 250° C. Results similar to those reported by Lin and Koenig for amorphous PET are also seen for electrospun PET. The slow crystallization kinetics of PET and the rapid solidification process of electrospinning results in the melting behavior shown in Figure 5.4. The crystallization

exotherm is indicative of PET that has been quenched, or at least cooled from the melt at relatively large undercoolings. Electrospun PET fibers are shown in Figure 5.5.

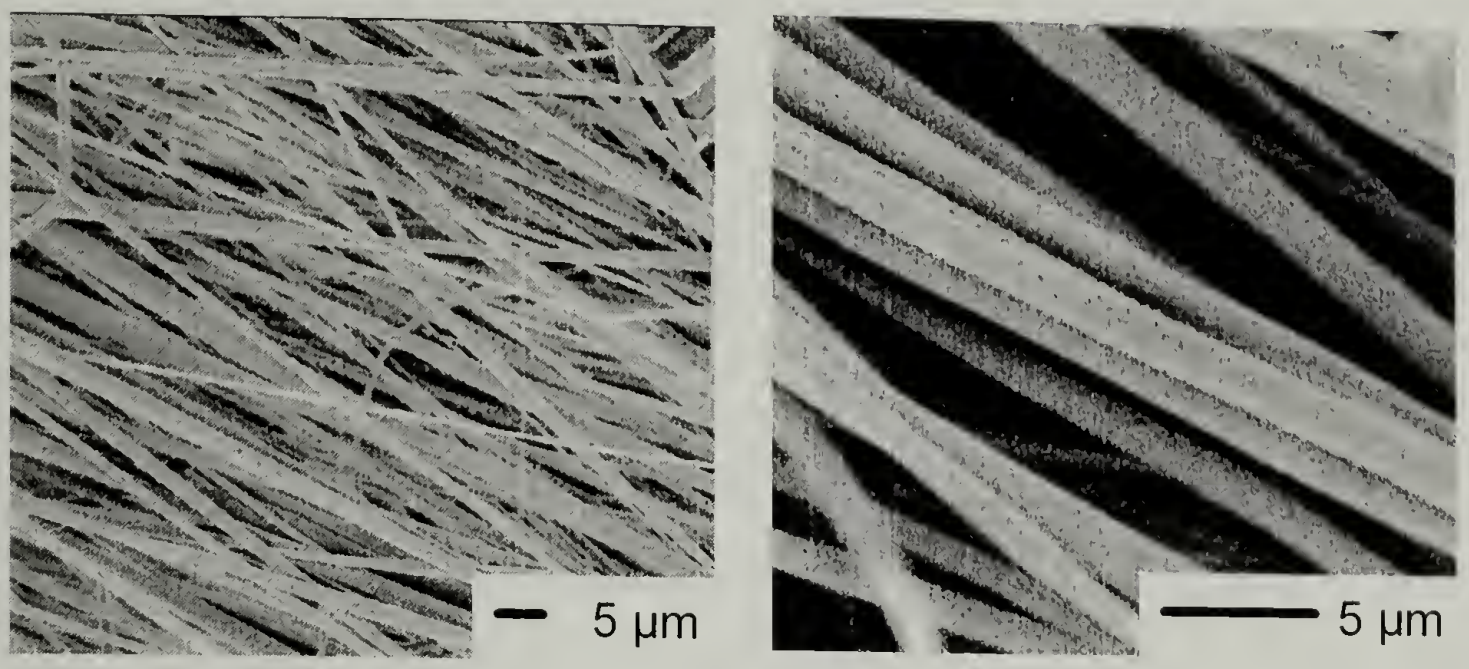

Figure 5.5 – Electrospun PET fibers (from 20% wt. solution).

Rapid solidification results in PET chains that become kinetically trapped in an amorphous state, until they are given sufficient time or heated to a temperature at which chain mobility is increased and the chains gain enough mobility to recrystallize, such as in a DSC heating. The crystallization and melting behavior seen for electrospun PET agrees with the perception of the electrospinning process as a rapid solidification of material, analogous to a thermal quench from the melt state.

Comparison of the electrospun PET to a solution cast PET film is complicated by the existence of residual solvent in the film. In order to show the effect of electrospinning compared to solution casting, both samples were allowed to dry at room temperature to avoid annealing affects of elevated temperature on crystalline

morphology. Electrospun PET and solution cast PET thermograms are compared in Figure 5.6.

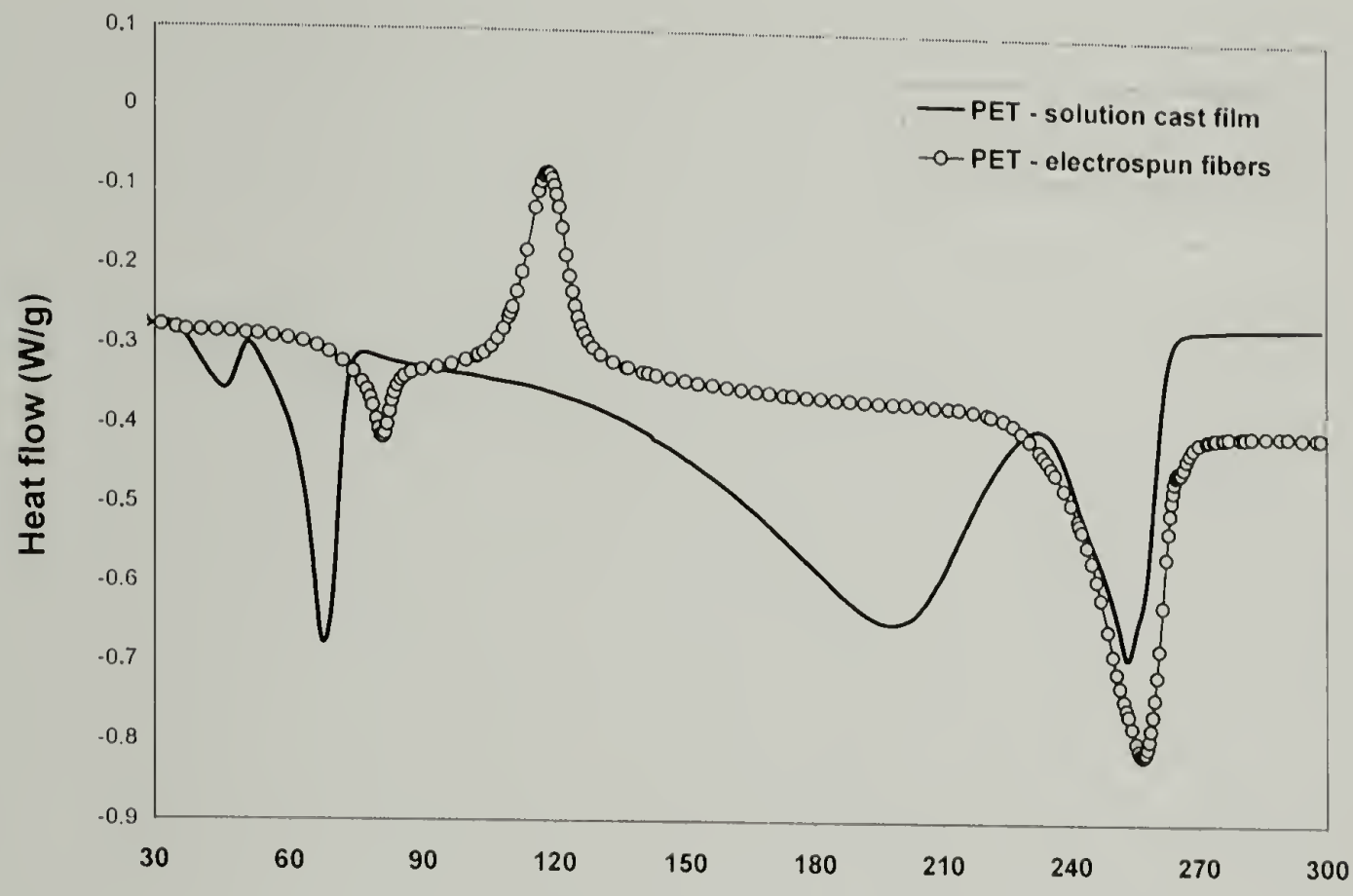

Figure 5.6 – DSC heating scans for electrospun and solution cast PET.

The electrospun material dried in air and shows no trace of residual solvent from the DSC thermogram. The solution cast PET film was put into a vacuum at room temperature for at least one week prior to DSC experiments, yet shows a large broad peak ranging from approximately 130° C to 190° C, which encompasses the boiling points of both co-solvents in the PET solution, tetrachloroethane and phenol, respectively. The predominant melting endotherm in the solution cast material coincides with that for the electrospun materials at approximately 260° C, however no

clear conclusions can be reached for the lower temperature endotherms observed in the solution cast material.

The second heating scan of electrospun PET—shown in figure 5.7, compared with the first heating scan—again shows a single melting endotherm similar to that seen for the PET pellet, indicating the metastable morphology in the electrospun PET fibers.

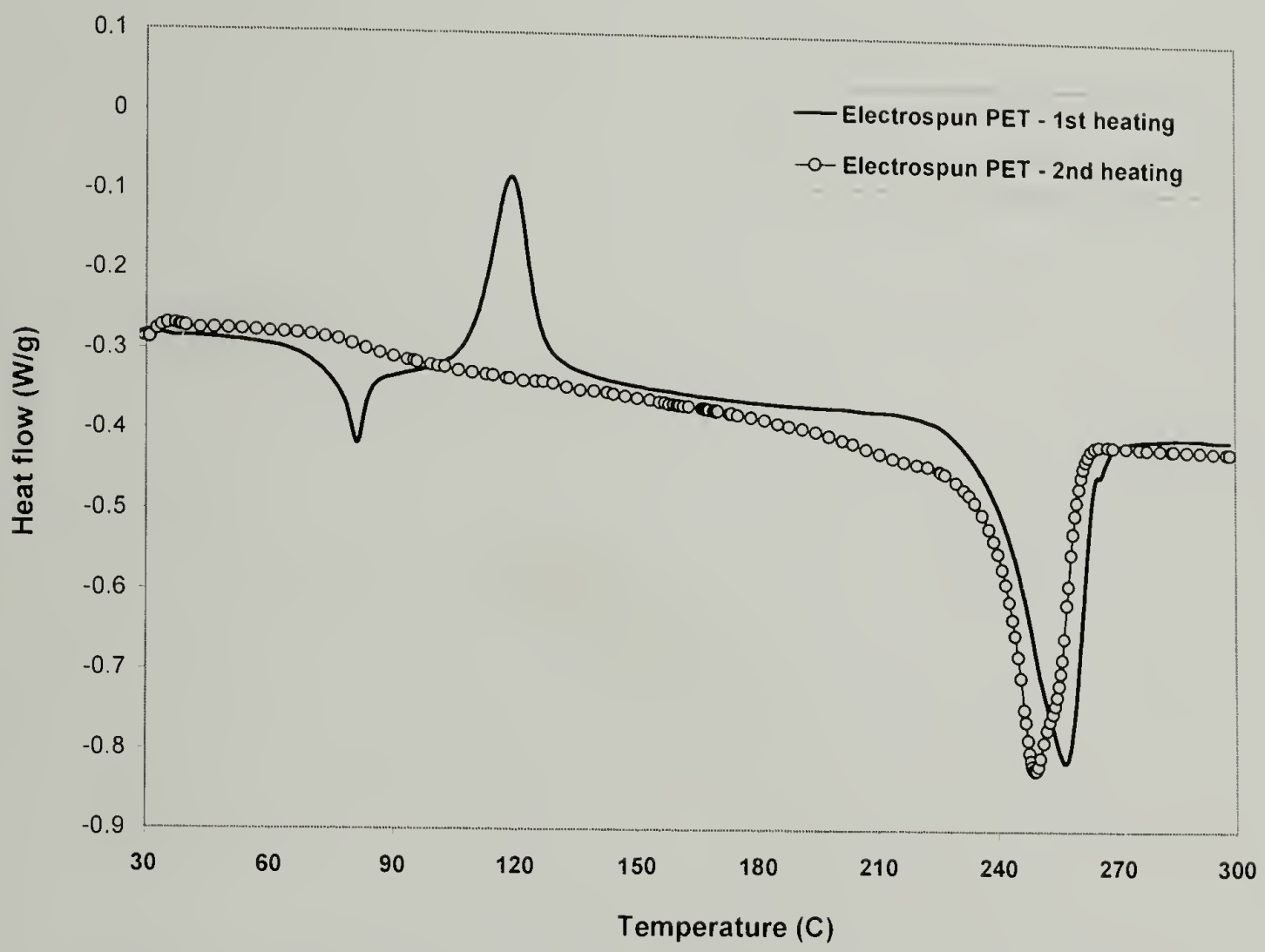

Figure 5.7 – First and second DSC heating scans for electrospun PET.

5.3.2 Poly(trimethylene terephthalate)

The first attempt to electrospin PTT fibers with an applied voltage of 8 kilovolts resulted in a polymer film, rather than a mat of fibers. The morphology of the material electrospun at 8 kV from 10% wt. solution is shown in Figure 5.8.

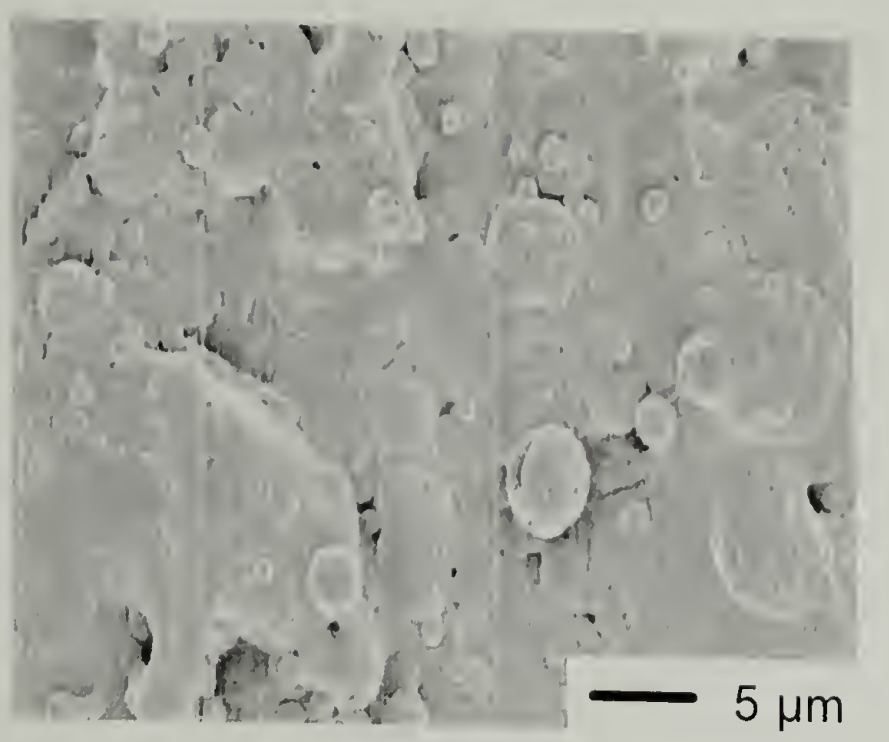

Figure 5.8 – Electrospun PTT (10% solution) at 8 kV.

The second attempt, electrospinning the 10% PTT solution at 13 kV resulted in formation of fibers, shown in Figure 5.9.

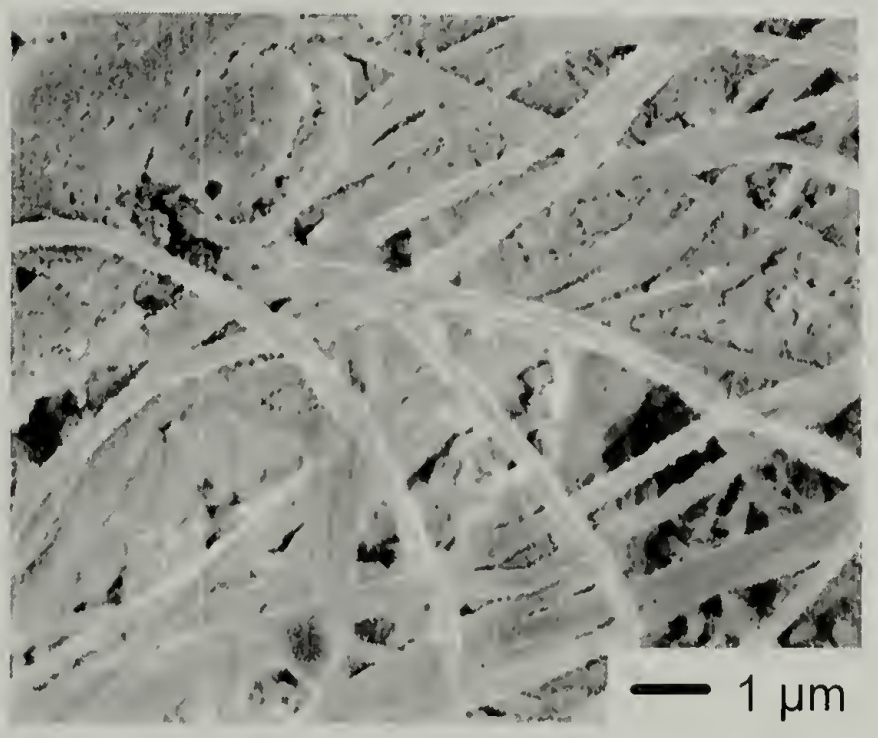

Figure 5.9 – Electrospun PTT (10% solution) at 13 kV.

The DSC seans for PTT electrospun at 8 kV and 13 kV, and for PTT pellet are compared in Figure 5.10. The material electrospun at 8 kV, which is not fibrous, shows a single melting endotherm, qualitatively similar to the melting behavior of the PTT pellet from which the solution was prepared.

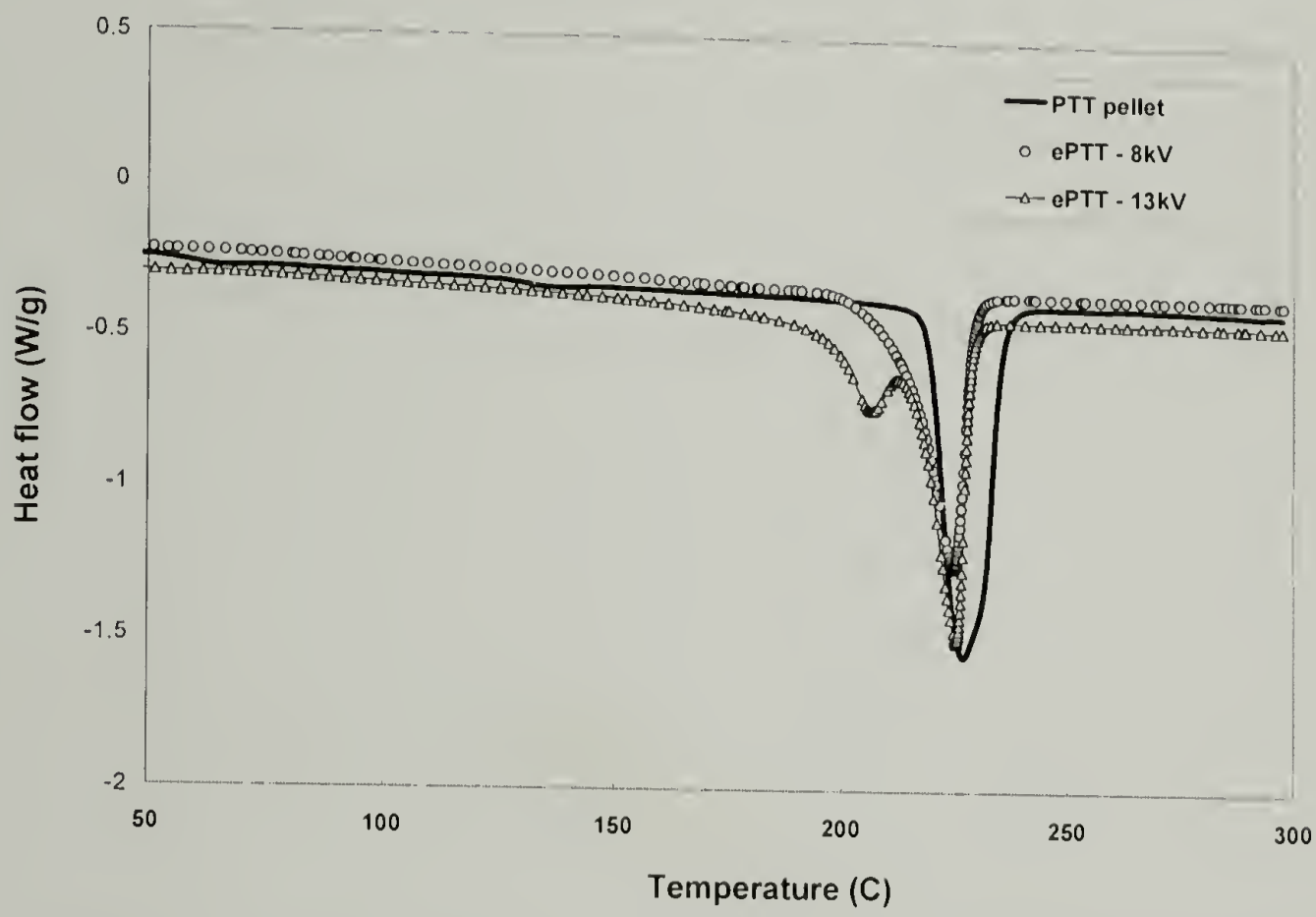

Figure 5.10 – DSC heating seans for PTT pellet and PTT electrospun at 8 kV and 13 kV.

PTT electrospun at 13 kV, which produces fibers, shows a double melting endotherm with a relatively small peak at lower temperature, approximately 210° C, and a larger peak at 225° C that corresponds to the melting temperature of the other two materials. The double melting peaks are observable only in the electrospun fibers which indicates a unique crystallization process occurring when fibers are formed. No exothermic heat is released in the temperature range between the melting endotherms suggesting that the two peaks are a result of two populations of crystal sizes, rather than

melting and recrystallization. The double melting behavior seen for the electrospun PTT resembles that seen for PTT crystallized from the melt at relatively large undercooling as studied by Chung and coworkers.[112] The thermogram for electrospun PTT resembles the those for PTT isothermally crystallized from the melt in the range of temperatures from 438° K to 448° K, which was at the lower end of temperatures included in the study. In their analysis, Chung et al. conclude that the two melting endotherms seen for PTT crystallized at large undercoolings are a result of two populations of lamellar stacks, and not melting by polymorphic crystals, as wide angle x-ray diffraction shows identical diffraction peaks for all cooling rates. The similarity in melting behavior between electrospun PTT and rapidly cooled PTT from the melt is consistent with the concept of electrospinning as a fiber spinning process which involves very rapid solvent evaporation in air and fast solidification of polymer fibers from solution while in flight to a target. The apparent two populations of crystallites may be produced by the initial solidification of the electrospinning fiber shell, corresponding to the low temperature endotherm, followed by relatively slower crystallization of the fiber core and allowing larger crystals to grow and producing the larger and higher temperature melting endotherm. In Figure 5.11, the heating scans of electrospun PTT fibers is compared with a solution cast film of PTT, to demonstrate that the fiber-spinning process from solution produces different results than other solution processing methods.

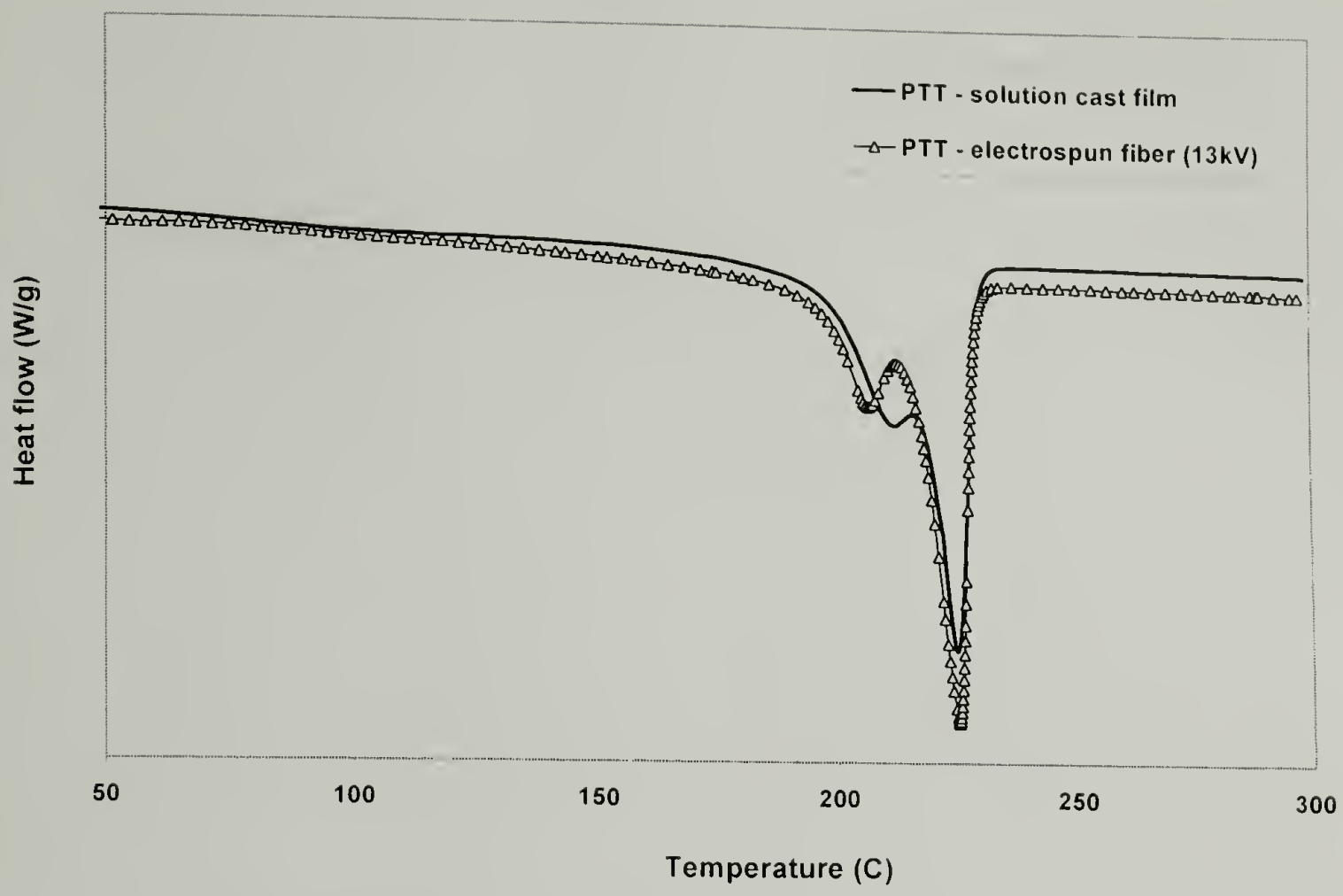

Figure 5.11 – DSC heating scans for PTT solution cast film and PTT electrospun fibers.

The solution cast PTT also shows a double melting behavior, although the small secondary peak is less distinct than the secondary peak in electrospun PTT. The DSC result for the soluton cast material makes sense compared to electrospun PTT. In the film, crystallization at the surface of the solution is relatively fast compared to in the bulk; this more rapidly crystallizing material causes the small low temperature melting shoulder. The electrospun material has much more surface area due to the cylindrical geometry and extremely fine diameter of the fibers, therefore surface crystallization is even more rapid that for the film cast from solution and surfaces are more abundant, resulting in a larger, more distinct low temperature melting endotherm for the electrospun material.

In the second heating scan of the electrospun PTT, the expected result is seen, that the melting behavior resembles that of the PTT pellet with a single melting endotherm at 230° C, indicating that the crystalline morphology present in the electrospun fibers is metastable. The first and second heating scans for electrospun PTT are shown in Figure 5.12.

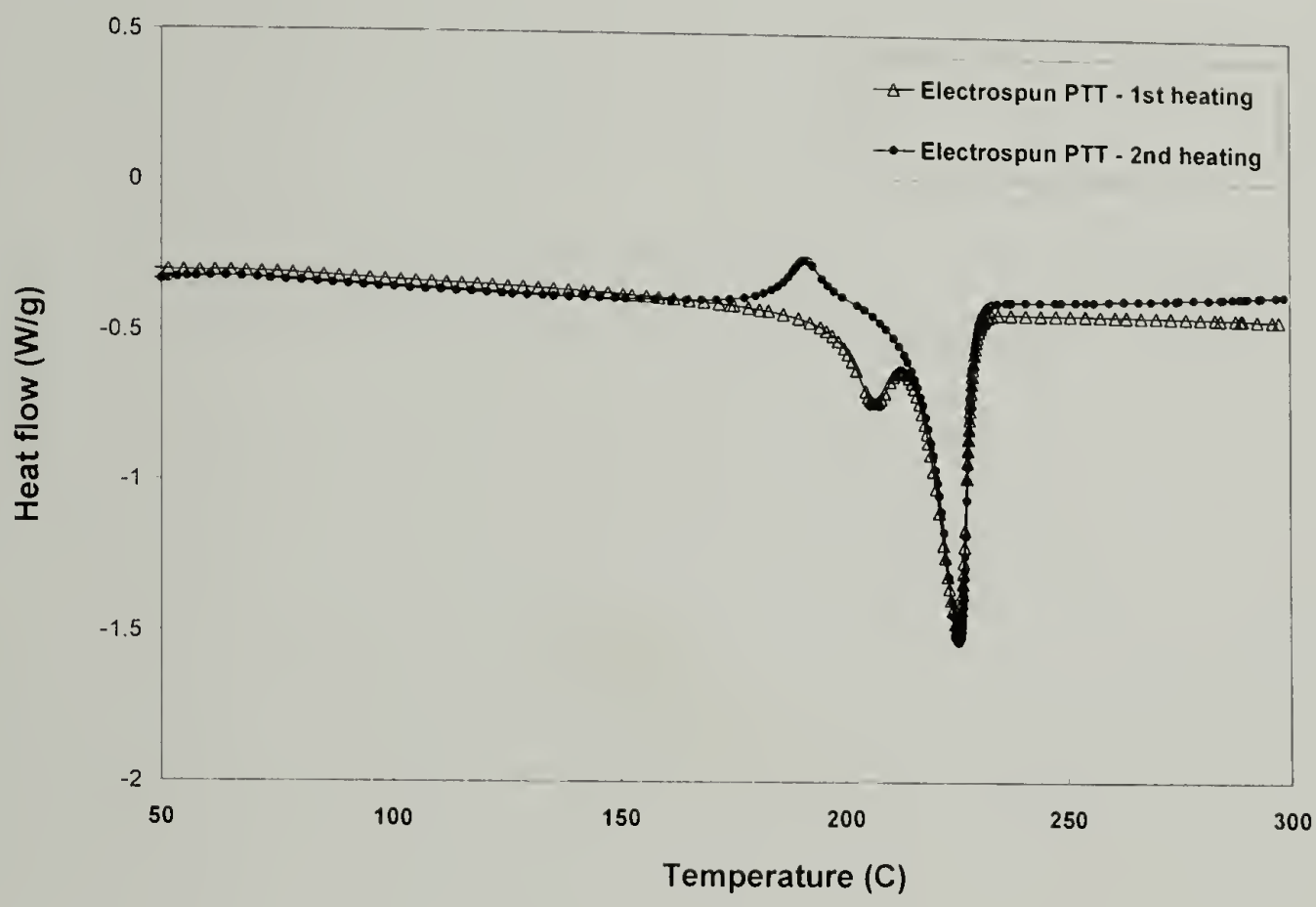

Figure 5.12 – First and second DSC heating scans for electrospun PTT.

5.3.3 Poly(butylene terephthalate)

DSC heating scans for PBT pellet, solution cast PBT film, and electrospun PBT fibers are shown in Figure 5.13.

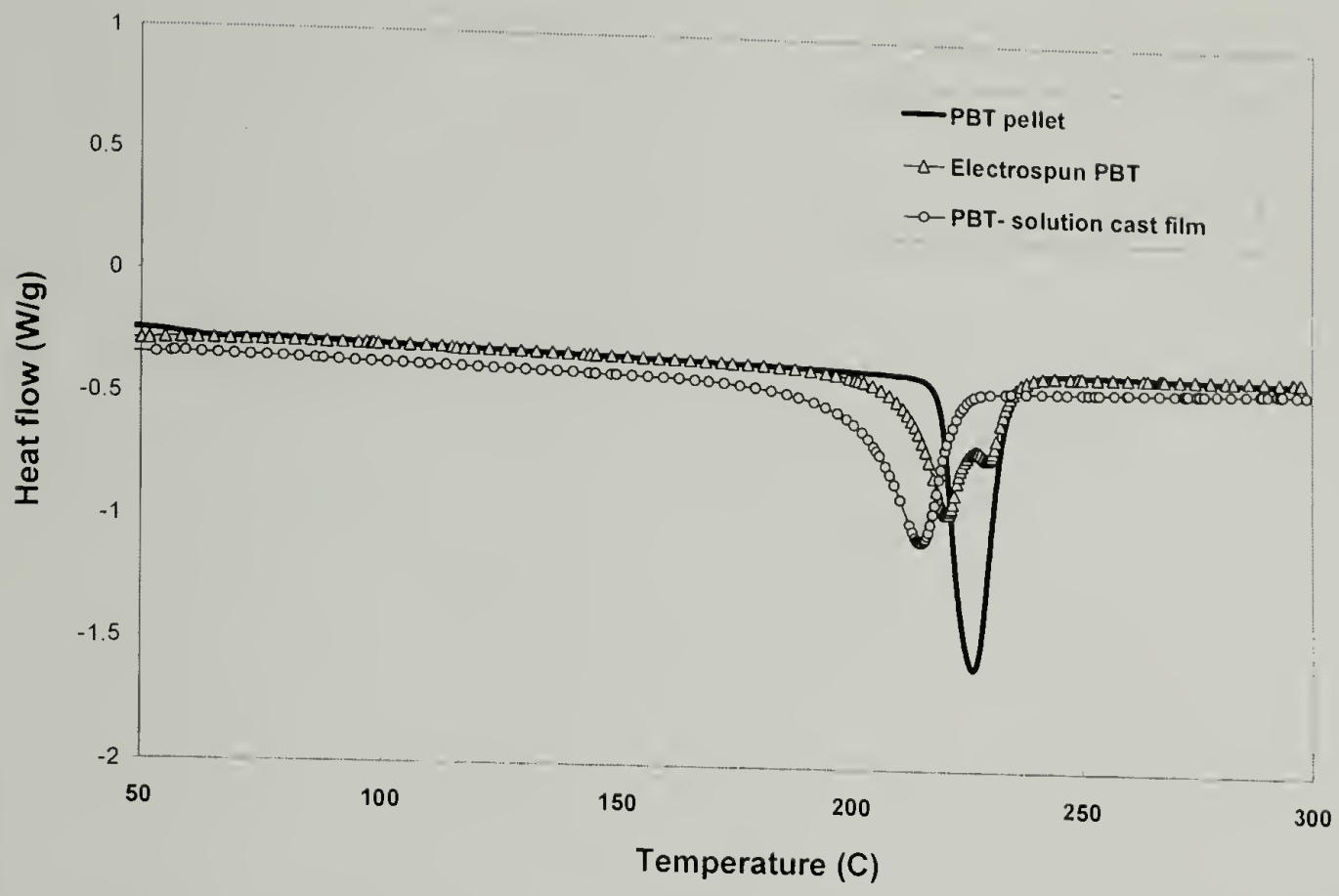

Figure 5.13 – DSC heating scans for PBT pellet, PBT solution cast film and electrospun fibers.

The PBT pellet shows a single relatively sharp melting endotherm at 226° C. The solution cast material also shows a single melting endotherm, although the peak is broader, has a lower degree of crystallinity and significantly lower in temperature than the pellet. The result from the solution cast material suggest that while a single population of crystal sizes appears to exist, crystallization from solution is relatively fast and leads to a distribution of crystal sizes, causing the broad melting endotherm. The electrospun PBT fibers, shown in Figure 5.14, show two melting endotherms upon first heating.

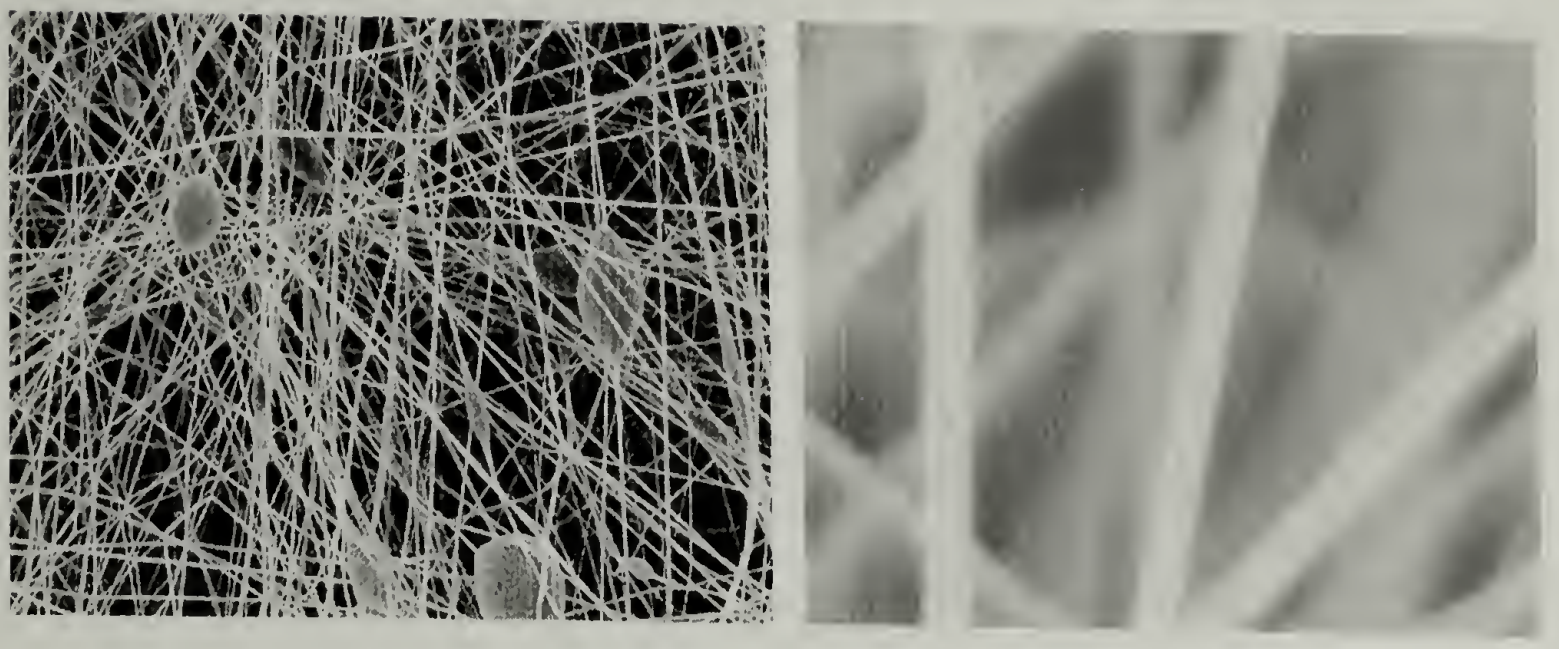

Figure 5.14 – Electrospun PBT fibers.

This type of melting behavior is similar to that observed for PBT crystallized from the melt at approximately 1.0-2.0 °C/min, as reported by Nichols and Robertson.[113] There is no exothermic heat between the temperature range of the two endotherms, indicating that the second peak is not a result of recrystallized material. As with PTT, the double melting endotherms are representative of two populations of crystal sizes, and not a consequence of crystalline polymorphism, which is shown in WAXD data by Yasuniwa and coworkers.[114] The overall crystallinity of the electrospun PBT is quite low compared to the bulk pellet, which is expected with the idea of rapid solidification associated with the electrospinning process. The second heating scan for electrospun PBT—Figure 5.15—again shows a single relatively sharp melting endotherm—preceeded by a small exotherm—as a result of the rapid quench with liquid nitrogen of the sample in the DSC after the first heating.

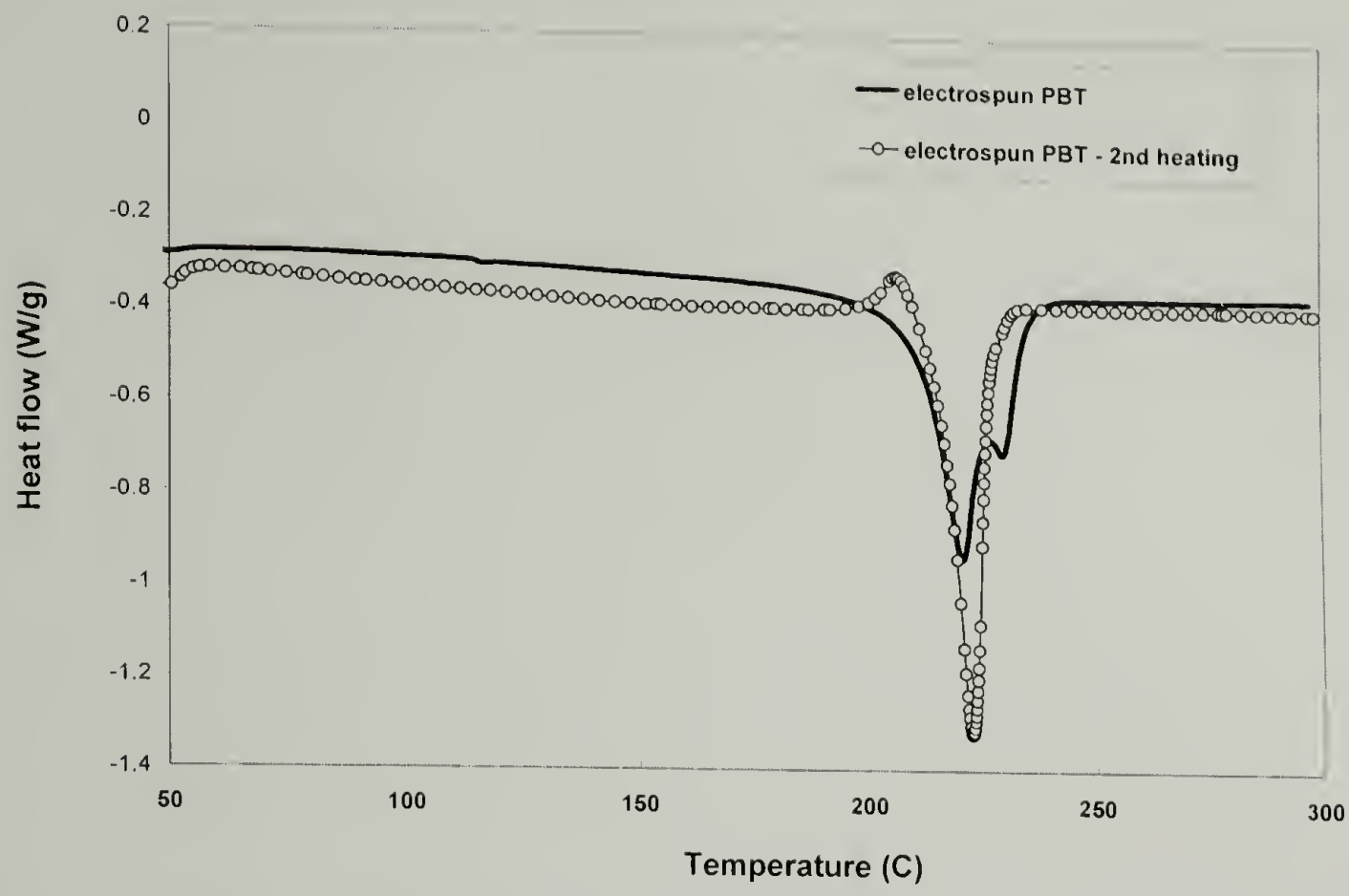

Figure 5.15 – First and second DSC heating scans for electrospun PBT.

5.4 Conclusions

This chapter attempts to give a simple analysis, based on melt crystallization studies reported in the scientific literature, of the observed melting behavior of three electrospun linear aromatic polyesters. The melting behavior of electrospun PET, PTT, and PBT have been compared to solution cast films and pellet forms of each polymer. In all three systems, the electrospun materials have unique melting behavior in the form of double melting endotherms on the first heating scans in differential scanning calorimetry. In accordance with the idea of electrospinning producing fibers by rapid solvent evaporation and fiber solidification, the melting behavior appears to reflect two crystallizations taking place during the electrospinning process. In each electrospun polymer, the relatively small melting endotherm may be caused by the small, imperfect crystals that are located at the shell of the electrospun fibers, which solidify rapidly due

to solvent evaporation. The subsequent, slower crystallization of the material at the core of the electrospun fibers accounts for the larger of the two melting endotherms seen in each electrospun system.

In addition to the similarity seen among all three electrospun systems in melting behavior, the overall crystallinity of each is lower in the electrospun material than the starting material in pellet form. Table 5.1 compares the crystallinity of the electrospun and pellet form of each polymer.

	ΔH_f (J/g)	**Overall Crystallinity (%)**	**Melting Temperature T_m (^oC)**
PET pellet	51.7	36.9	259
Electrospun PET	40.9	29.2	80 / 256
PTT pellet	78.7	54.0	227
Electrospun PTT (13kV)	73.6	50.5	205 / 225
PBT pellet	66.3	45.6	226
Electrospun PBT	52.4	36.7	220 / 230

Table 5.1 – Crystallinity and melting temperatures for bulk and electrospun PET, PTT, and PBT.

The metastable crystalline morphology of this family of electrospun linear aromatic polyesters presents an interesting set of materials for future work in annealing and mechanical post-treatment of the electrospun fibers. The differences in crystallinity illustrated above in Table 5.1 may manifest themselves in fibers that are more ductile with increased drawability, and the potential to achieve materials ultimately of higher

strength and stiffness. The ability to electrospin aligned fibers has been demonstrated with PET in Figure 5.4, and should be easily extended to PTT and PBT, as well. The potential exists to produce highly oriented PET, PTT and PBT fibers with diameters on the nanoscale.

CHAPTER 6

SUMMARY AND SUGGESTIONS FOR FUTURE WORK

Electrospun materials have been shown to possess many unique characteristics and properties. The most obvious novelty of the process is the extremely fine diameter of fibers produced, typically 2-3 orders of magnitude smaller than conventional solution or melt spun polymer fibers. This quality alone has led many researchers to investigate a variety of electrospun polymers as potentially useful in applications for composites, filters, bioscaffolds, catalyst support, and others.

In this thesis, some electrospun polymers have shown unique mechanical, optical, and thermal behavior. Electrospun thermoplastic polyurethanes have uncharacteristic mechanical behavior relative to the bulk materials from which they are electrospun. In a variety of polymers, a color change phenomenon occurs when polymer solutions containing carbon black are electrospun to form white fiber mats, and subsequently return to black in color when heated to a characteristic temperature. A family of electrospun linear aromatic polyesters shows unique melting behavior compared to their bulk analogs.

The results presented in this thesis indicate that much remains to be fulfilled in terms of understanding the physical properties of electrospun materials. In terms of mechanical properties, even just the group of materials referred to as thermoplastic polyurethane elastomers presents a wide range of materials to electrospin and study mechanical behaviors, based on the chemistry of the polymer. By studying a range of TPU's, with varying relative amounts of hard and soft segment contents, a clearer

picture may be reached concerning the effects of electrospinning on the morphology and organization of hard and soft phases in electrospun TPU fibers, and how those changes manifest themselves in a change of mechanical behavior.

The color change phenomenon discussed in Chapter 4 has also opened possibilities for additional study. The effect of carbon black filler size and loading can be systematically studied, as well as optimizing electrospinning conditions—solution concentration, solvents, applied voltage—to achieve the most distinct color change possible from solution to electrospun mat. Also, the concept of color change can be extended to pigments of color, and further it is conceivable that a fiber mat consisting of several different polymers, each carrying a different color, can produce a mat upon which color images could be made, each color exposable by a specific intensity or wavelength of radiation.

The melting behavior of PET, PTT, and PBT show interesting characteristics. What remains to be studied for these electrospun polymers is the crystal structure, to determine if any change is produced by electrospinning. In addition, the mechanical properties of the electrospun fibers are certain to be influenced by this change of crystallinity, and perhaps show that the fibers produced by electrospinning are more/less processable in terms of post-treatment with drawing and/or annealing. In general, the effect of electrospinning on polymer crystallinity requires further study.

Perhaps most important for electrospinning, as far as a viable commercial process for the production of nanoscale fibers, is the volume of materials that can be produced. Output presents one of the most difficult challenges to the process, and must

be addressed, in terms of production rate and the effect of spinning rate on orientation and strength, if the potential applications for these unique materials are to be realized.

APPENDIX

THERMOPLASTIC POLYURETHANE CHEMISTRY

Soft segment chemistry

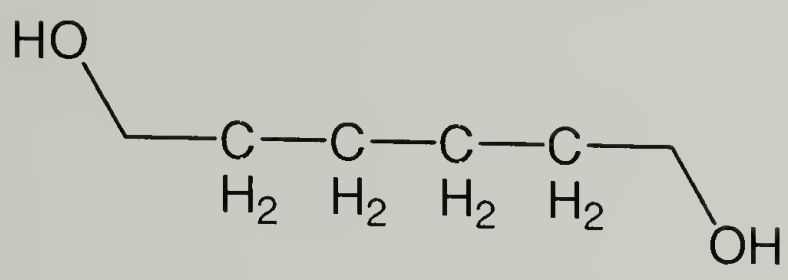

tetramethylene glycol ether

Hard segment chemistry

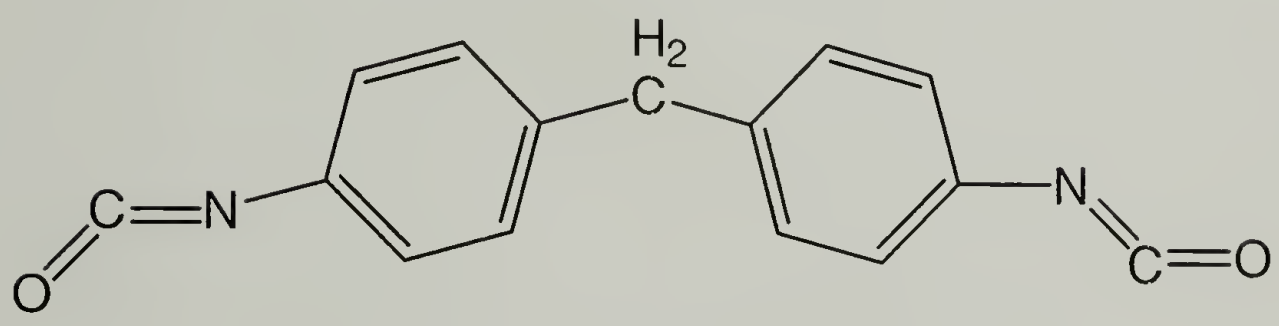

4,4'- methyl bisphenyl diisocyanate (MDI)

BIBLIOGRAPHY

1. W Gilbert. *On the Loadstone and Magnetic Bodies and on the Great Magnet theEarth*. **1600**

2. JF Cooley. *U.S. Patent 692,631*. **1902**.

3. WJ Morton *U.S. Patent 705,691*. **1902**.

4. A Formhals *U.S. Patent 1,975,504*. **1934**.

5. A Formhals, *U.S. Patent 2,116,942*. **1938**.

6. CL Norton. *U.S. Patent 2,048,651*. **1936**.

7. J Zeleny. *The Physical Review*, **1917**, *X(I)*, 1.

8. AL Huebner. *J. Fluid Mech*. **1969**, *38*(4), 679.

9. JR Melcher, EP Warren. *J. Fluid Mech*. **1971**, *47*(1), 127.

10. GI Taylor. *Proc. Roy. Soc. London*, **1964**, *A280*, 383.

11. GI Taylor. Proc. Roy. Soc. London, **1966**, *A291*, 145.

12. GI Taylor. *Proc. Roy. Soc. London*, **1969**, *A313*, 453.

13. YM Shin, MM Hohman, MP Brenner, GC Rutledge. *Applied Physics Letters*, **2001**, *78*(8), 1149.

14. YM Shin, MM Hohman, MP Brenner, GC Rutledge. *Polymer*, **2001**, *42*, 9955.

15. PK Baumgarten. *J. Colloid Interface Sci*. **1971**, *36*, 71.

16. SB Warner, A Buer, SC Ugbolue, GC Rutledge, YM Shin. *National Textile Center Annual Report* No. 83-90, **2000**

17. DH Reneker, AL Yarin, H Fong, S Koombhongse. *J. Appl. Phys*. **2000** *87*(9), 4531,

18. PG de Gennes. *J. Chem. Phys*. **1974**, *60*, 5030.

19. H Chang, AS Lodge, *Rheol. Acta*, **1972**, *11*, 127.

20. JS Stephens, DB Chase, JF Rabolt. *Macromolecules*, **2004**, *37*, 877.

21. R Dersch, T Liu, AK Schaper, A Greiner, JH Wendorff. *J. Polym. Sci: Part A. Polym. Chem.* **2003**, *41*, 545.

22. S Megelski, JS Stephens, DB Chase, JF Rabolt. *Macromolecules*, **2002**, *35*, 8456.

23. B Ding, HY Kim, SC Lee DR Lee, KJ Choi. *Fibers and Polymers*, **2002**, *3*(2), 73.

24. A Buer, SC Ugbolue SB Warner. *Textile Res. J.* **2001**, *71*(4), 323.

25. KH Lee, HY Kim YM La, DR Lee NH Sung. *J. Polym. Sci: Part B. Polym Phys.* **2002**, *40*, 2259.

26. MM Bergshoef, GJ Vansco. *Adv. Mater.* **1999**, *11*(16), 1362.

27. X Fang, DH Reneker. *J. Macromol. Sci. – Phys.* **1997**, *B36*(2), 169.

28. S Sikigara, M Gandhi, J Ayutsede, M Micklus F Ko. *Polymer*, **2003**, *44*, 5721.

29. JA Matthews, GE Wnek, DG Simpson, GL Bowlin. *Biomacromolecules*, **2002**, *3*, 232.

30. G Srinivasan, DH Reneker. *Polym. International*, **1995**, *36*, 195.

31. L Larrondo, RSJ Manley. *J. Polym. Sci: Part B. Polym Phys.* **1981**, *19*, 909.

32. L Larrondo, RSJ Manley . *J. Polym. Sci: Part B. Polym Phys.* **1981**, *19*, 933.

33. PK Kahol, NJ Pinto. *Synth. Met.* **2004**, *140*, 269.

34. X Zong, S Ran, D Fang, BS Hsiao, B Chu. *Polymer*, **2003**, *44*, 4959.

35. H Fong, DH Reneker. J. *Polym. Sci: Part B. Polym. Phys.* **1999**, *37*, 3488.

36. Y Dror, W Salalha, RL Khalfin, Y Cohen, AL Yarin, E Zussman. *Langmuir*, **2003**, *19*, 7012.

37. A Koski, K Yim, S Shivkumar. *Mat. Letters*, **2004**, *58*, 493.

38. MG McKee, GL Wilkes, RH Colby TE Long. *Macromolecules*, **2004**, *37*, 1760.

39. JM Deitzel, J Kleinmeyer, D Harris, NC Beck Tan. *Polymer*, **2001**, *42*, 261.

40. JWS Rayleigh. *Philos. Mag.* **1892**, *34*, 145.

41. H Fong, I Chun, DH Reneker. *Polymer*, **1999**, *40*, 4585.

42. KH Lee, HY Kim, HJ Bang, YH Jung, SG Lee. *Polymer*, **2003**, *44*, 4029.

43. ED Boland, GE Wnek, DG Simpson, KJ Pawlowski, GL Bowlin. *J. Macromol. Sci.—Pure Appl. Chem.* **2001**, *A38*(12), 1231.

44. GE Martin, ID Cockshott, FJT Fildes. *US Patent 4,044,404*. **1977.**

45. H Planck, P Ehrler. *US Patent 4,474,630*. **1984.**

46. TV How. *US Patent 4,552,707*. **1985.**

47. W Simm. *U.S. Patent 3,994,258*. **1976.**

48. H Schrueder-Gibson, P Gibson, K Senecal, M Sennett, J Walker, W Yeomans, D Ziegler, PP Tsai. *J. Adv. Mat.* **2002**, *34*(3), 44.

49. YJ Ryu, HY Kim, KH Lee, HC Park, DR Lee. *European Polym. J.* **2003**, *39*, 1883.

50. D Li, Y Xia. *Nano Letters*, **2003**, *3*(4), 555.

51. H Dai, J Gong, H Kim, D Lee. *Nanotech.* **2002**, *13*, 674.

52. P Viswanathamurthi, N Bhattarai, HY Kim, DR Lee. *Scripta Materialia*, **2003**, *49*, 577.

53. P Viswanathamurthi, N Bhattarai, HY Kim, DR Lee, *Nanotech.* **2004**, *15*, 320.

54. Y Wang, R Furlan, I Ramos, JJ Santiago-Aviles. *Appl. Phys. A*, **2004**, *78*, 1043.

55. D Li, T Herricks, Y Xia. *Appl. Phys. Letters*, **2003**, *83*(22), 4586.

56. H Guan, C Shao, S Wen, B Chen, J Gong, X Yang. *Mat. Chem. Phys.* **2003**, *82*, 1002.

57. N Dharmaraj, HC Park, BM Lee, P Viswanathamurthi, HY Kim, DR Lee. *Inorg. Chem. Commun.* **2004**, *7*, 431.

58. H Guan, C Shao, B Chen, J Gong, X Yang. *Inorg. Chem. Commun.* **2003**, *6*, 1409.

59. SV Fridrikh, JH Yu, MP Brenner, GC Rutledge. *Physical Review Letters*, **2003**, *90*(14), Art. No. 144502.

60. A Theron, E Zussman, AL Yarin. *Nanotech.* **2001,** *12*, 384.

61. E Zussman, A Theron, AL Yarin. *Applied Physics Letters*, **2003**, *82*(6), 973.

62. S Fennessey, RJ Farris. *Polymer*, **2004**, *45*(12), 4217.

63. I Chun, DH Reneker, H Fong, X Fang, J Deitzel, N Beck Tan, K Kearns. *J. Adv. Mat.* **1999**, *31*(1), 36.

64. A Pedicini, RJ Farris. *Polymer*, **2003**, *44*, 6857.

65. JM Deitzel, JD Kleinmeyer, JK Hirvonen, NC Beck Tan. Polymer, **2001**, *42*, 8163.

66. P Gibson, H Schreuder-Gibson. Int. Nonwovens Tech. Conf. **2003**.

67. D Li, Y Wang, Y Xia. Adv. Mater. **2004**, *16*(4), 361.

68. JC Halpin, SW Tsai. U.S. Air Force Materials Laboratory Report, AFML-TR 67-423, **1969**.

69. MS Khil, HY Kim, MS Kim, SY Park, D-R Lee. *Polymer*, **2004**, *45*, 295.

70. KH Lee, HY Kim, YJ Ryu, KW Kim, SW Choi. *J. Polym. Sci.: Part B: Polym. Phys.* **2003**, *41*, 1256.

71. R Sen, B Zhao, D Perea, ME Itkis, H Hu, J Love, E Bekyarova, RC Haddon. *Nano Letters*, **2004**, *4*(3), 459.

72. X Zong, S Ran, D Fang, BS Hsiao, B Chu. *Polymer*, **2003**, *44*, 4959.

73. W-J Li, CT Laurencin, EJ Caterson, RS Tuan, FK Ko. *J. Biomed. Mat. Res.* **2002**, *60*(4), 613.

74. JS Kim and DH Reneker. *Polymer Composites*, **1999**, *20*(1), 124.

75. R. Bonart, L.Morbitzer, G.Hentze. *J. Macromol. Sci.- Phys.* **1969**, *B3*(2), 337.

76. Estes GM, Seymour RW, Cooper SL. *Macromolecules* **1971**, *4*, 452.

77. Hermans PH. *Contributions to the Physics of Cellulose Fibers*. Amsterdam: Elsevier, **1946**.

78. Fraser, RDB. *J Chem Phys* **1953**, *21*, 1511.

79. R. Falabella, Ph.D. Dissertation **1980**.

80. JC West, JT Koberstein, A Lilaonitkul, SL Cooper, *ACS Polymer Prepriuts*, **1975**, *16*, 523.

81. RM Christensen. *Mechanics of Composite Materials*. John Wiley & Sons, New York. **1979**.

82. S. Backer, D.R. Petterson, *Textile Res. J.* **1960**, *30*, 704.

83. S. Bais-Singh, B.C. Goswami, *J. Textile Inst.* **1995**, *86*(2), 271.

84. J.W.S. Hearle, P.J. Stevenson, *Textile Res. J.* **1963**, *33*, 877.

85. J.W.S. Hearle, P.J. Stevenson, Textile Res. J. **34**, 181 (1964)

86. L. Rangtong, Y. Haojing, C. Caiyuan, *J. of China Textile Univ. (Eng. Ed.)*, **1998**, *15*(1), 10.

87. L. Zuopan, C. Caiyuan, *J. of China Textile Univ. (Eng. Ed.)* **1999**, *16*(2), 43.

88. T. Liao, S. Adanur, J-Y. Drean, *Textile Res. J.* **1997**, *67*(10), 753.

89. L.J. Gibson, M.F. Ashby. *Cellular Solids: structure and properties*. Cambridge Univ. Press; New York. **1997**.

90. D.J. Durian, D.A. Weitz, D.J. Pine. *Science*, **1991**, *252*, 686.

91. K.Fuchs, Chr. Friedrich, J. Weese, *Macromolecules*, **1996**, *29*, 5893.

92. S. Wu, *J.Polym.Sci:Part B:Polym.Phys.* **1989**, *27*, 723.

93. JM Huang, FC Chang. *J. Polym. Sci. Polym. Phys.* **2000**, *38*, 934.

94. N Dangseeyun, P Srimoaon, P Supaphol, M. Nithitanakul. *Thermochimica Acta*, **2004**, *409*, 63.

95. RC Roberts, *Polymer*, **1969**, *10*, 117.

96. PJ Holdsworth, A Turner-Jones, *Polymer*, **1971**, *12*, 195.

97. JP Bell, T Murayama, *J. Polym. Sci, A-2*, **1969**, *7*, 1059.

98. RC Roberts, *J. Polym. Sci., Part B*, **1970**, *8*, 381.

99. GE Sweet, JP Bell, *J. Polym. Sci., A-2*, **1972**, *10*, 1273.

100. DL Nealy, TG Davis, CJ Kibler, *J. Polym. Sci., A-2*, **1970**, *8*, 2141.

101. HH Chuah, *Chem. Fiber Int.* **1996**, *46*(6), 424.

102. HS Brown, HH Chuah, *Chem. Fiber Int.* **1997**, *47*(1), 72.

103. K Dangayach, HH Chuah, W Gergen, P Dalton, F Smith, *Plastics—Saving Planet Earth*, 55th ANTEC Proc. **1997**, 2097.

104. WT Chung, WJ Yeh, PD Hong, *J. Applied Polym. Sci.* **2002**, *83*, 2426.

105. RS Stein, A Misra, *J. Polym. Sci, Phys. Ed.* **1980**, *18*, 327.

106. JT Yeh, J Runt, *J. Polym. Sci., Phys. Ed.* **1989**, *27*, 1543.

107. SZ Cheng, R Pan, B Wunderlich, *Makromol. Chem.* **1988**, *189*, 2443.

108. S Hobbs, CF Pratt, *Polymer*, **1975**, *16*, 462.

109. S Hobbs, CF Pratt, *Polymer*, **1976**, *17*, 12.

110. S Fakirov, N Avramova, J Schultz. *J. Angew Makromol Chem.* **1986**, *140*, 63.

111. S-B. Lin, J.L. Koenig. *J. of Polym. Sci: Polym. Symp.* **1984**, *71*, 121.

112. W-T. Chung, W-J. Yeh, P-D. Hong. *J. of Applied Polym. Sci.* **2002**, *83*, 2426.

113. ME Nichols, RE Robertson, *J. of Polym. Sci. Part B: Polym. Phys.* **1992**, *30*, 755.

114. M Yasuniwa, S Tsubakihara, T Murakami. *J. Polym. Sci. Part B: Polym. Phys.* **2000**, *38*, 262.